SUNSET GROUP

INIFTA
CONICET
UNLP
FACULTAD DE CIENCIAS EXACTAS
DEPARTAMENTO DE QUÍMICA

Small Angle X-Ray Scattering

Lisandro J. Giovanetti

Surface and Nanostructures Studies based on Synchrotron Experimental Techniques Group.
INIFTA. Fac. de Cs. Exactas. Universidad Nacional de La Plata - CONICET
Diagonal 113 y Calle 64. (1900) La Plata. Buenos Aires - Argentina.
TE: (+54 221) 425 7430 - Ext: 144 / 123
WEB: http://nano.fisica.unlp.edu.ar
E-mail: lisandro@fisica.unlp.edu.ar

Bibliografía

- A Guinier “X-ray Diffraction in Crsytals, Imperfect Crystals and Amorphous Bodies” Freeman, 1963
- C. Cantor and P. Schimmel “Biophysical Chemistry part II: Techniques for the study of Biological Strcutre and Function” Freeman, 1980
- O. Glatter and O. Kratky “Small-angle X-ray Scattering” Academic Press 1982
- See Dmitri Svergun’s web site at http://www.embl-hamburg.de/Externalinfo/Research/Sax

Small Angle X-Ray Scattering

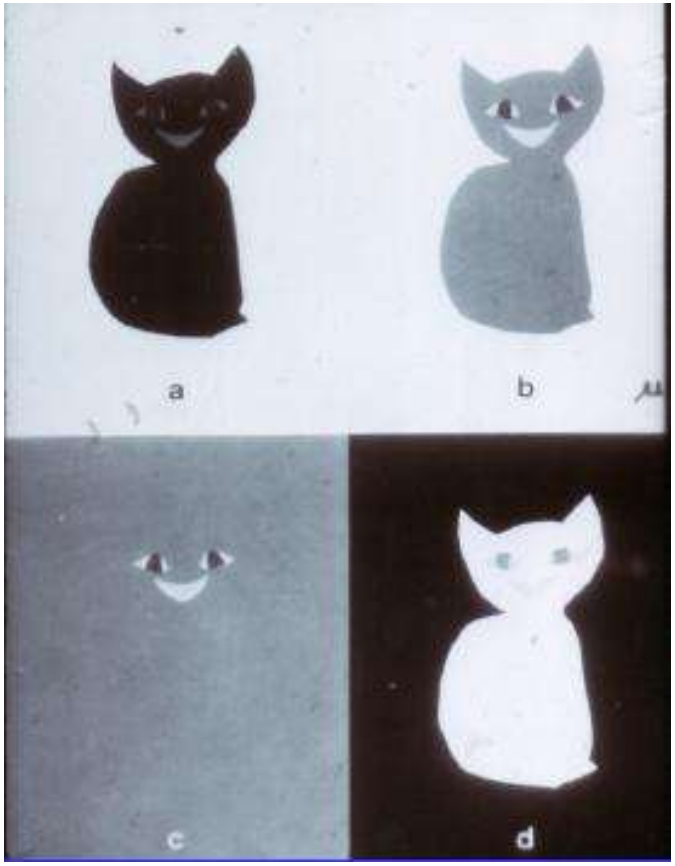

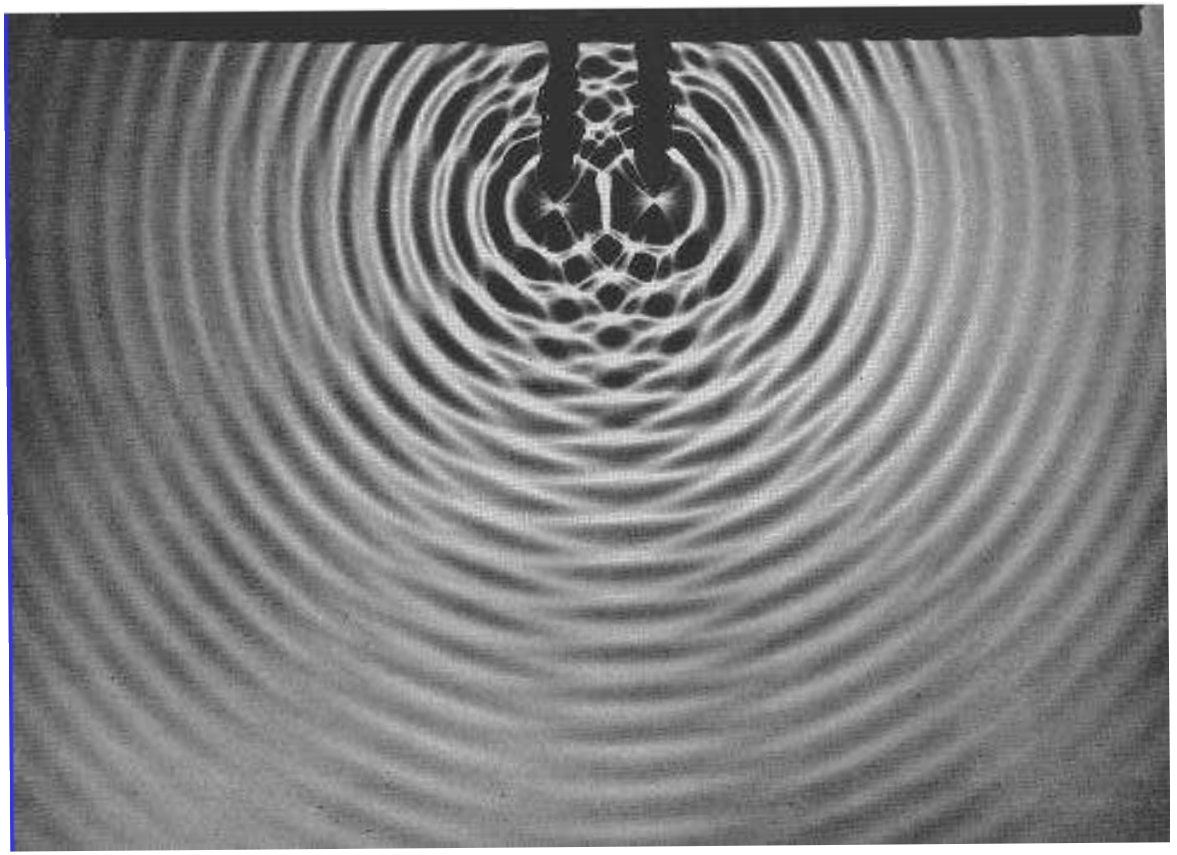

Small Angle X-Ray Scattering

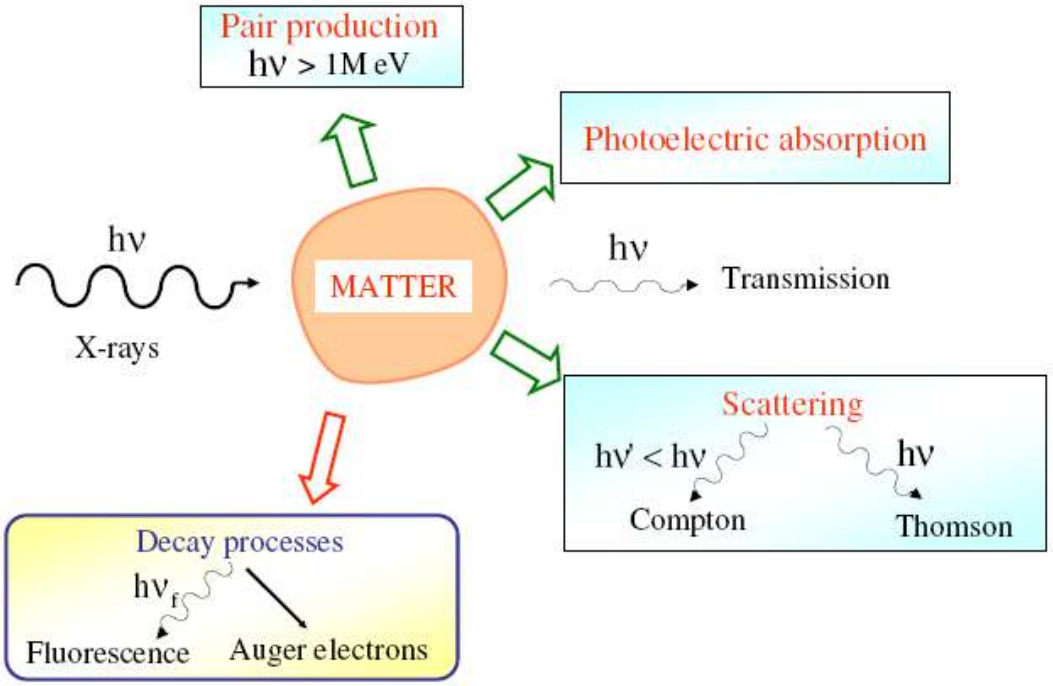

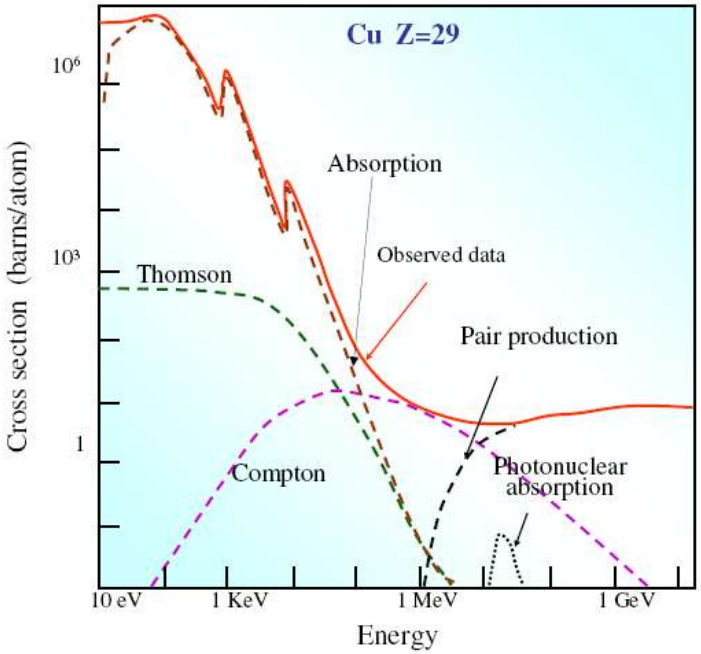

Scattering phenomenon and interference

X-ray is traveling wave…

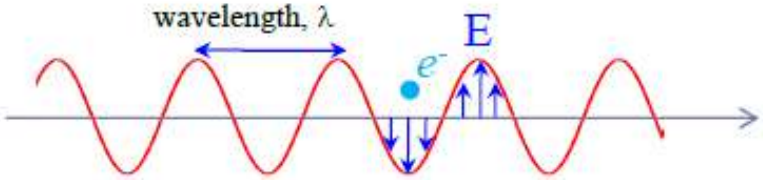

X-ray electric field hits electron…

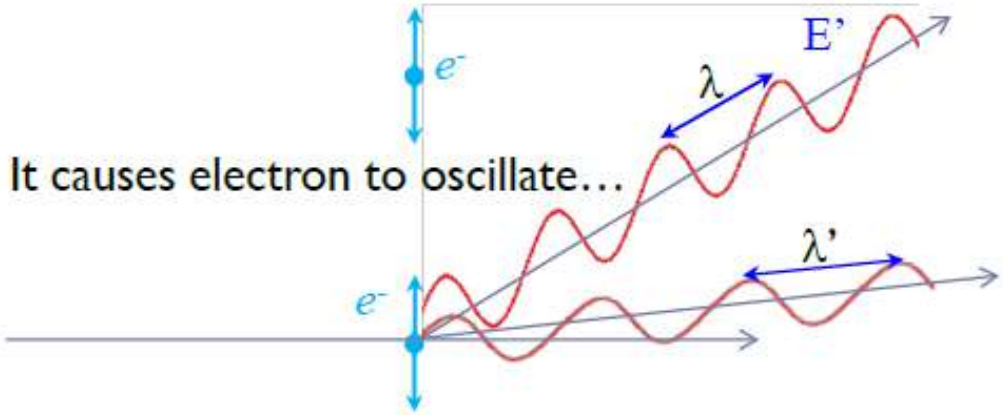

It causes electron to oscillate…

And make it radiate secondary X-ray!
This is scattering!

X-ray Wave function:

$$E(t) = E_0 e^{i(2\pi\nu t + \phi_0)}$$

frequency: $\nu = c/\lambda$
Initial phase: ϕ_0
Phase change: $\Delta\phi = 2\pi d/\lambda$ (radian)
after travelling distance d.

Elastic scattering: $\lambda \rightarrow \lambda$ not change
Inelastic (Compton) scattering: $\lambda \rightarrow \lambda'$ changed

If the scattered X-ray has the same wavelength of the original X-ray, it is called elastic/coherent scattering (no energy loss). If the wavelength of the scattering is changed (longer), it is inelastic/incoherent/Compton scattering (there is an energy loss)

X-ray interacts with atoms

Inelastic scattering is very weak and often ignorable for bound electrons, for example electron in atoms. Besides elastic and inelastic scattering, atoms absorb X-ray and emit fluorescence X-ray, especially at the absorption edges.

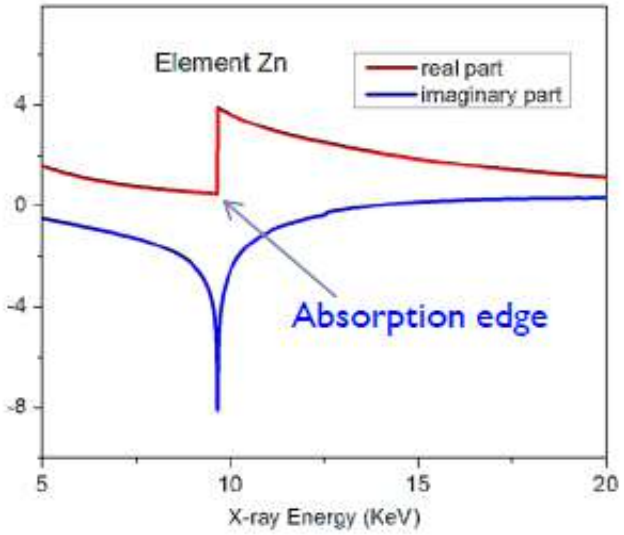

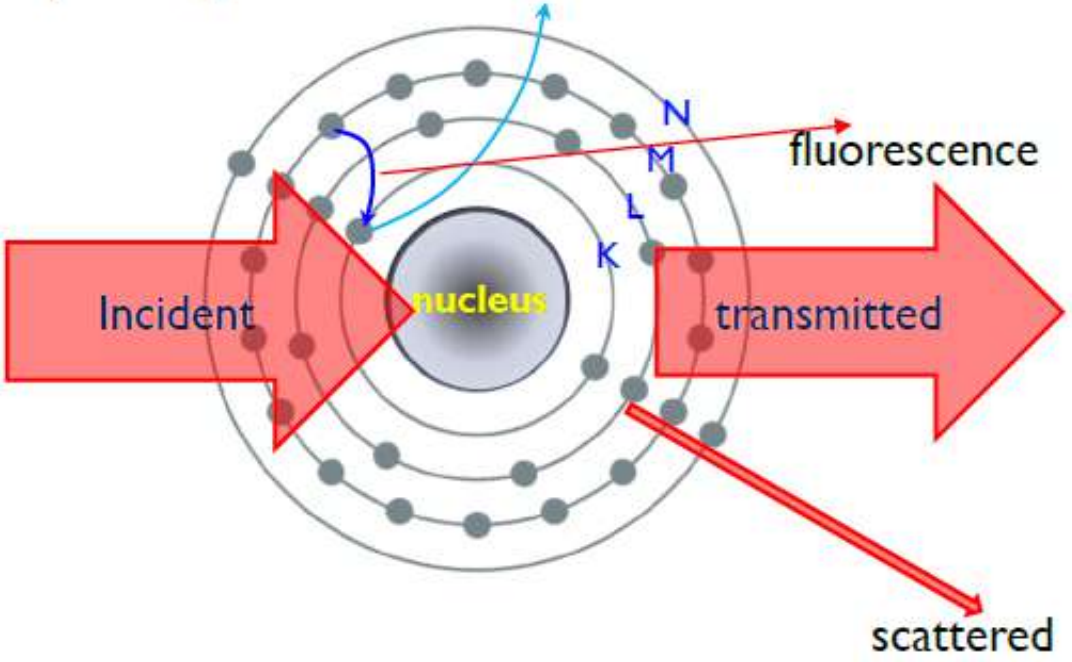

- Fluorescence X-ray has lower energy or longer wavelength due to energy loss.
- Both Inelastic scattering and fluorescence X-ray only add background to scattering data because they don't interfere with elastically scattering x-ray due to different wavelength!
- However, stay away the absorption edges when choose X-ray radiation energy for scattering to avoid problematic fluorescence X-ray background.

X-ray measures distance/structure by interference

- Interference in pond:

  Interference pattern of water waves codes distance between sources

- Elastic scattering Interference:

  Elastic X-ray scattering interferes.

  Before hit the scatterers, the X-ray plane waves travel with same phase (in phase). When hit the scatterers, X-ray waves are scattered. When two scattered X-ray waves arrive at a detector pixel with same phase (they are in phase), they enhance each other (constructive interference). If they arrive a pixel with opposite phases (out of phase), they cancel each other (deconstructive interference). The interference pattern on detector encodes the distances among scatterers.

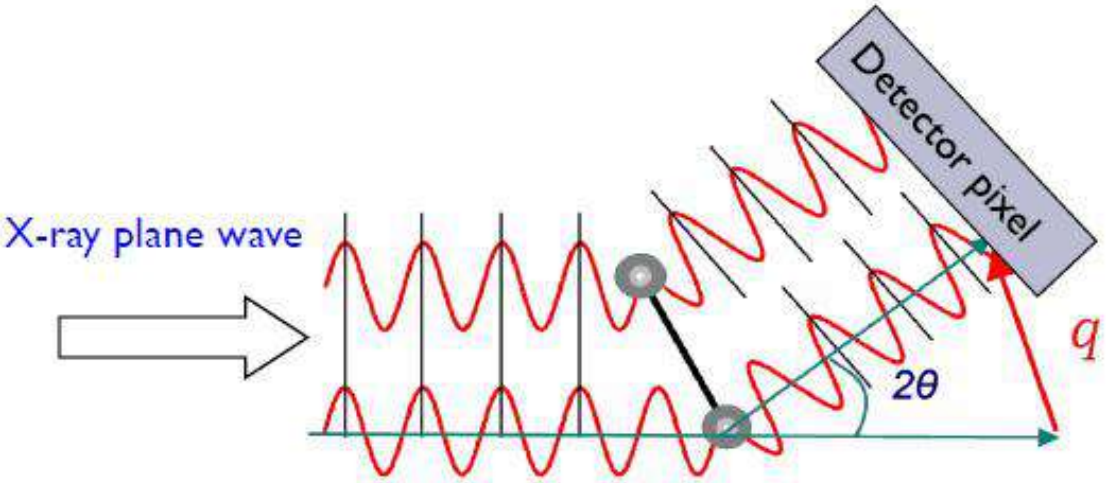

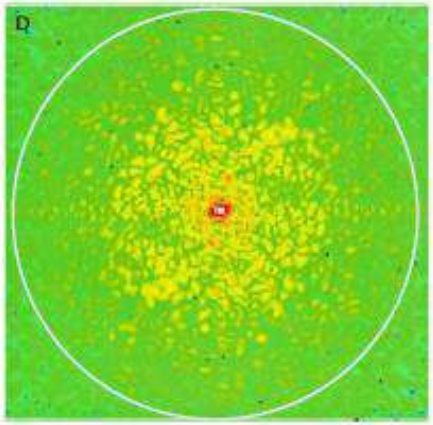

X-ray wave Interference pattern

X-ray scattering

Geometrical apporach

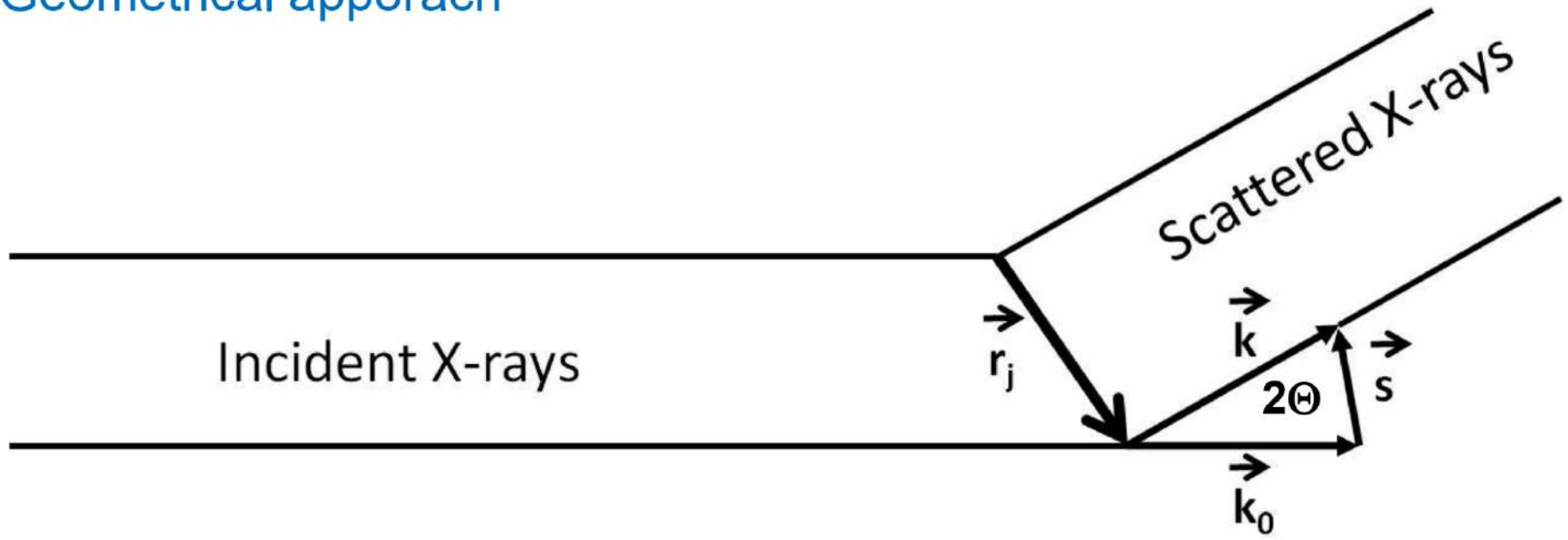

Scattering vector $\vec{s} = (\vec{k} - \vec{k}_0)$

Scattering angle 2Θ

X-ray scattering

Scattering from a single electron

For a single scattering process the amplitude $\boldsymbol{A_j}$ of scattered X-ray photons can be described as a plain wave scattered by an ensemble of atoms:

$$A_j = b_j \, e^{-i\frac{2\pi}{\lambda}\left(\vec{k}_0 - \vec{k}\right)\cdot\vec{r}}$$

With b_j is the scattering cross section, the r_j describes the inner distance vector and the vector k_0 is the wave vektor of the incident wave.

X-ray scattering

Scattering from an ensemble

Within an particle, the scattering amplitudes of all atoms have to be summed up:

$$A\left(\vec{k}\right) = \sum_j b_j \, e^{-i\frac{2\pi}{\lambda}\left(\vec{k}_0 - \vec{k}\right)\cdot\vec{r}_j}$$

Or, using $\vec{s} = (\vec{k} - \vec{k}_0)$ as **scattering vector**

$$A\left(\vec{s}\right) = \sum_j b_j \, e^{-i\frac{2\pi}{\lambda}\vec{s}\cdot\vec{r}_j}$$

Problema de las fases

Instrumentalmente solo se puede medir cantidad de fotones. Es decir intensidad dispersada. La intensidad se relaciona con el cuadrado de la amplitud de la onda. Es decir se pierde la fase.

$$\Psi = A.\exp(i\phi)$$ Descripción genérica de una onda

$$I = \Psi.\Psi^* = A.\exp(i\phi).A.\exp(-i\phi) = A^2$$

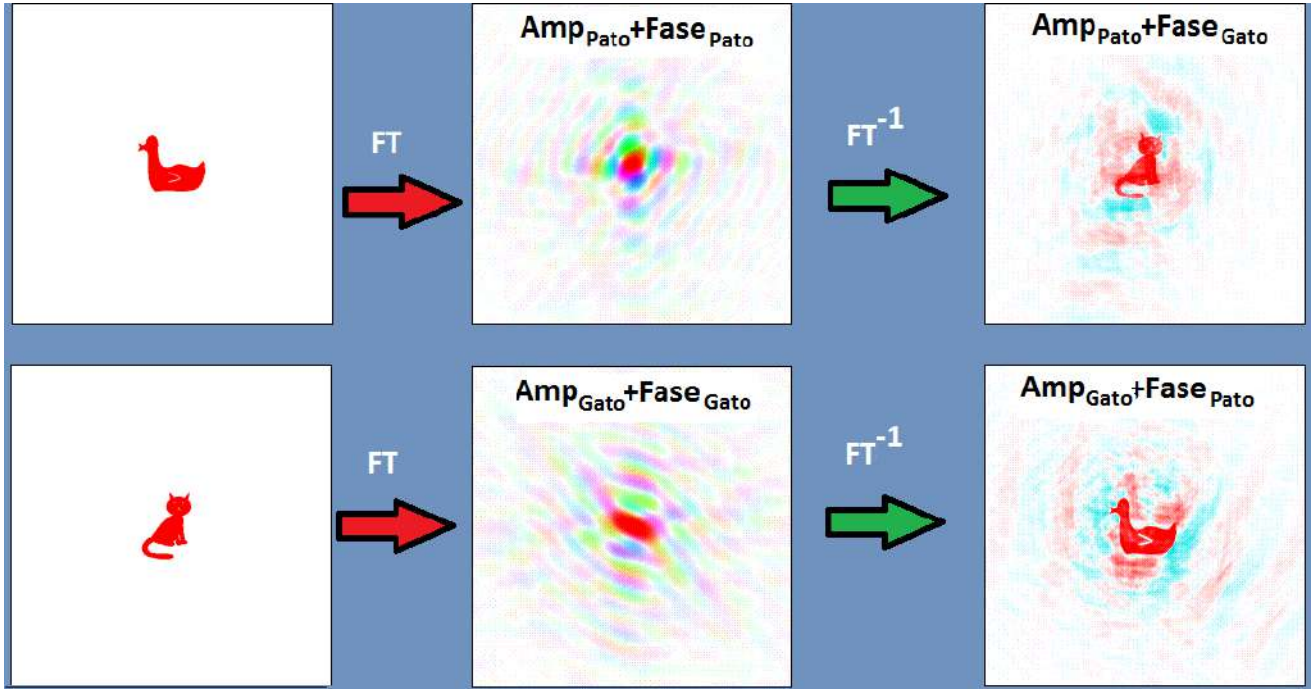

PROBLEMA: Como se observa en el ejemplo la fase contiene la mayoría de la información.

En consecuencia los resultados que se obtienen por SAXS no poseen interpretación única. Conocimientos previos de la muestra son necesarios.

X-ray scattering

Scattering intensity

The scattering amplitude is experimentally not accessible, but the scattering intensity. The intensity is the product of the scattering amplitude with ist complex conjugate and results to:

$$AA^* = I(\vec{s}) = \sum_j \sum_k b_j \, b_k \, e^{\vec{s} \cdot \vec{r}_{jk}}$$

With the vector r_{jk} as inner distance vector, pointing from the j^{th} scatting center to the k^{th} scattering center.
The b_j are the atomic scattering densities. They depend on the number of electrons of the atom and the heavier an atom the higher is b_j.

X-ray scattering

Atomic scattering factors

The atomic scattering factor is the Fourier Transform of the atomic electron density.

It can be calculated by quantum mechanics and can be found at International Tables of Crystallography, Volume C

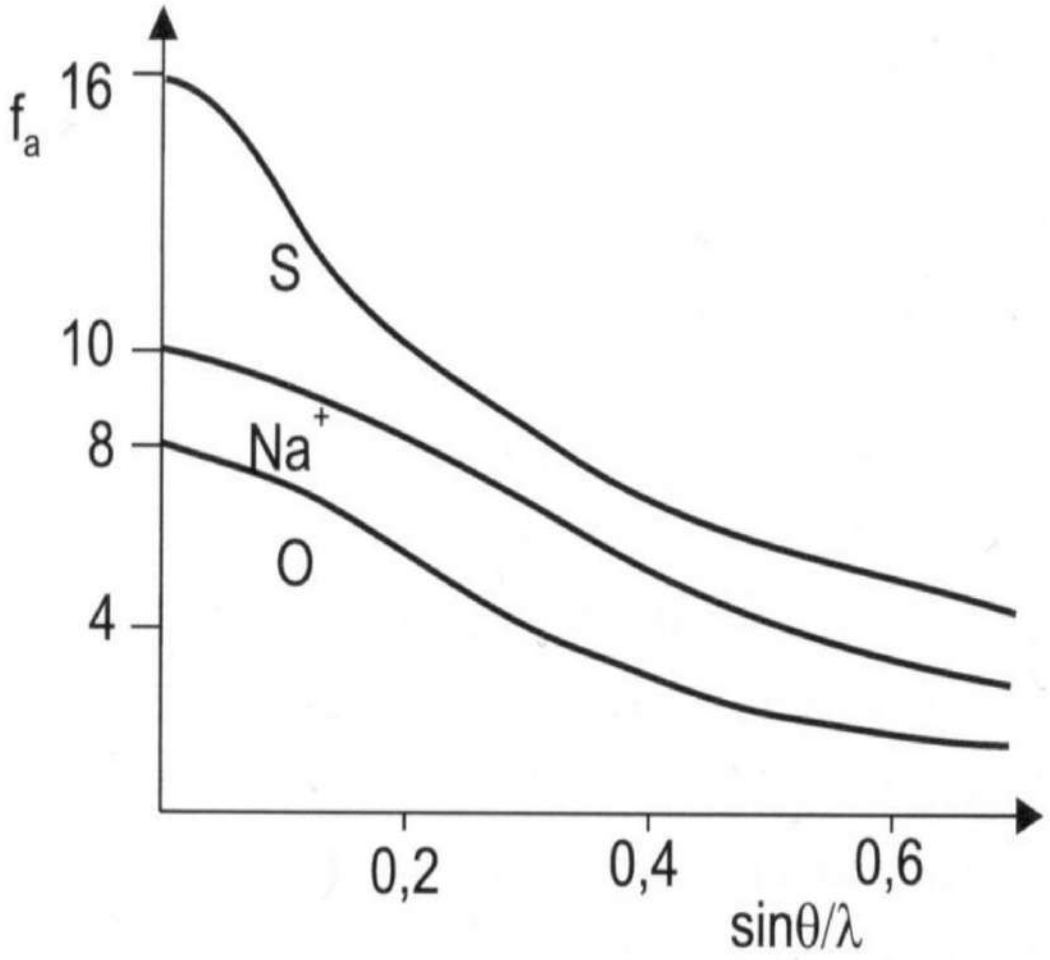

X-ray scattering

Electron density

As seen on the atomic scattering factors, the scattering density of the depends not only on the number of electrons, but as well on the distribution of these electrons around the atom.

This electron density ρ can be defind as follows:

$$b_j = \rho_j \, dV_j$$

With the dV_j as the volume element surrounding the scattering center.

The reconstitution of the electron density $\rho(r)$ and its distribution in the particle is the aim of every X-ray scattering or diffraction experiment.

X-ray scattering

Electron density

The effective scattering density depends on the electron density of the surrounding of the atom.
A net electron density can be defined by subtracting the electron density of the enironment ρ_S:

$$\Delta\rho(\vec{r}) = \rho(\vec{r}) - \rho_S$$

The average value of the excess density is called contrast, which is typically very small for biological objects containing light atoms only.

Solution X-ray scattering measures the contrast / electron density difference

In vacuum, x-ray scattering directly measures Z number.

Solution sample scattering:

$$I_{molecule} = I_{solution} - I_{solvent}$$

What X-ray scattering measures:

$$\Delta\rho(\vec{r}) = \rho_m(\vec{r}) - \rho_s(\vec{r})$$

excess electron density/scattering length against solvent/buffer

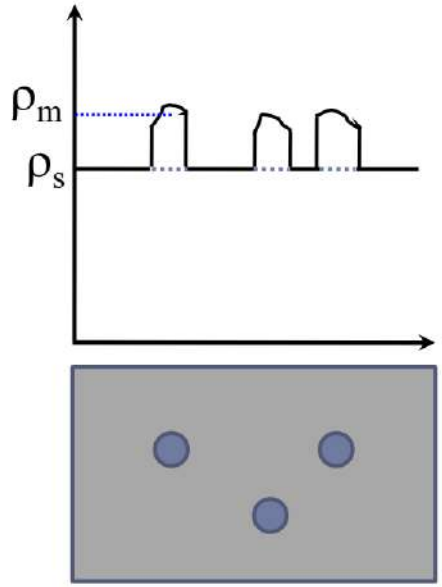

In vacuum: $A(\vec{r}) = \rho_m(\vec{r})e^{i\vec{q}\bullet\vec{r}}$

In solution: $A(\vec{r}) = \Delta\rho(\vec{r})e^{i\vec{q}\bullet\vec{r}}$

Solution X-ray scattering contrast matching:

Increasing solvent electron density, X-ray scattering contrast match occurs at average spatial scale [I(q~0) → 0], but electron density difference still exist locally / at high spatial resolution scale.

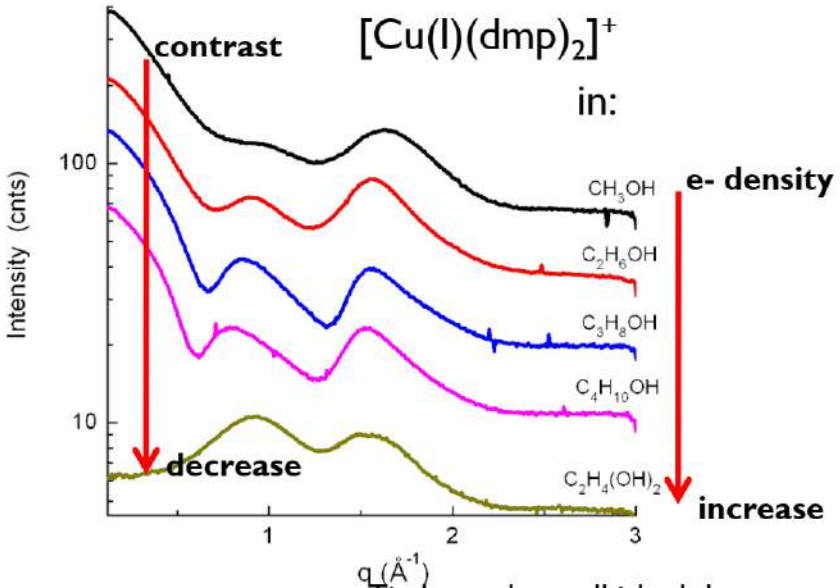

X-ray scattering

Scattering from dilute samples

In the ideal dilute solutions the scattering intensity from the entire sample will be isotropic and proportional to the scattering from the single particle averaged over all orientations Ω.

Averaging of the term $\left\langle e^{\vec{s}\cdot\vec{r}_{jk}} \right\rangle_{\Omega} = \frac{\sin sr_{jk}}{sr_{jk}}$ lead to:

$$I(s) = \sum_j \sum_k \rho(r_j)\rho(r_k)\frac{\sin sr_{jk}}{sr_{jk}}$$

X-ray scattering

Scattering from dilute samples

The vectors s and r are now reduced to their absolut value, which lead to a significant loss of information in the SAXS pattern compared to e.g. crystallographic data

$$I(s) = \int_0^\infty p(r) \frac{\sin sr}{sr} \, dr \qquad s = |\vec{s}| = \frac{2\pi}{\lambda} \sin 2\Theta$$

Debye 1915

The p(r) function is called the pair distance distribution function.

The I(s) is the Fourier-Transform of the p(r) function.

X-ray scattering

Pair distance distribution function p(r)

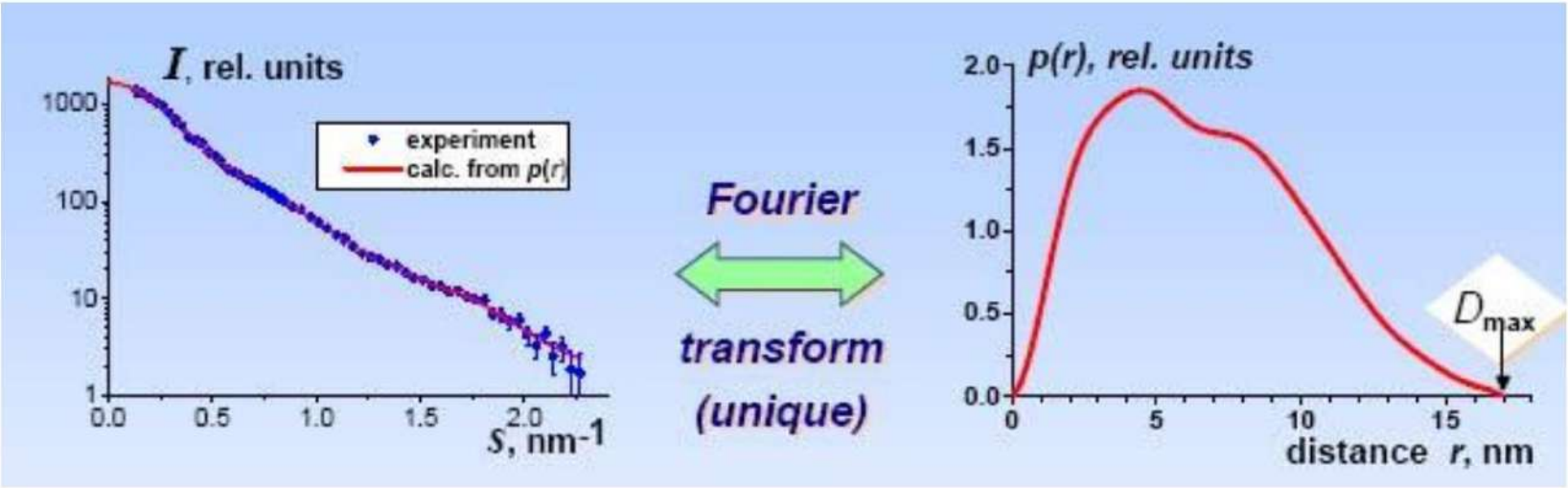

$$I(s)=4\pi\int_{r=0}^{\infty}p(r)\frac{\sin(sr)}{sr}dr \qquad p(r)=\frac{1}{2\pi^2}\int_{s=0}^{\infty}s^2 I(s)\frac{\sin(sr)}{sr}ds$$

Distance distribution function

"**how often which distance**" appears in the particle

From crystal and fiber diffraction to solution scattering

Interference patterns of objects vary along with the samples' nature, including the symmetry of matrix of molecules embedded and the freedom of molecules in the matrix.

	Single Crystal	Fiber/ Membrane	Powder/ Micro-crystals	Solution
Sample states		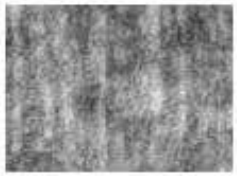		
Interference pattern	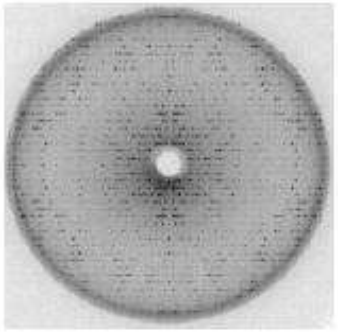	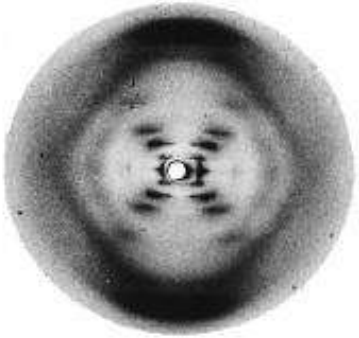	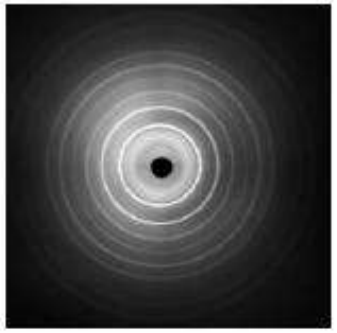	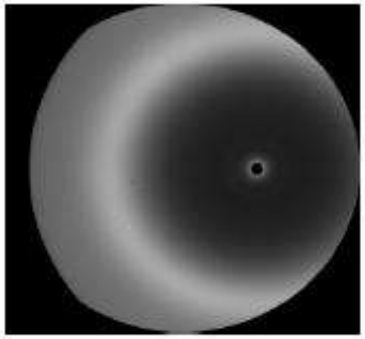
matrix symmetry and molecular freedom	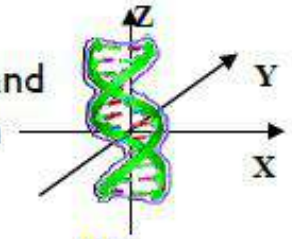	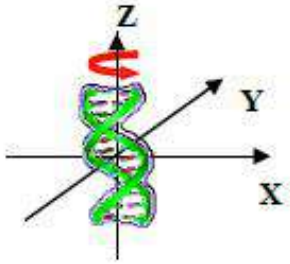	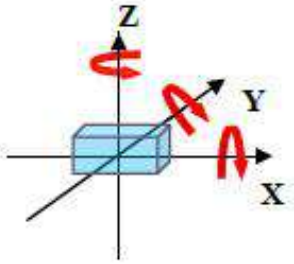	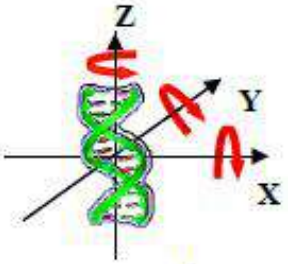

Matrix symmetry: high ← low

Molecular freedom: low → high

¿Qué podemos medir con SAXS?

SAXS es una técnica **no destructiva** que se emplea para caracterizar diversos sistemas condensados

Sistemas líquidos – dispersiones líquidas

Proteínas en solución

Coloides inorgánicos

Nano-emulsiones

Polímeros

micelas

Sistemas semisólidos-sólidos

Materiales en polvo

Polímeros

Geles

Grasas/ceras

Superficies

films

polímeros

Interfases líquidas

¿Qué podemos obtener de un experimento SAXS?

Información estructural

Sistemas diluidos:
- Forma y tamaño (distribución de tamaño)
-Volumen de objetos dispersores
-Área
- Masa molecular

Sistemas concentrados:
-Estructuras periódicas largo alcance
- Arreglos supra moleculares
- distancia entre dispersores
- etc

Fibras

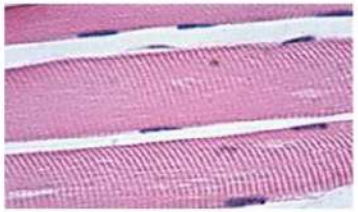

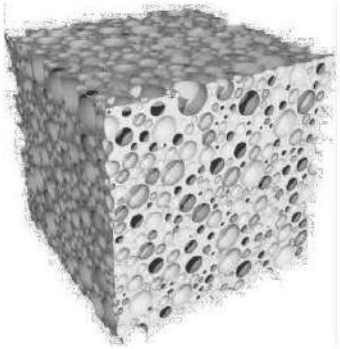

Material poroso

Coloides

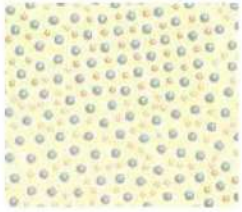

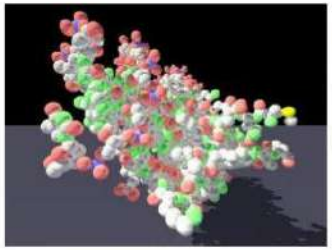

Proteínas en solución

Morfología de polímeros

Small Angle X-Ray Scattering

Muestras monodispersas

Sistemas diluidos

Factor de forma: transformada de Fourier del objeto

En caso de muestras isotrópicas:

$$I(q) = 4\pi \int p(r) \frac{sen(qr)}{qr} dr \qquad I(q) = NP(q)$$

p(r) función de distribución de a pares y P(q) es una función llamada factor de forma.
P(q) <-> p(r) mediante una transformada de Fourier.

Sistemas concentrados

$$I(q) = NP(q)S(q)$$

Aparece una nueva función llamada factor de estructura. S(q)

S(q): Fenómenos de interferencia

Existen pocos factores de estructura analíticos.

form factor for sphere

The form factors of some objects with simple shapes have analytical formula expression, for example, sphere. Sphere is a widely used model in characterizing the size or size distribution of globular particles in structural biology and nanoscale material science.

Sphere with homogenous electron density and radius R:

$$F(q) = \frac{3(\sin(qR) - qR\cos(qR))}{(qR)^3}$$

$$I(q) = F^2(q) = \left(\frac{3(\sin(qR) - qR\cos(qR))}{(qR)^3} \right)^2$$

From the scattering curve, we can estimate the radius of the sphere:

$$R \approx \frac{4.493}{q_{01}}$$

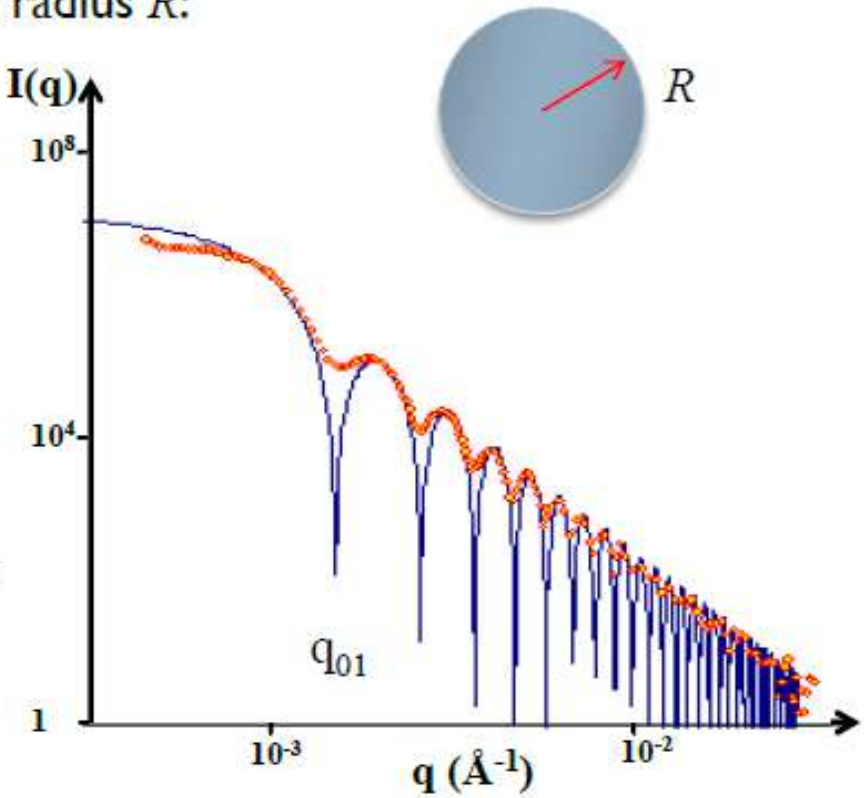

- Scattering profile of silica spheres (red) and simulation based on perfect sphere (blue)
- Discrepancy of silica scattering from sphere model due to size polydispersity, imperfect spherical shape, etc.

SAXS: figuras geométricas homogéneas

$$A(q,R) = \frac{\sin(qR) - qR\cos(qR)}{(qR)^3}$$

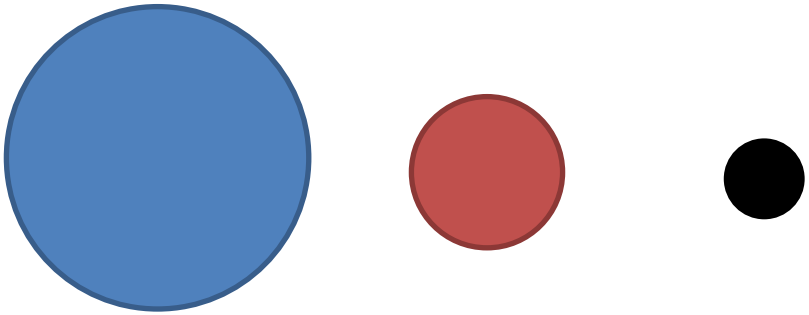

El objeto más sencillo de representar es una esfera homogenea. La amplitud es una función analítica.

Un incremento en el radio de la esfera desplaza el patrón la dispersión a ángulos menores.

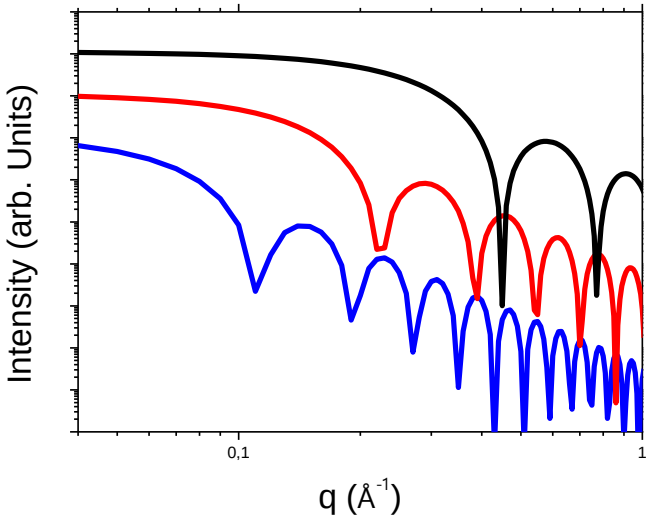

SAXS: figuras geométricas homogéneas

Intensidad relativa de SAXS para diversas figuras geométricas.

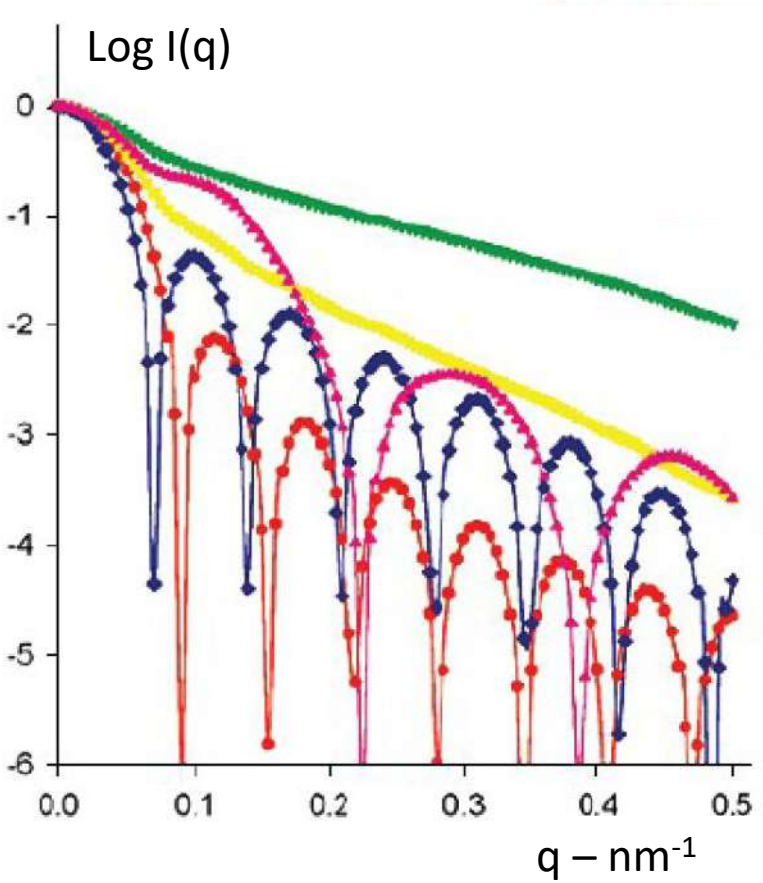

Esfera sólida

Esfera hueca

"Pesas"

Discos planos

Cilindros

SAXS: Efecto de polidispersidad de tamaños

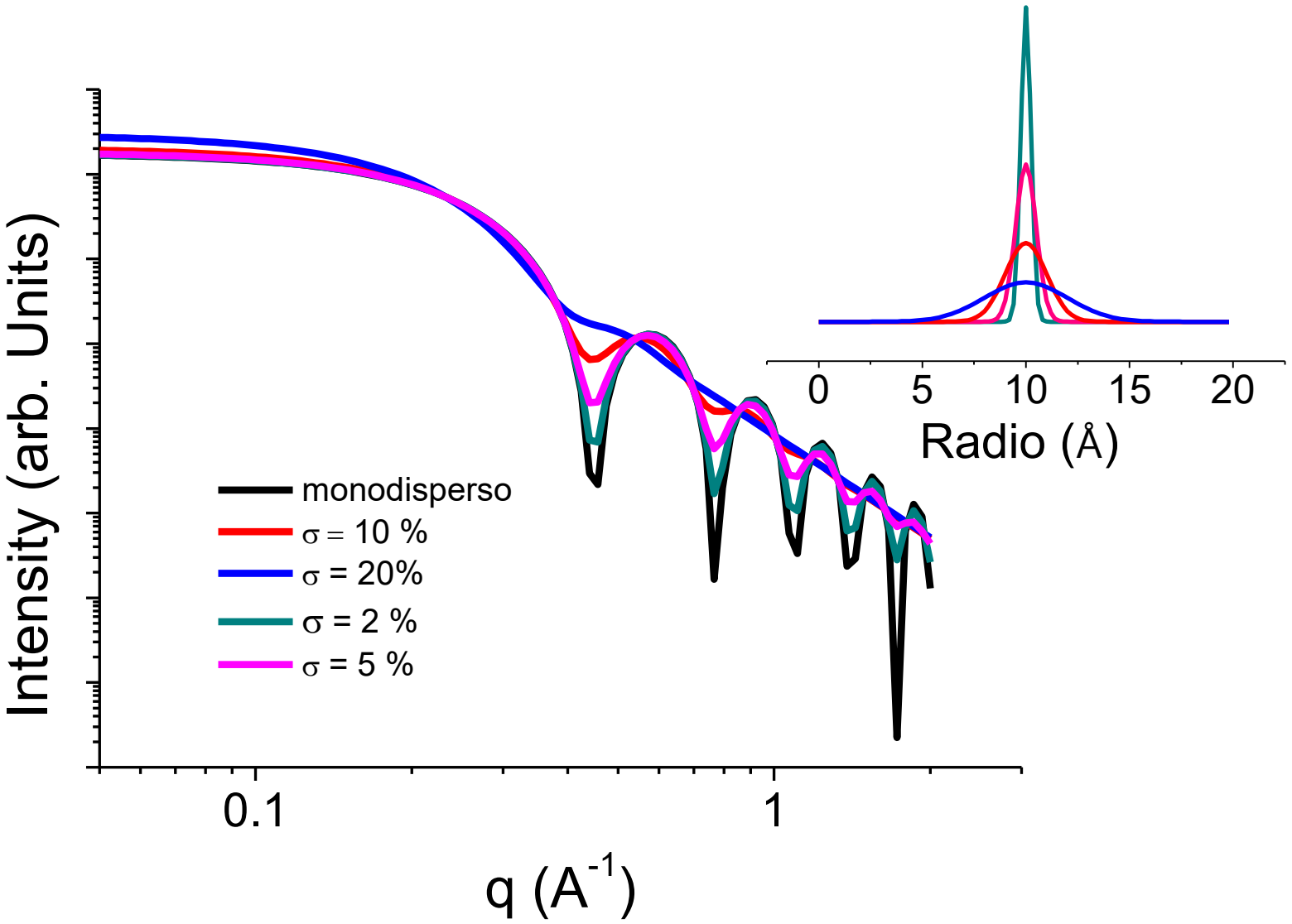

¿Es una figura homogénea una buena representación de una nanopartícula?

$$P_{cubo} = \frac{2}{\pi}\int_0^{\pi/2}\int_0^{\pi/2}\left[\frac{\sin(q.a/2.\sin\alpha\cos\beta)}{q.a/2.\sin\alpha\cos\beta}\frac{\sin(q.a/2.\sin\alpha\sin\beta)}{q.a/2.\sin\alpha\sin\beta}\frac{\sin(q.a/2.\cos\alpha)}{q.a/2.\cos\alpha}\right]^2 \sin\alpha.d\alpha d\beta$$

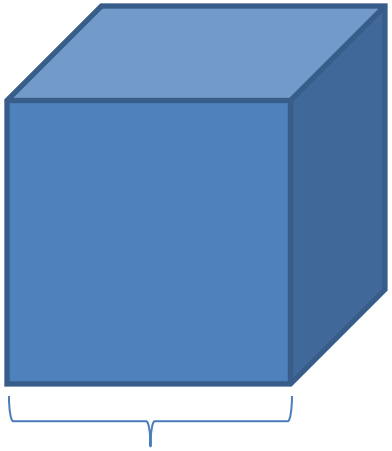

a= 4 nm

Las partículas, coloides, proteínas, están compuestos por átomos (sistemas discretos). Los modelos de dispersión calculados anteriormente exhiben los patrones de dispersión para figuras geométricas homogéneas (continuo).

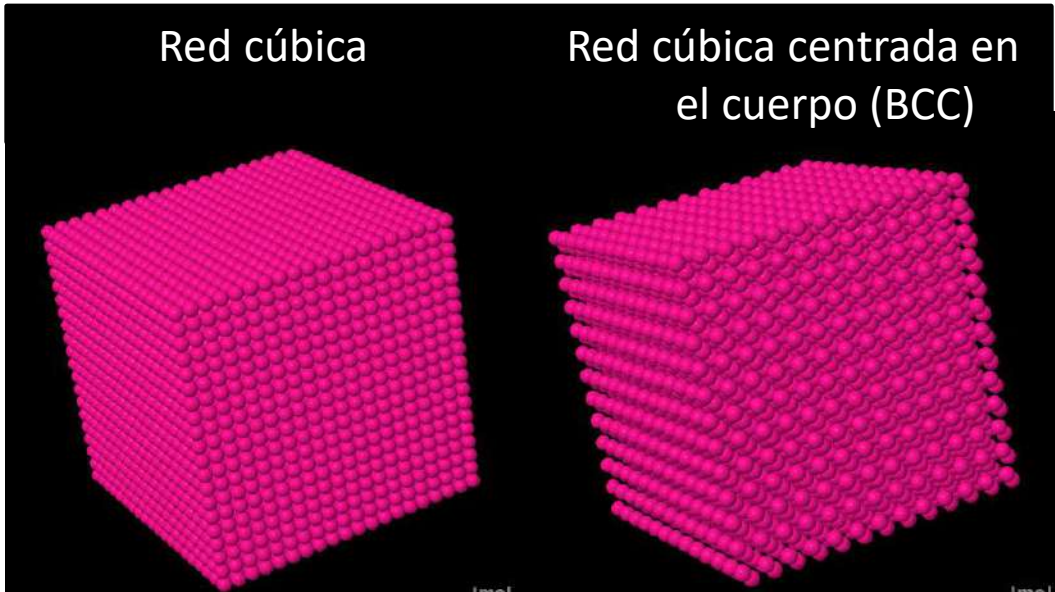

Se proponen dos cubos (a=b=c) de similar tamaño con motivos diferentes de partículas esféricas (¿átomos?)

¿Es una figura homogénea una buena representación de una nanopartícula?

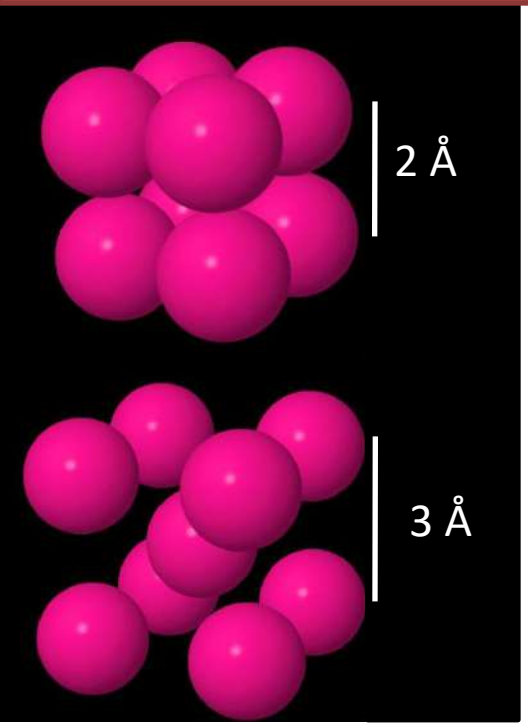

Se simularon partículas nanométricas cúbicas compuestas por esferas de 1 Å de radio cada una.

Hay que tener en cuenta que la simetría en cada caso es diferente, pero sobre todo la distancia entre unidades esféricas.

Los patrones de dispersión son similares en ambos casos y el cubo homogéneo ajusta perfectamente las curvas.

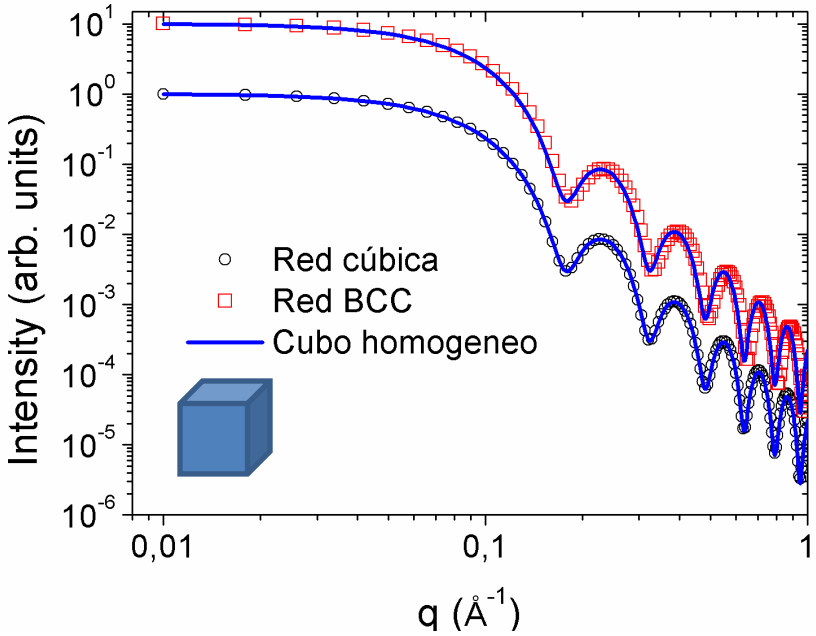

¿Es una figura homogénea una buena representación de una nanopartícula?

En un experimento de dispersión de rayos X a bajos ángulos se analizan las frecuencias espaciales bajas (q->0). Para poder estimar las diferencias entre las nanopartículas habría que estudiar la intensidad registrada a ángulos altos (experimento de difracción).

Conclusión:
En un experimento de dispersión se analiza la densidad electrónica media!

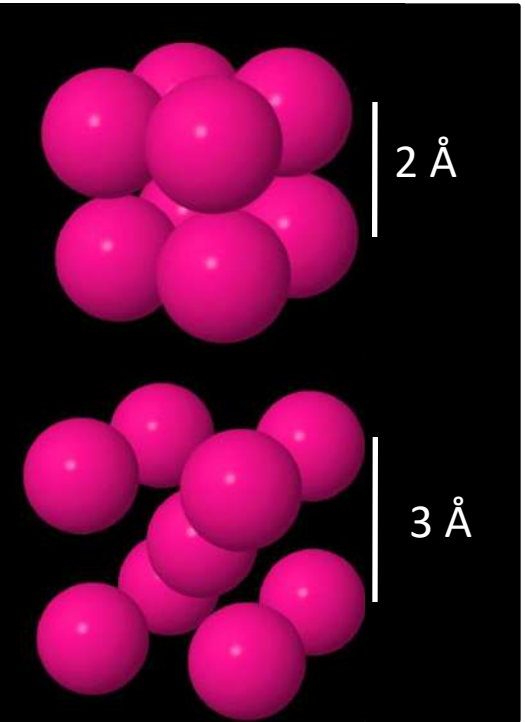

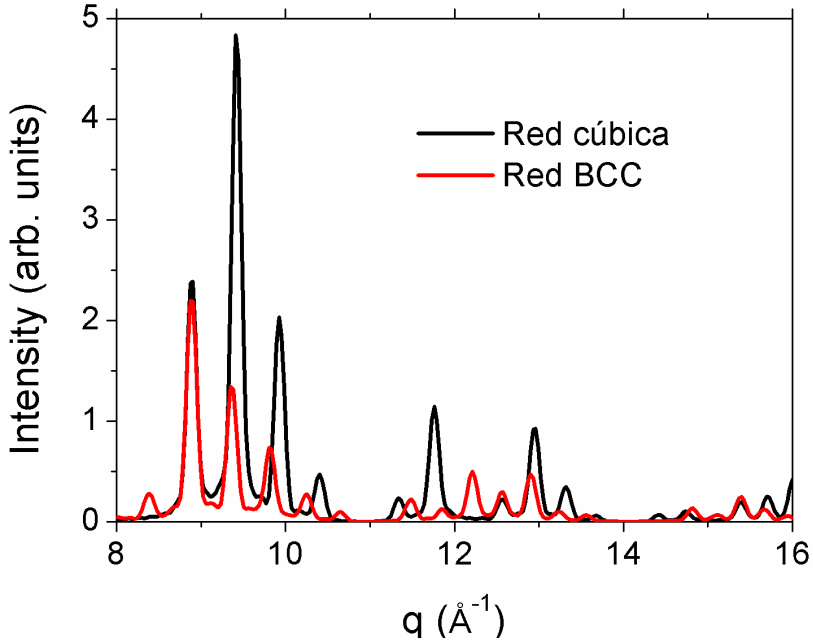

Estrategias de análisis: Invariantes

Primer análisis sobre curvas SAXS

$$Q = \frac{1}{V}\int_0^\infty q^2 I(q)dq = 2\pi^2\phi_1\phi_2(\Delta\rho)^2$$

Fracción de volumen

Constraste

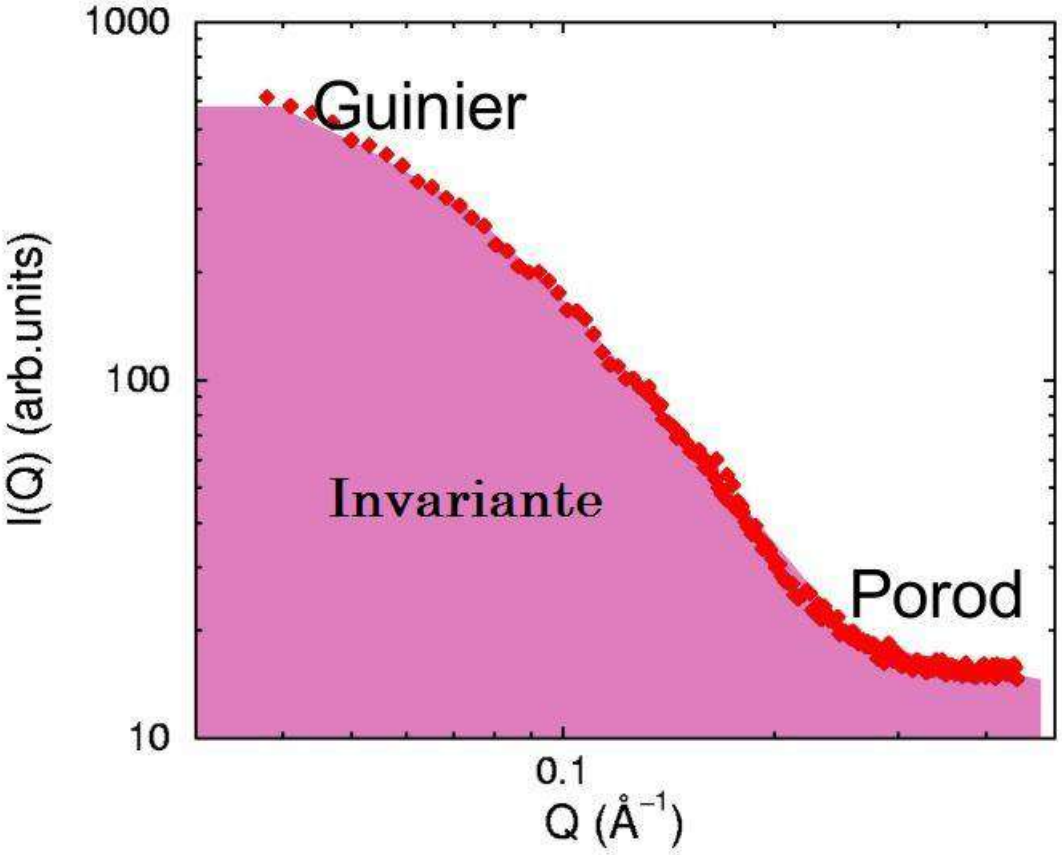

Estrategias de análisis: Invariantes

X-ray scattering

Radius of gyration – Guinier plot

Expanding the sin-function in the scattering intensity I(s) in a series

$$\left(\frac{\sin sr}{sr} = 1 - \frac{s^2r^2}{6} + \frac{s^4r^4}{120} - \cdots\right)$$

, the Debye-Function can be expressed as

$$I(s) \cong \int_0^\infty p(r)\left(1 - \frac{s^2r^2}{6} + \cdots\right)dr = \int_0^\infty p(r)\,dr - \frac{s^2}{6}\int_0^\infty p(r)\,r^2dr + \cdots$$

Estrategias de análisis: Invariantes

X-ray scattering

Radius of gyration – Guinier plot

The second moment of the distance distribution function p(r) is given by:

$$\int_0^\infty p(r)\, r^2\, dr$$

and the radius of gyration Rg can be introduced in analogy with classical mechanics:

$$Rg^2 = \frac{1}{2} \frac{\int_0^\infty p(r)\, r^2\, dr}{\int_0^\infty p(r)\, dr}$$

Estrategias de análisis: Invariantes

X-ray scattering

Radius of gyration – Guinier plot

Putting the things together one gets:

$$I(s) \cong \int_0^\infty p(r)\left(1 - \frac{Rg^2}{6}s^2 + \cdots\right)dr$$

And finally the Guinier approximation:

$$I(s) \cong I_0\, e^{-\frac{Rg^2}{3}s^2}$$

Guinier and Fournet 1955

Estrategias de análisis: Invariantes

X-ray scattering

Radius of gyration – Guinier plot

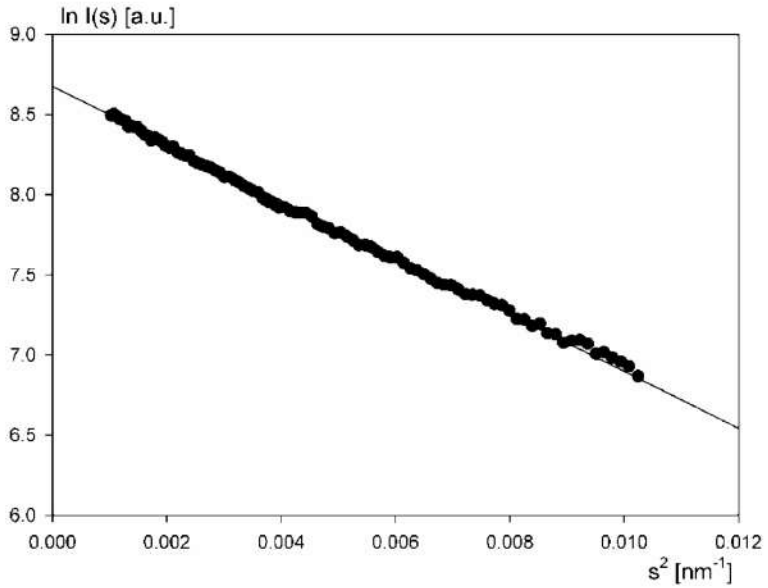

Guinier-Approximation:

- every scattering curve is for sRg < 1.2 a Gauss function
- In the so called Guinier-Plot (ln I versus s^2) the Rg can be calculated from the slope of the plot
- The Rg is directly related to the form and the mass distribution of the particle

$$\ln I(s) = -\frac{Rg^2}{3} s^2 + \ln I_0$$

Estrategias de análisis: Invariantes

The Rg is historically the first structural parameter determined from the SAXS data (Guinier and Fournet 1955), yielding direct information about the particle size and shape.

The value of I_0 is proportional to the squared number of electrons in the particle and to the particle concentration, so that absolute measurements allow one to determine the molecular mass of the solute.

Estrategias de análisis: Invariantes

X-ray scattering

Guinier approximation

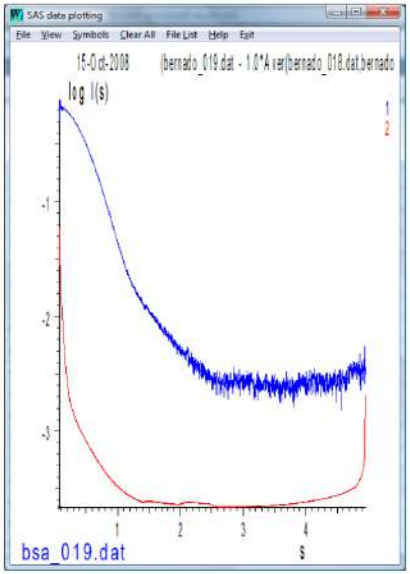

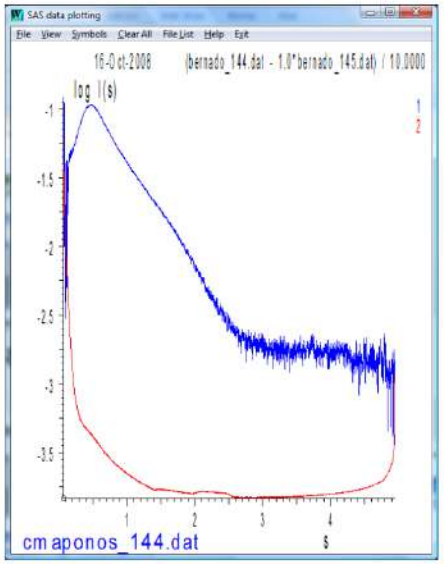

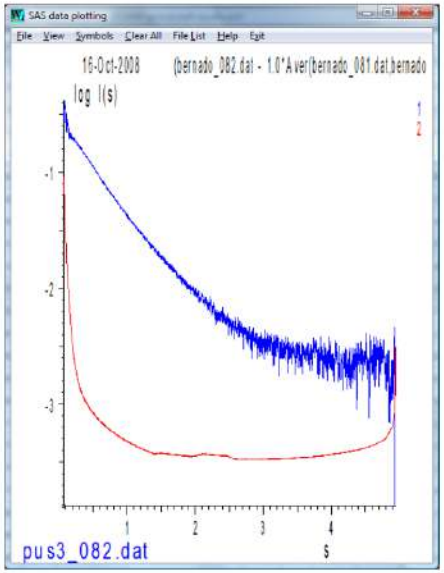

Deviations from the ideal protein solution are easily visible in the Guinier plot!

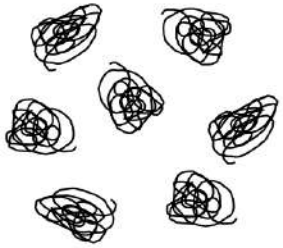

Ideal solution of particles

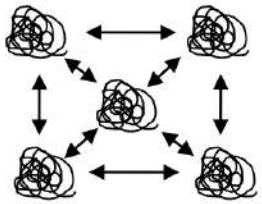

Repulsive particle interactions

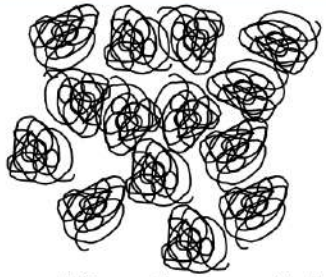

Attractive particle interactions

Estrategias de análisis: Invariantes

X-ray scattering
Kratky plot

Kratky plots ($I(s)\cdot s^2$ versus s) can be used to identify disordered states and distinguish them from globular particles.

The scattering intensity of a globular protein has a Gaussian-like shape at small s and decays approximately as $1/s^4$ at high s yielding a bell-shaped Kratky plot with a well defined maximum.

In the case of an unfolded protein, the Kratky plot also presents a plateau over a specific range of s, which is followed by a monotonic increase.

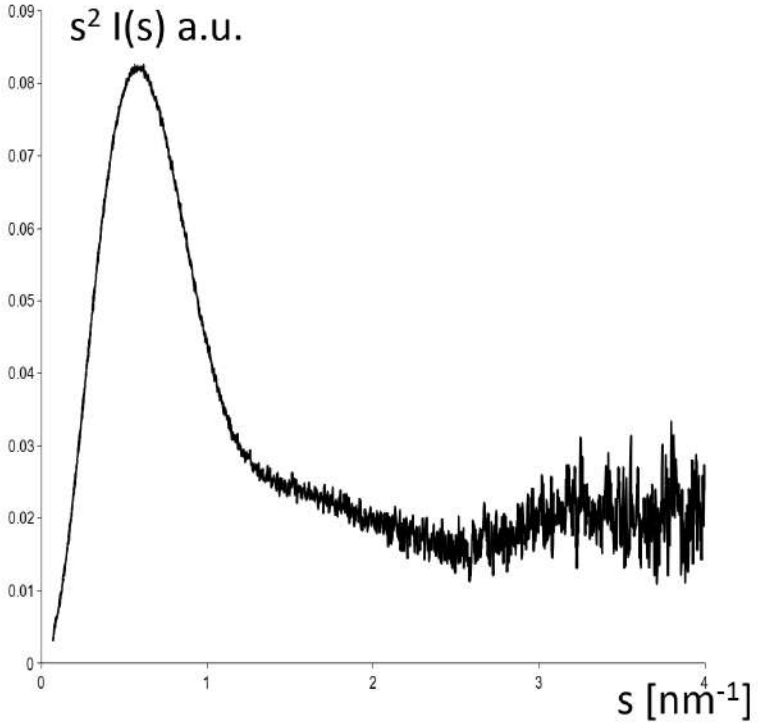

Estrategias de análisis: Invariantes

The Kratky plot is typically used to analyze the conformation of proteins, but can be used to analyze the random walk model of polymers.

A Kratky plot can be made by plotting:

$I(s)*s^2$ versus s.

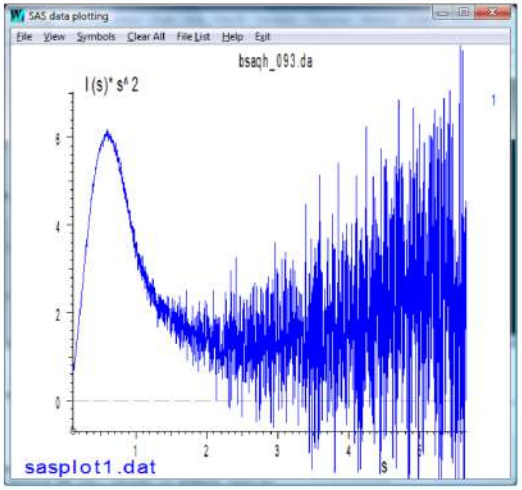

Folded globular protein

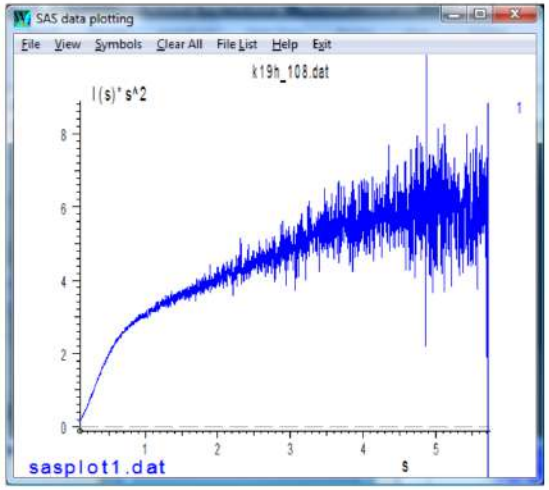

Completely unfolded protein

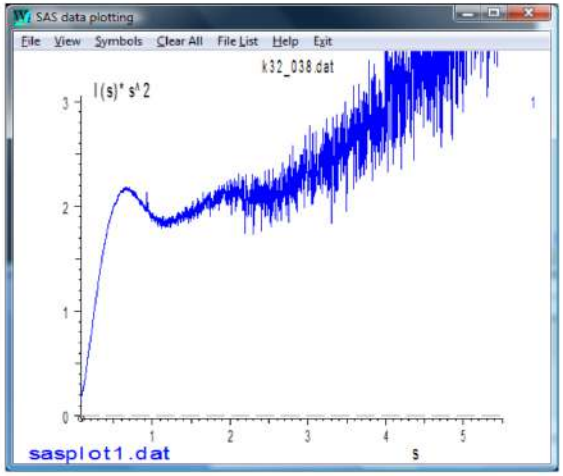

Partially folded protein

Estrategias de análisis: Invariantes

X-ray scattering
Porod invariant

Another important overall value computed from the SAXS data is the so-called Porod invariant Q:

$$\int_0^\infty s^2 I(s)\, ds = Q$$

Porod 1951

Contrary to R_g, the Porod invariant depends only on the particle volume and not on its form.

For the Porod analysis, the behavior of the scattering intensity at higher scattering vectors plays a significant role.

This higher angle part of the *I(s)* corresponds to the small interparticle distances.

Therefore in the high *s* regime the scattering from the internal structure and in particular near the particle surface S is dominating the signal.

Estrategias de análisis: Invariantes

For compact particles, the asymptotic behavior at large *s* is described as

$$I(s) \approx \frac{K}{s^4}$$

introducing K as a constant depended on surface of the scattering particle.

This specific surface value can be estimated directly from the asymptotic behavior of the plot

s^4 I(s) versus s

(Porod plot) at high s.

Estrategias de análisis: Invariantes

Límite de porod

$$q^4 I(q) \xrightarrow[q\to\infty]{} 2\pi(\Delta\rho)^2 V.A$$

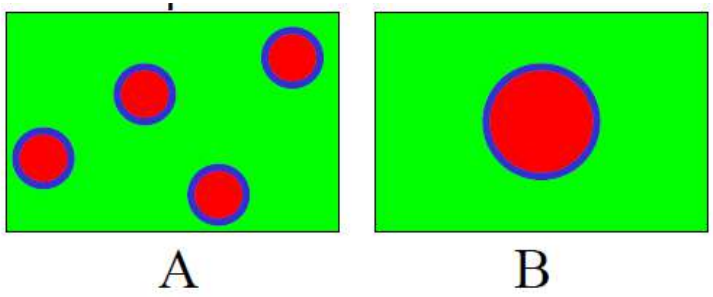

A posee mayor límite de Porod que B

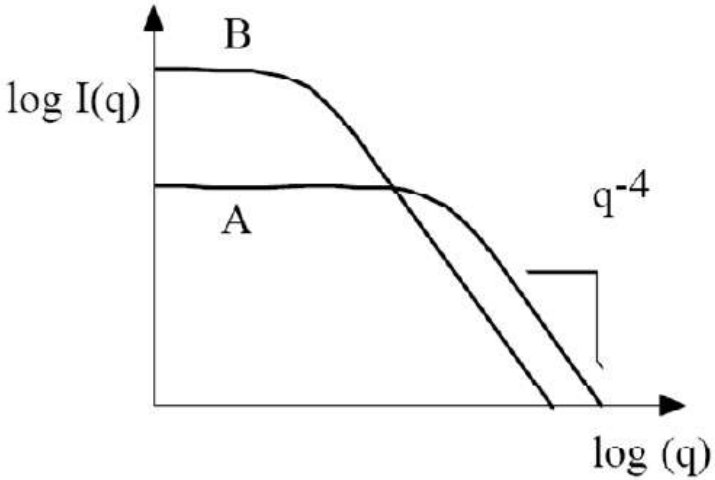

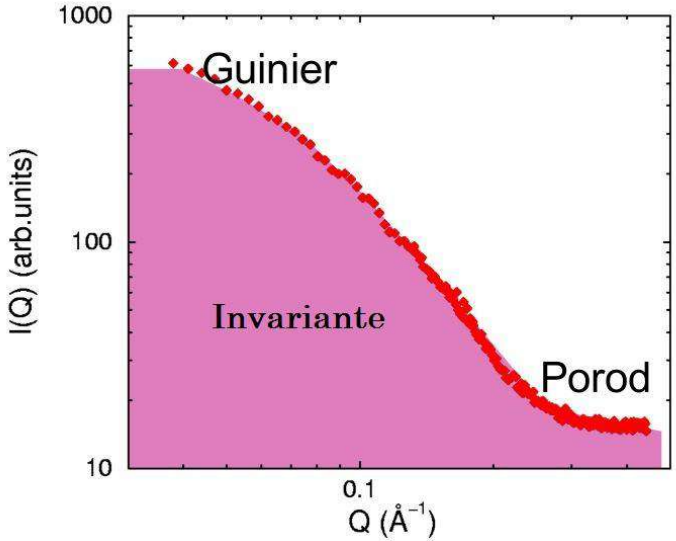

Estrategias de análisis: Invariantes

X-ray scattering

Porod plot

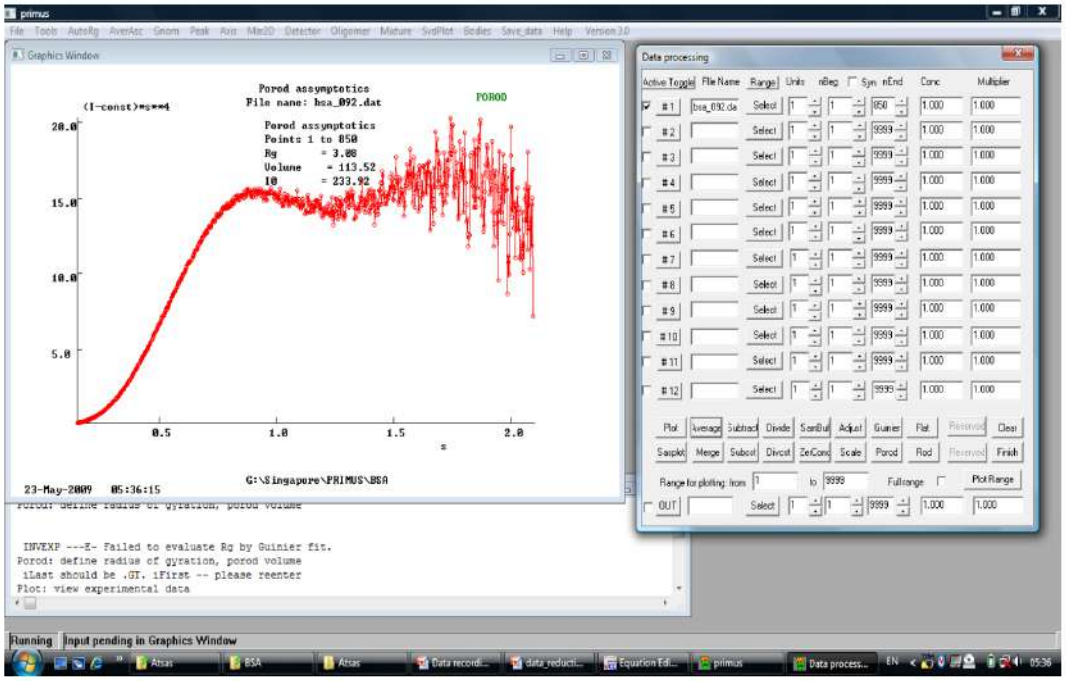

Porod approximation:

$I(s) = K*s^{-4}$

$$\frac{K}{Q} \propto \frac{S}{V}$$

$$Q = \int_{s=0}^{\infty} s^2 I(s)\, ds$$

Q = Porod invariant

$\frac{S}{V}$ shape to volume ratio

Rule of thumb: Porod volume is approximately two times molecular weight

Estrategias de análisis: p(r)

p(r)

- Distribution of distances of atoms from centroid
- Autocorrelation function of the electron density
- 1-D: Only distance, not direction
  - No phase information
  - Can be determined unambiguously from SAXS pattern if collected over wide enough range
  - 20:1 ratio qmin :qmax usually ok

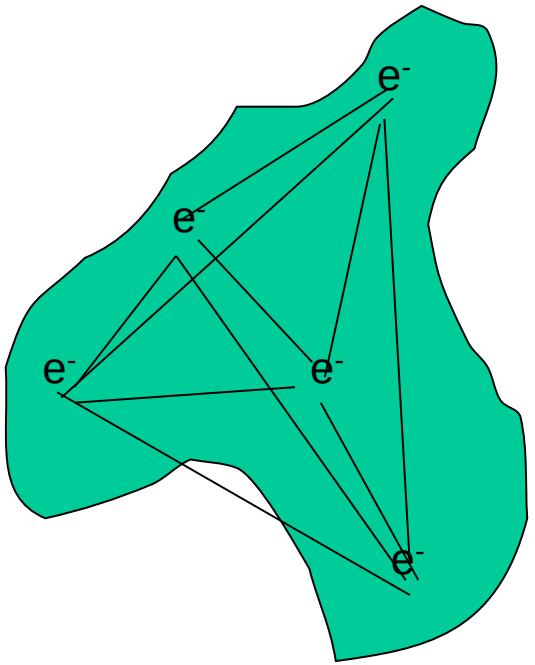

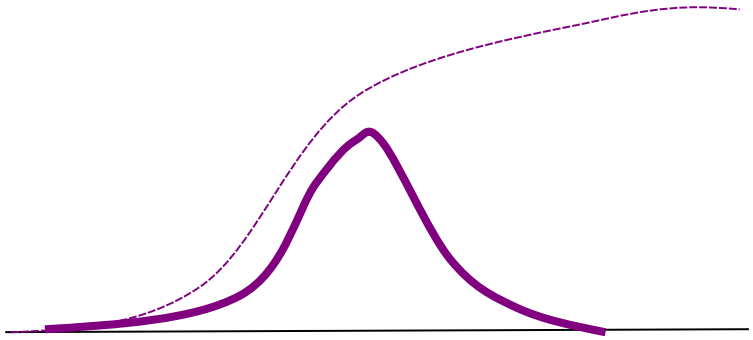

P(r) & Intensity related by Fourier transform pair*

$$I(\vec{q}) = 4\mathrm{p} \int_0^{¥} p(r) \frac{sin(q.r)}{q.r} .dr$$

$$p(r) = \frac{1}{2\mathrm{p}^2} \int_0^{¥} I(q) \, .qr.sin(qr).dq$$

* This is a fourier sine transform because of symmetry (see Glatter & Kratky)

Estrategias de análisis: p(r)

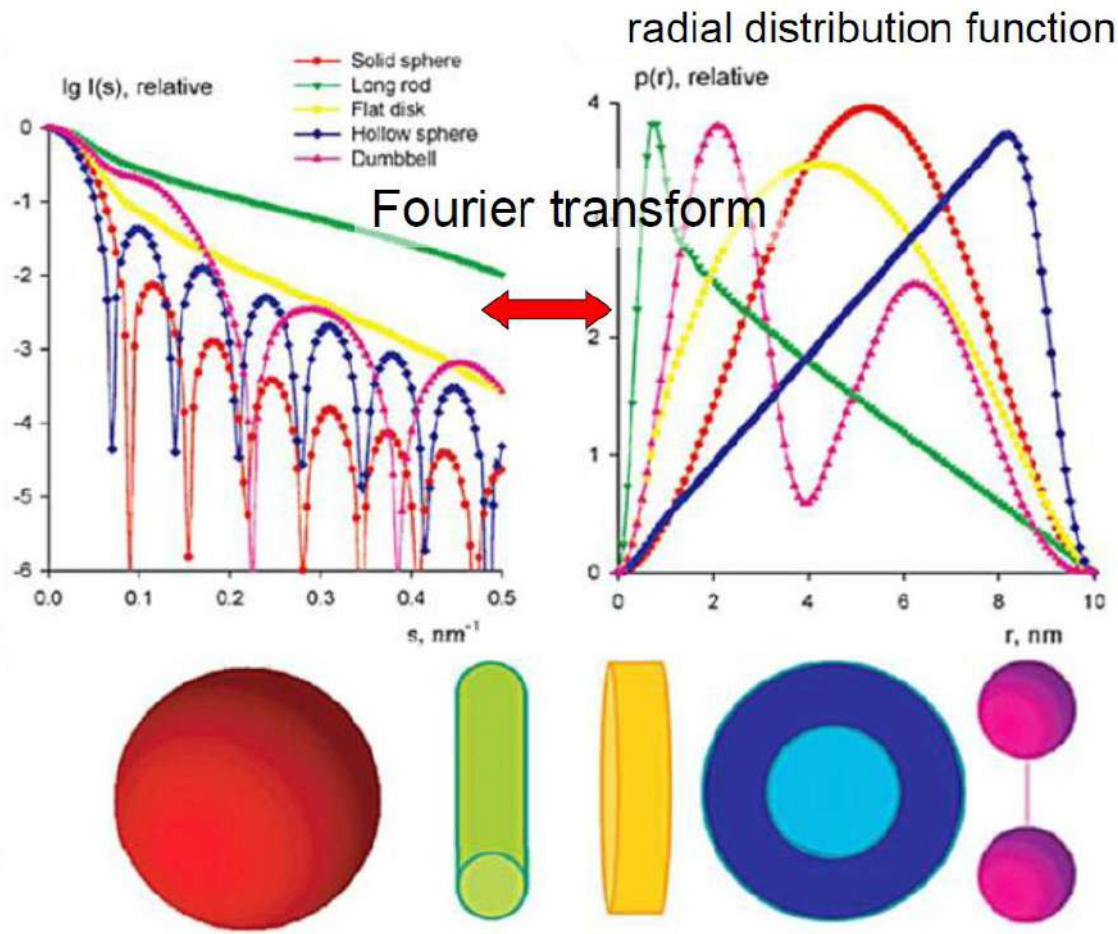

Se invierte la ecuación:

$$I(q) = 4\pi \int p(r) \frac{sen(qr)}{qr} dr$$

El fin es obtener la función de distribución radial p(R)

Estrategias de análisis: p(r)

Ab initio program DAMMIN

Using simulated annealing, finds a compact dummy atoms configuration X that fits the scattering data by minimizing

$$f(X) = \chi^2[I_{\exp}(s), I(s, X)] + \alpha P(X)$$

where χ is the discrepancy between the experimental and calculated curves, *P(X)* is the penalty to ensure compactness and connectivity, $\alpha > 0$ its weight.

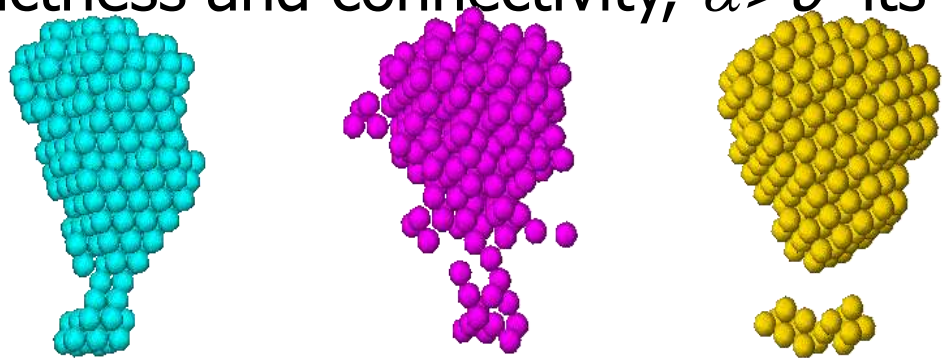

compact

loose

disconnected

Estrategias de análisis: p(r)

Local and global search

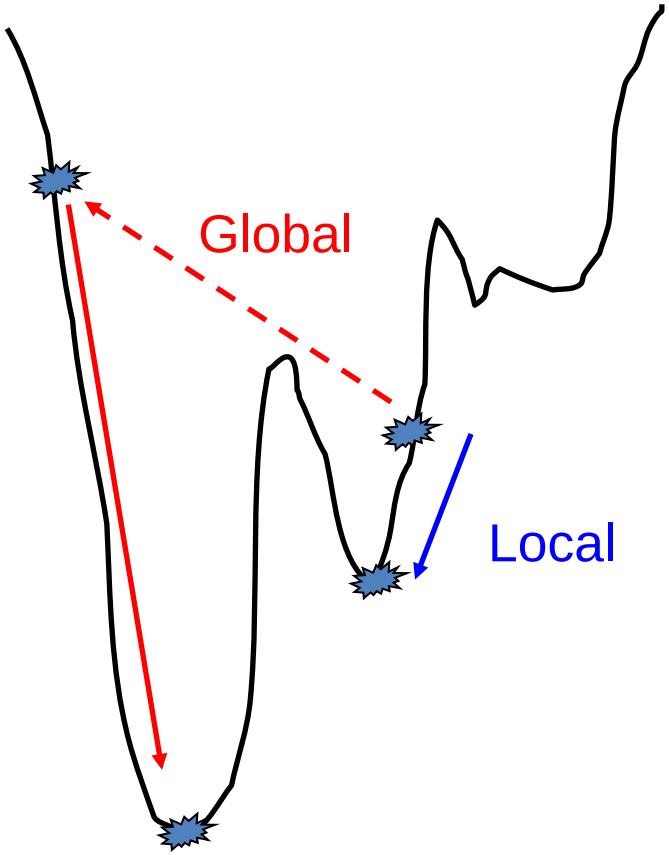

- Local search always goes to a better point and can thus be trapped in a local minimum
- To avoid local minima, global search must be able go to a worse point

Estrategias de análisis: p(r)

S1 shape reconstruction

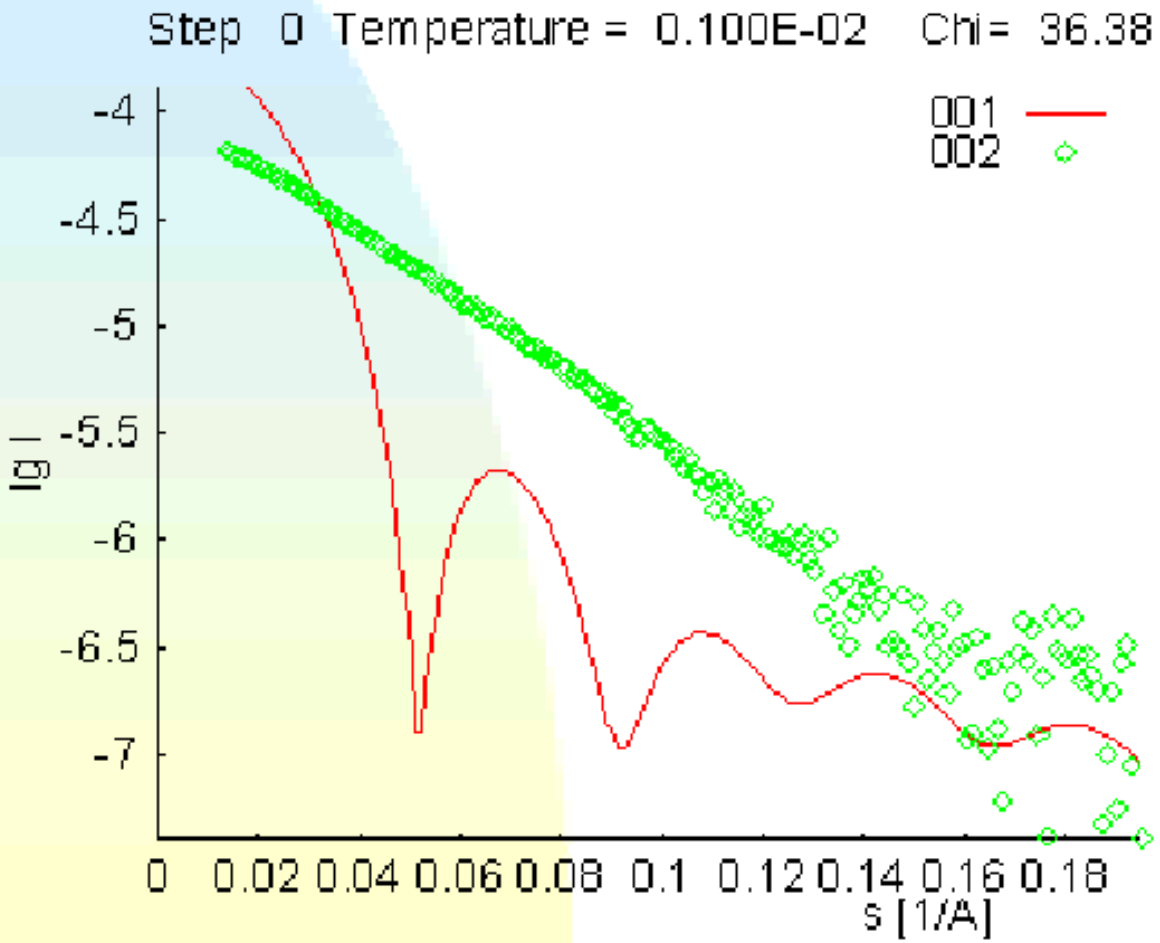

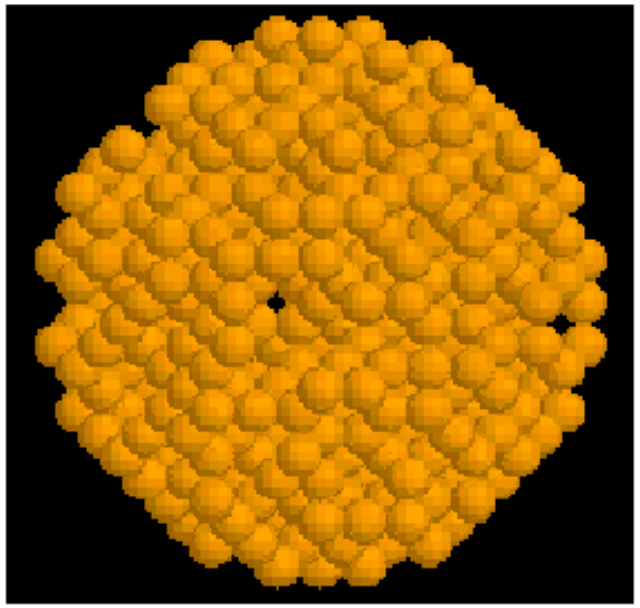

Estrategias de análisis: Modelos físicos- Ajuste por mínimos cuadrados

Extraer información de los patrones de SAXS a través de modelos físicos implica generalmente optimizar ecuaciones no lineales.
La figura de mérito que suele emplearse para calcular la bondad del ajuste es el χ^2

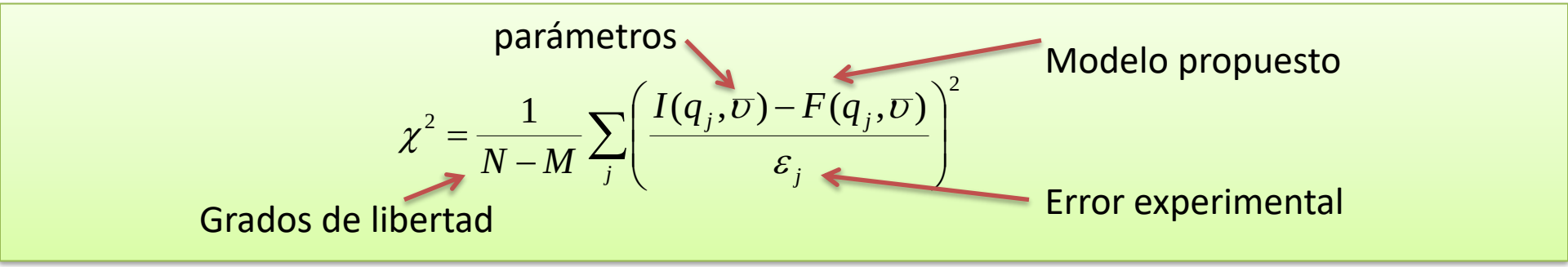

Existen diversos programas disponibles para realizar el análisis de los patrones de dispersión: SASfit, SASview, Irena (plataforma Igor), IsGISAXS, etc.

Microemulsiones

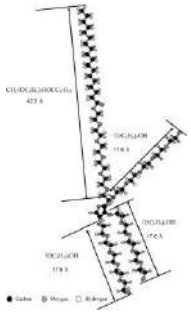

Se denominan microemulsiones a aquellas emulsiones nanométricas termodinámicamente estables.

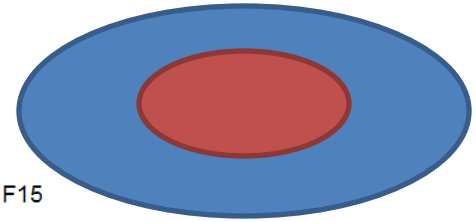

Modelo propuesto:
Elipsoide de revolución
core shell monodisperso

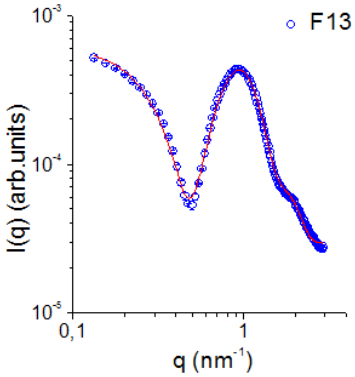

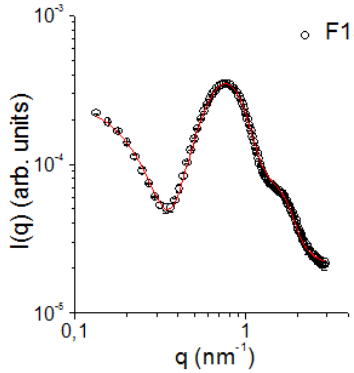

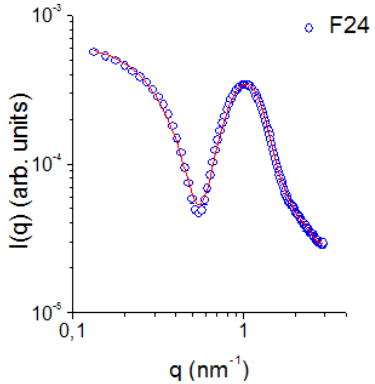

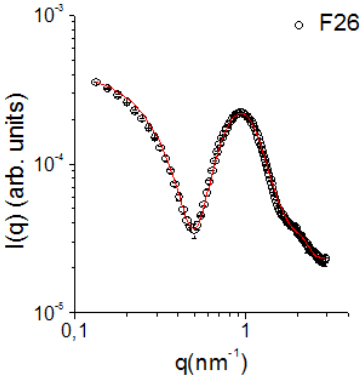

Tween 80 es un emulsionante neutro que forma micelas cilíndricas.

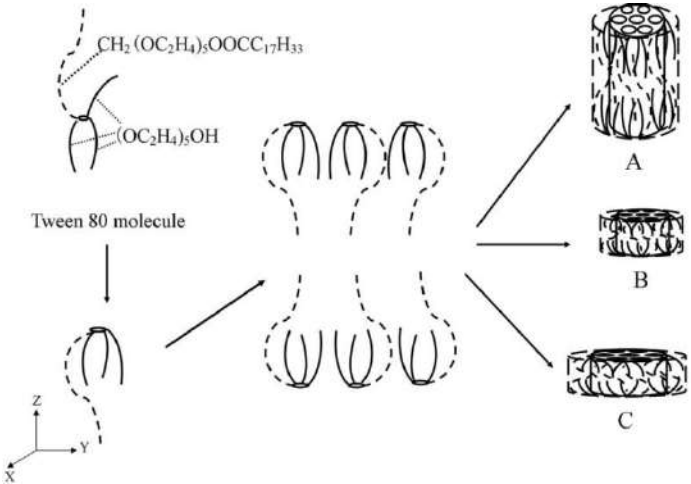

Nanopartículas metálicas

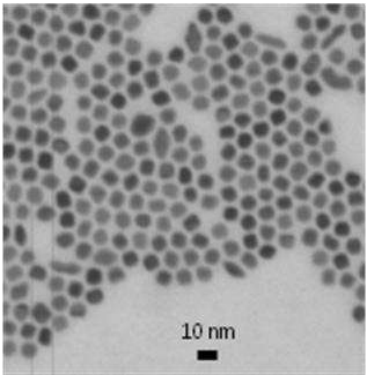

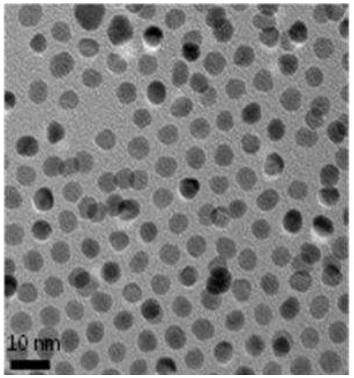

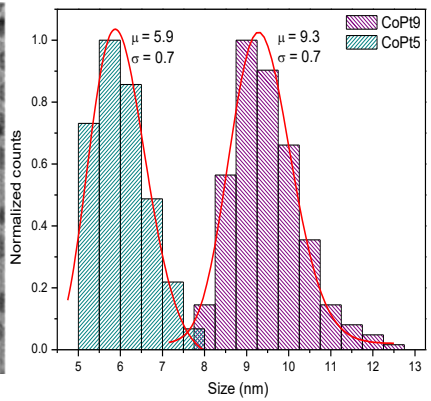

Issue 14, 2018 Previous Article Next Article

From the journal: Nanoscale

Unexpected compositional and structural modification of $CoPt_3$ nanoparticles by extensive surface purification†

Check for updates

Martin D. Mizrahi, Galyna Krylova, Lisandro J. Giovanetti, José M. Ramallo-López, Yuzi Liu, Elena V. Shevchenko *b and Félix G. Requejo*a

Author affiliations

Abstract

We combined synchrotron small angle X-ray scattering, X-ray fluorescence and extended X-ray absorption fine structure spectroscopy to probe the structure of chemically synthesized $CoPt_3$ nanoparticles (NPs) after ligand removal *via* the commonly accepted solvent/nonsolvent approach. We showed that the improved catalytic

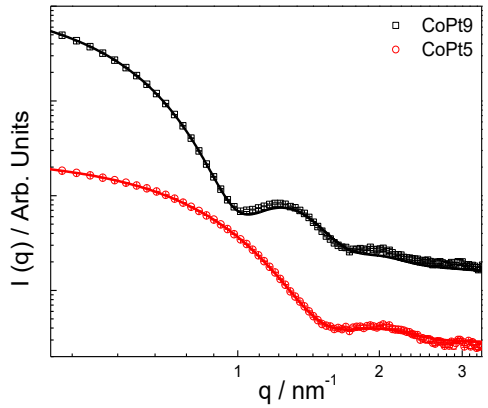

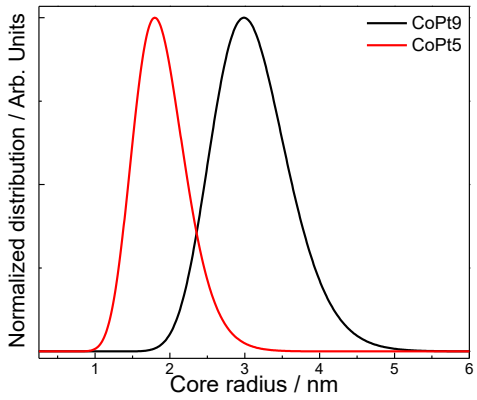

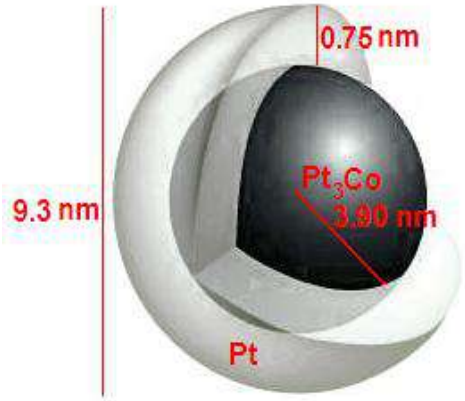

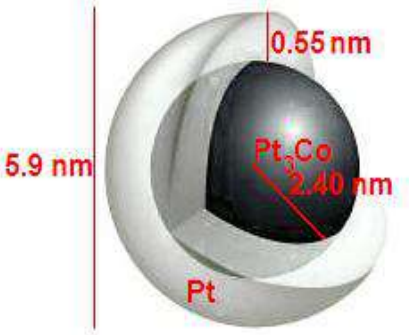

Non diluted systems

"Dilute gas"

(uncorrelated holes)

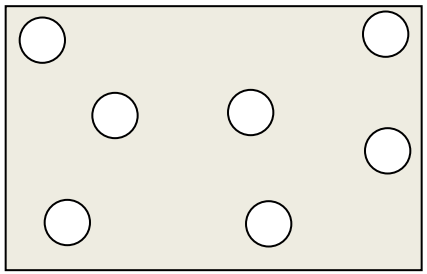

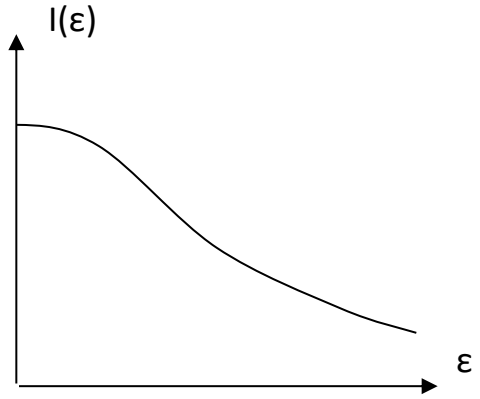

"Liquid"

(short range correlation)

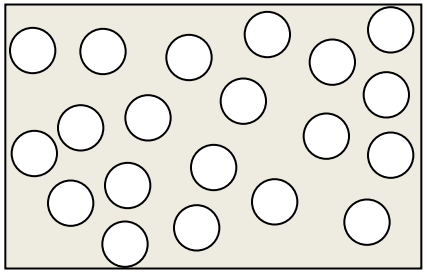

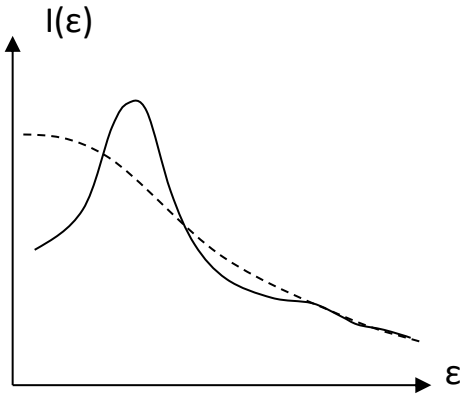

"Solid"

(2D crystalline order)

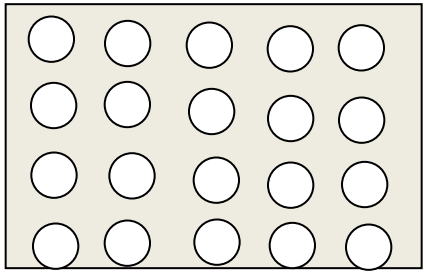

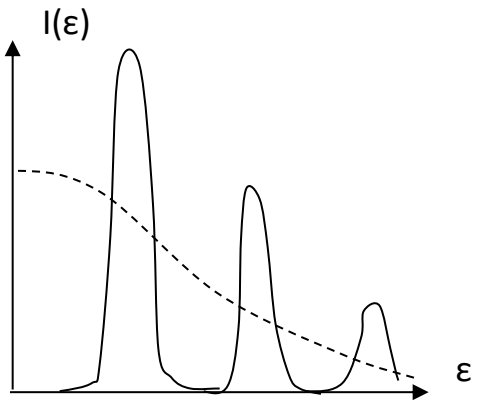

Non diluted systems

$$I(q) = N \cdot I_1(q) \cdot S(q)$$

Interpretation of S(q)

$$I(q) = N \cdot I_1(q) \cdot S(q)$$

Shape

Structure (correlation)

A semi-empirical structure function that describes the spatial correlation of colloidal spherical objects embedded in a homogeneous matrix, derived using the Born–Green approximation, is given by Guinier (1955):

$$S(q) = \frac{1}{1 + k \cdot \Phi(q, d)} \qquad \Phi(q, d) = 3\frac{\sin(qd) - qd\cos(qd)}{(qd)^3}$$

AgNW / Acetone

NANOGAP

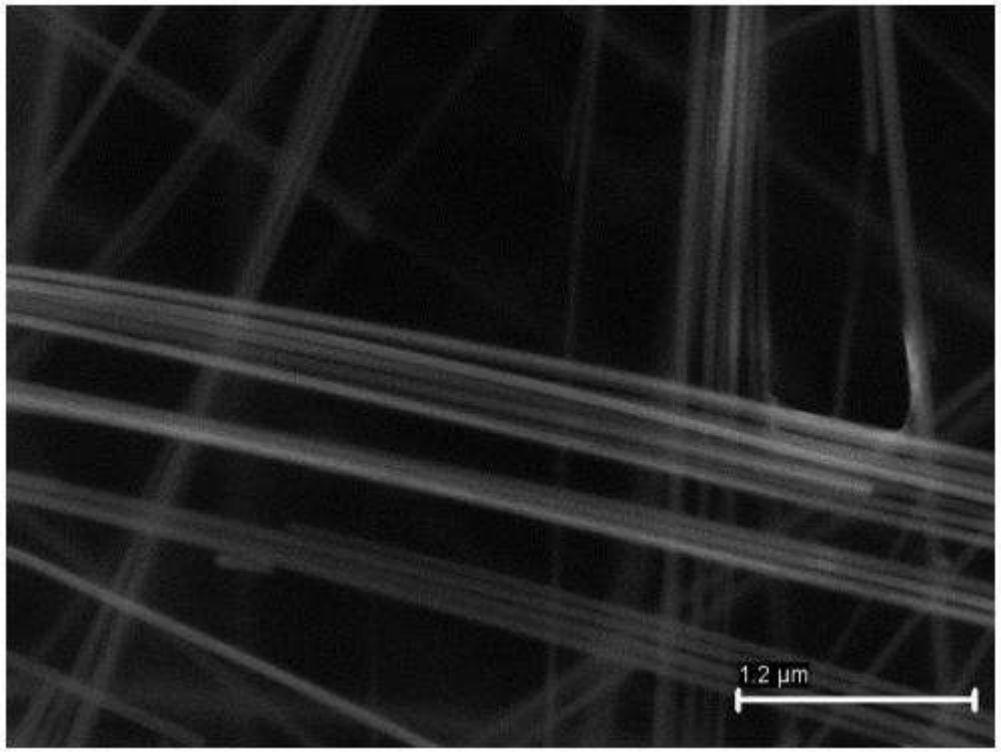

<R> = 30 nm

s / <R> = 20 %

Original curve

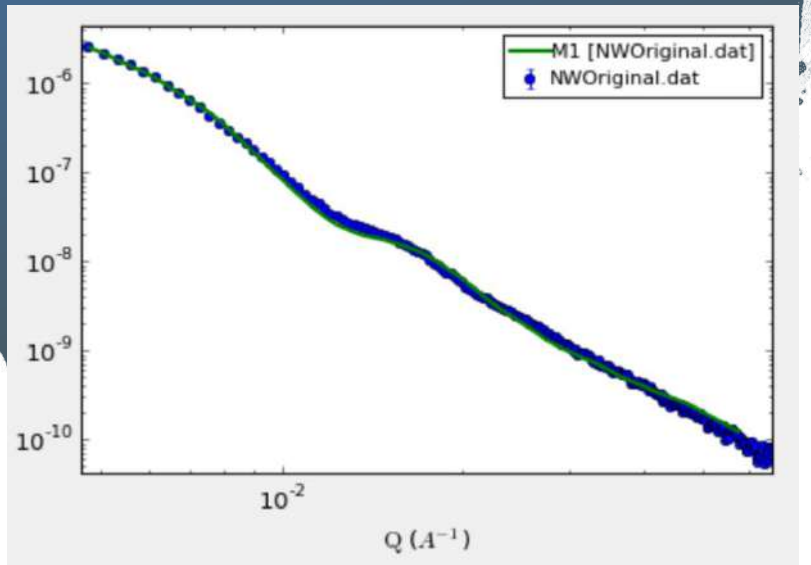

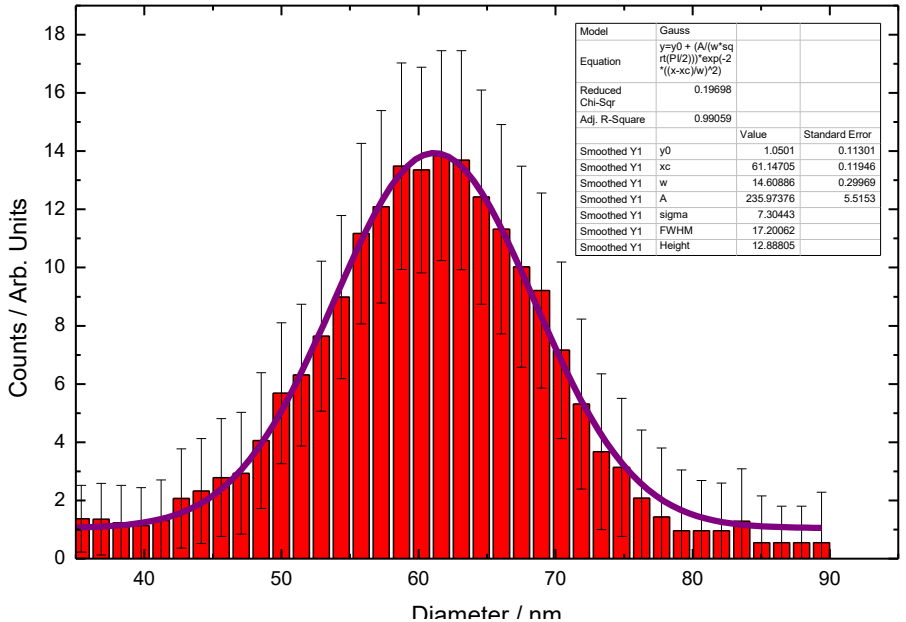

Journal of APPLIED CRYSTALLOGRAPHY
submit subscribe open access search this article

J Appl Crystallogr. 2015 Jun 1; 48(Pt 3): 962–969.
Published online 2015 May 22. doi: 10.1107/S1600576715007347
PMCID: PMC4453982
PMID: 26089769

McSAS: software for the retrieval of model parameter distributions from scattering patterns

I. Bressler,[a,*] B. R. Pauw,[b,*] and A. F. Thünemann[a]

Author information · Article notes · Copyright and License information Disclaimer

Abstract

Go to:

A user-friendly open-source Monte Carlo regression package (*McSAS*) is presented, which structures the analysis of small-angle scattering (SAS) using uncorrelated shape-similar particles (or scattering contributions). The underdetermined problem is solvable, provided that sufficient external information is available. Based on this, the user picks a scatterer contribution model (or 'shape') from a comprehensive library and defines variation intervals of its model parameters. A multitude of scattering contribution models are included, including prolate and oblate nanoparticles, core–shell objects, several polymer models, and a model for densely packed spheres. Most importantly, the form-free Monte Carlo nature of *McSAS* means it is not necessary to provide further restrictions on the mathematical form of the parameter distribution; without prior knowledge, *McSAS* is able to extract complex multimodal or odd-shaped parameter distributions from SAS data. When provided with data on an absolute scale with reasonable

Aged for 10 days
S(q) approximated by I(q)/ $I(q)_{Initial}$

2.5 % Acetone/AgNW solution

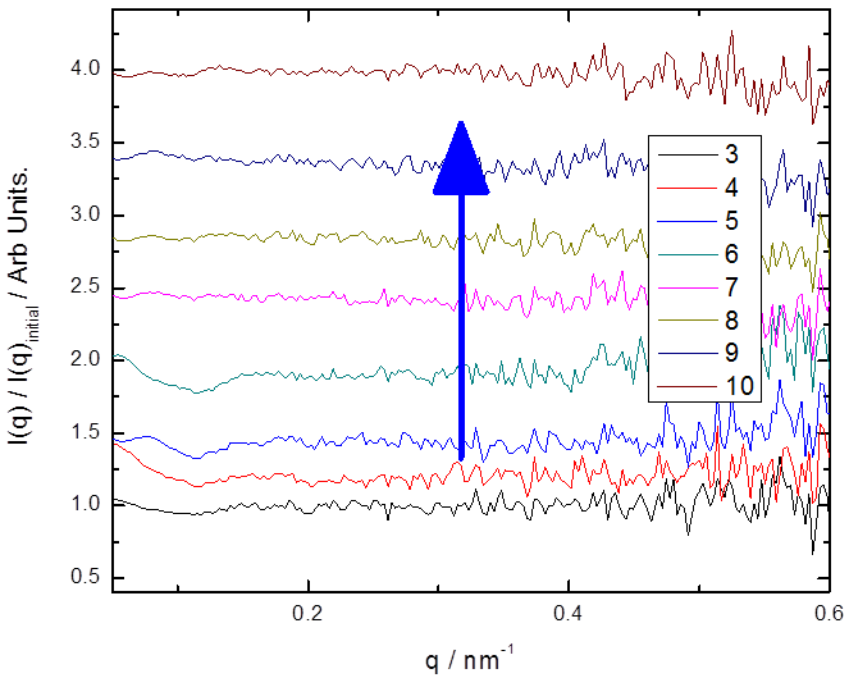

4.5 % Acetone/AgNW solution

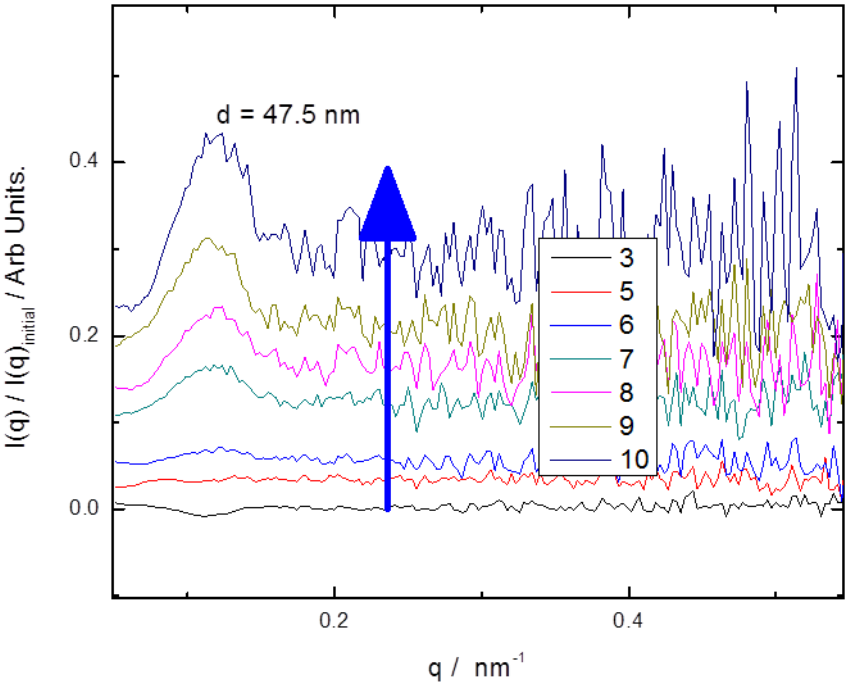

Integration of S(q) as an indication of “the strength” correlation between AgNW

2.5 % Acetone/AgNW solution

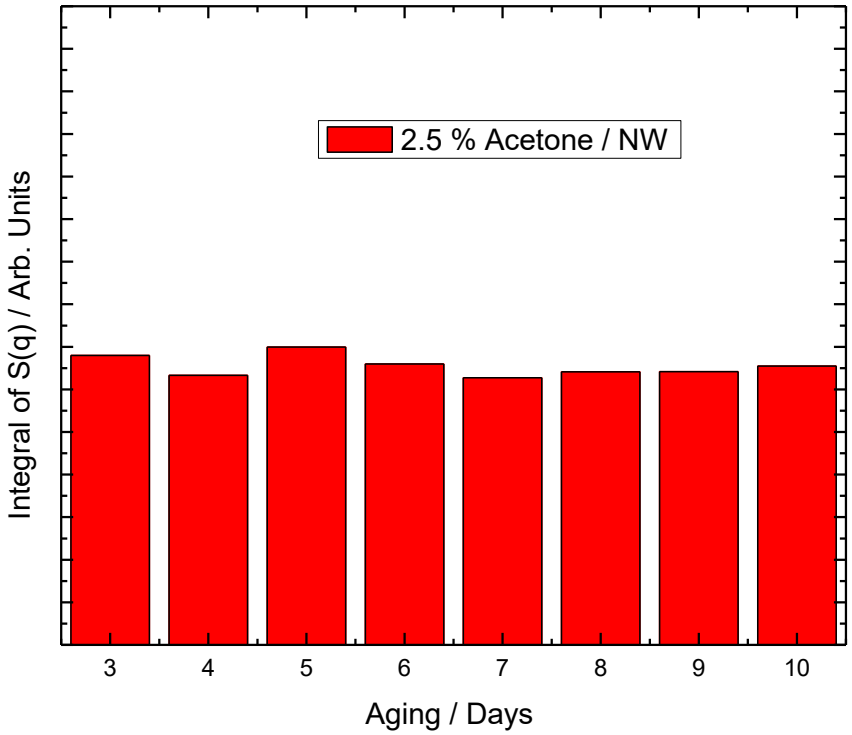

4.5 % Acetone/AgNW solution

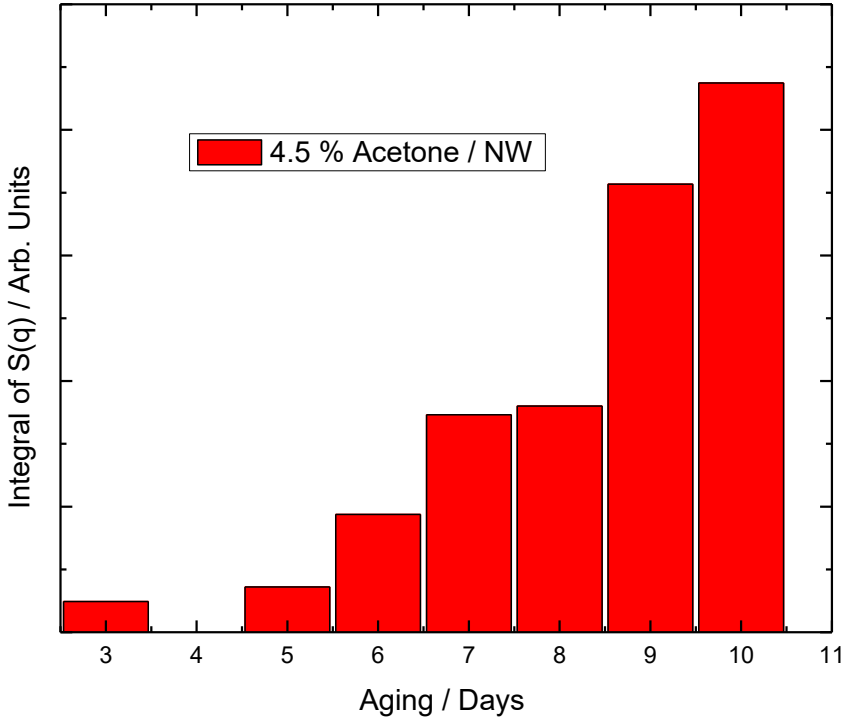

Spherical nano-objects embedded in a solid matrix
Dense systems

$$I(q) = N.I_1(q).S(q)$$

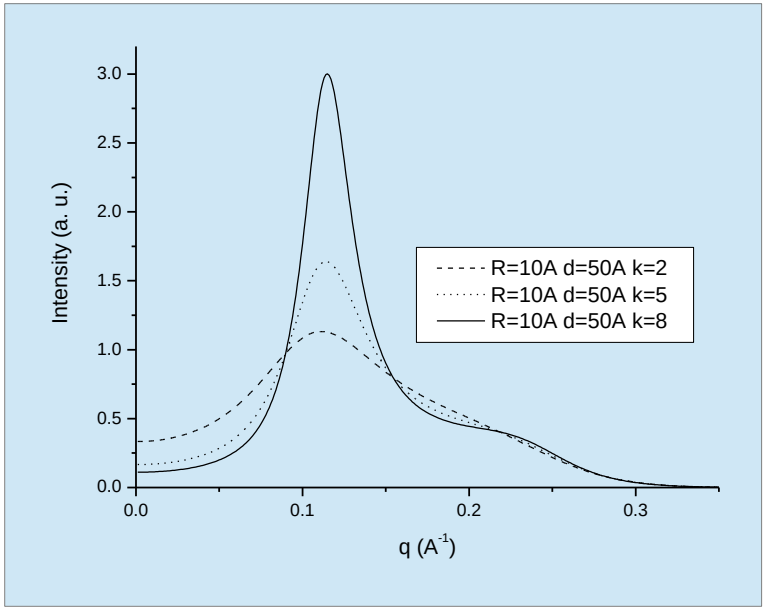

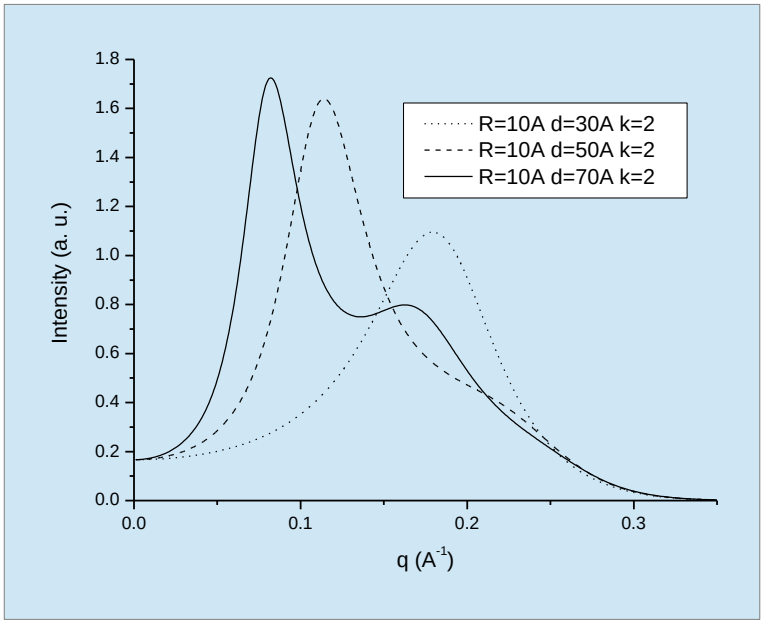

$$S(q) = \frac{1}{1 + k\Phi(qd)}$$

$$\Phi(qd) = 3\frac{sin(qd) - qdcos(qd)}{(qd)^3}$$

$$d = \frac{2\pi}{q_{max}}$$

Interpretation of S(q)

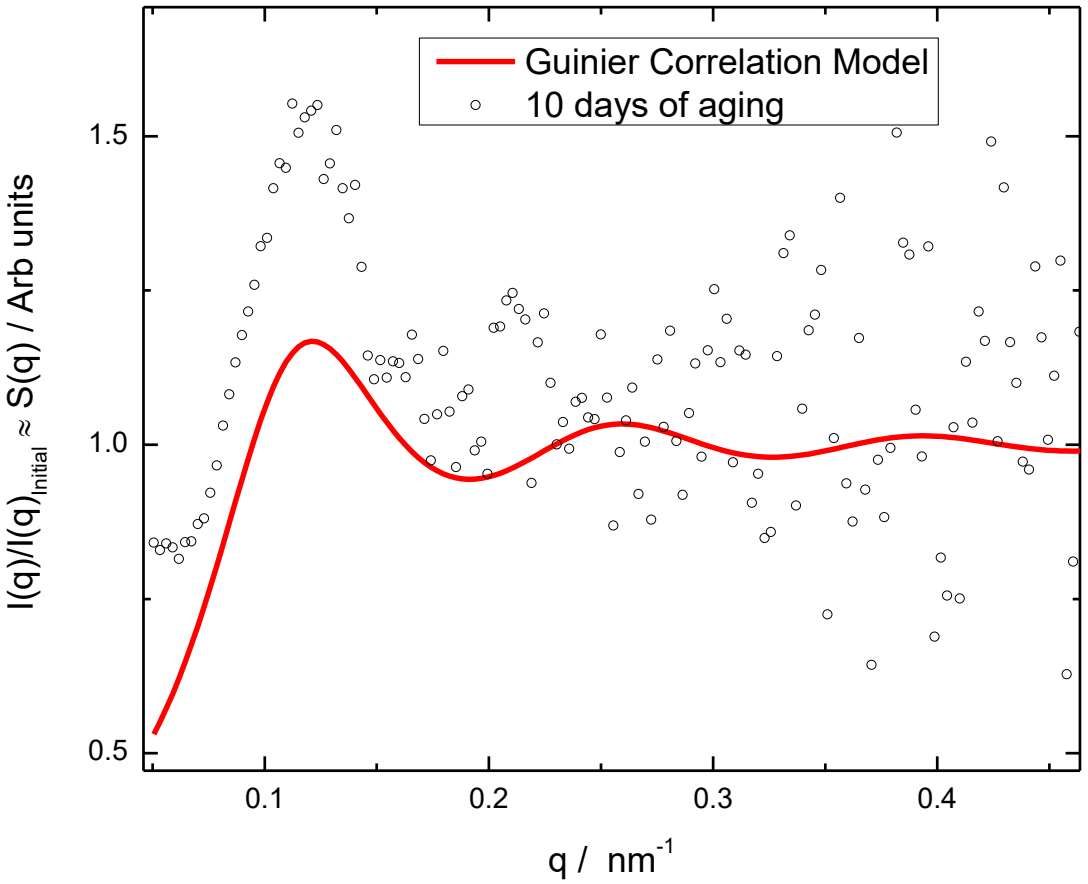

Red curve is a simulation of S(q) using a correlation distance of 48 nm.

Fractal objects: $I(q)=N.I_1(q).S(q)$

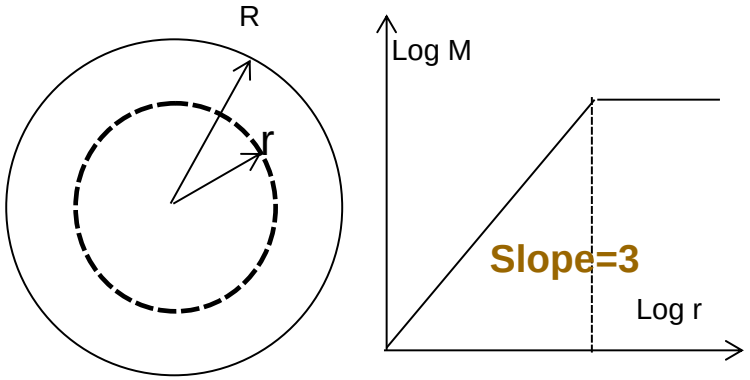

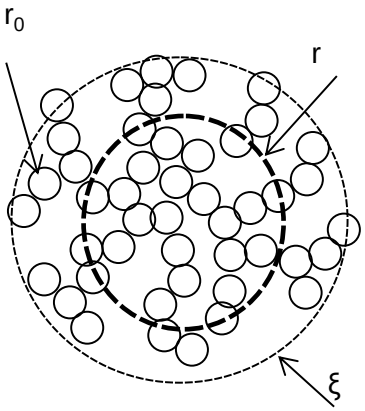

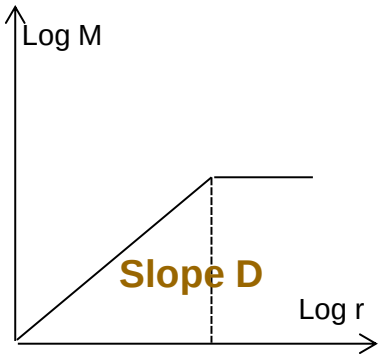

Homogeneous object

$M(r) = a.r^3$

Fractal object

$M(r) = a.r^D$ or:

$$N(r) = \left(\frac{r}{r_0}\right)^D$$

$$\frac{N}{V}g(r) = \frac{N}{V} + \left(\frac{D}{4\pi r_0^D} r^{D-3}\right) e^{-r/\xi}$$

$$S(q) = 1 + \frac{D}{r_0^D} \int_0^\infty r^{D-1}\, e^{-\frac{r}{\xi}} \frac{sinqr}{qr}\, dr$$

I(0)

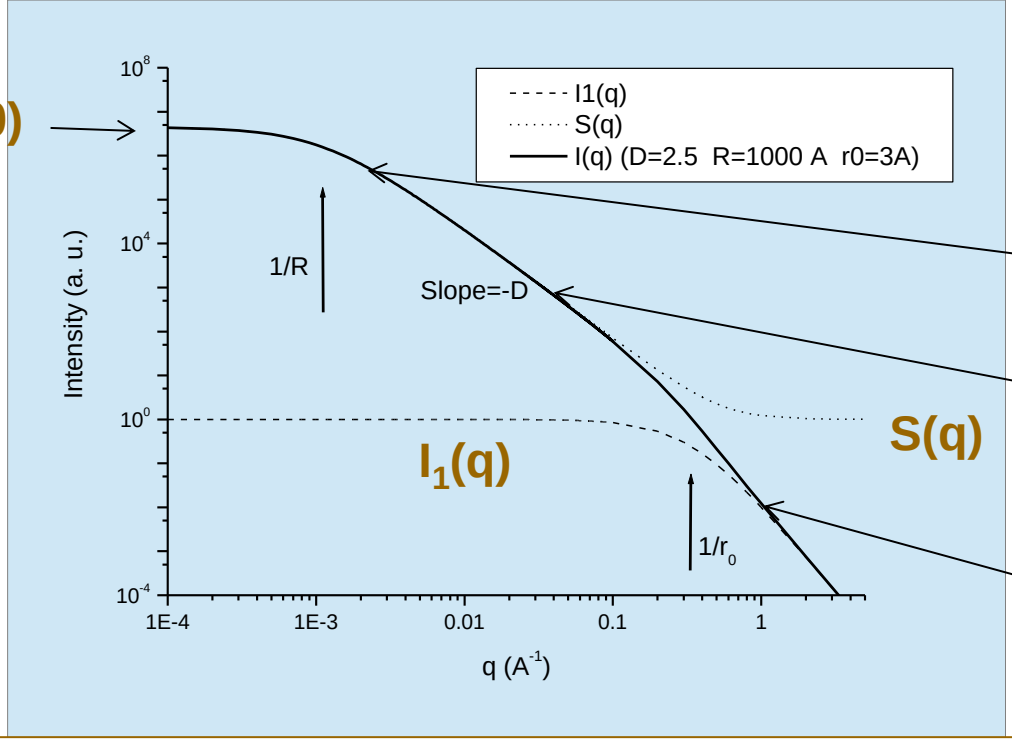

Guinier

I(q)=a.q^{-D}

S(q)

$I_1(q)$

I(q)=N.I_1(q).S(q)

Porod

$q = 0$ $\quad I(0)= \Gamma(D+1).\left(\frac{\xi}{r_0}\right)^D \quad \xi = \left[\frac{D(D+1)}{2}\right]^{-1/2} R_g \quad I(0)= a.R_G^D$

$q \to 0$ **(Guinier)** $\quad S(q)= S(0)\left\{1 - \left[\frac{D(D+1)}{6}\right]\xi^2 q^2\right\} \simeq S(0).e^{-\frac{R_g^2 q^2}{3}} R_g = \left[\frac{D(D+1)}{2}\right]^{1/2} \xi$

$1/\xi << q << 1/r_0 \quad I(q) \propto q^{-D}$

q >> 1/ro **(Porod)** $\quad I(q) \propto q^{-4}$

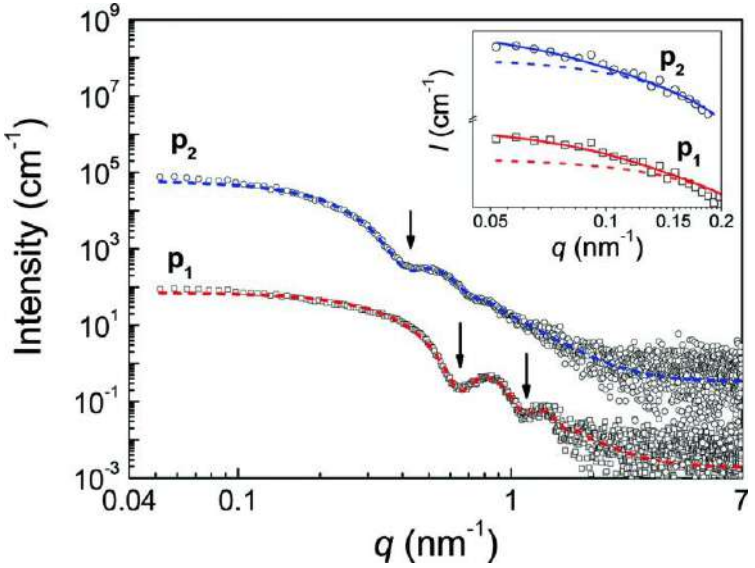

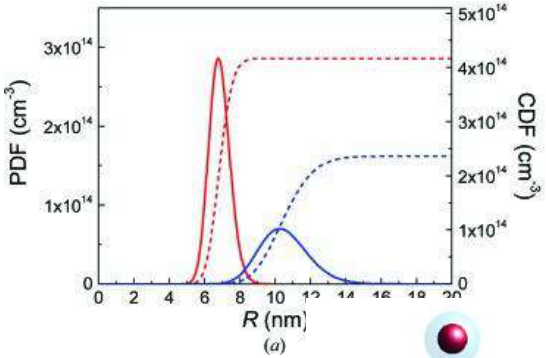

Sample p$_1$


Sample p$_2$

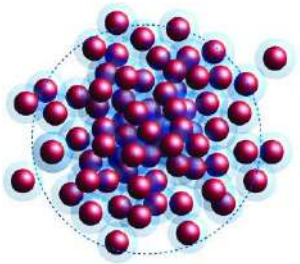
Sample p$_3$

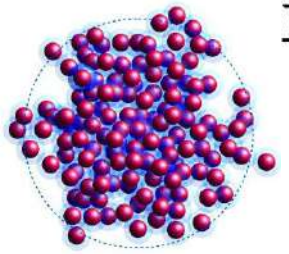
Sample p$_4$

Journal of APPLIED CRYSTALLOGRAPHY
submit subscribe open access search this article

J Appl Crystallogr. 2017 Apr 1; 50(Pt 2): 481–488.
Published online 2017 Mar 14. doi: 10.1107/S1600576717002370
PMCID: PMC5377343
PMID: 28381973

SAXS analysis of single- and multi-core iron oxide magnetic nanoparticles

Wojciech Szczerba,[a,b] Rocio Costo,[c] Sabino Veintemillas-Verdaguer,[c] Maria del Puerto Morales,[c] and Andreas F. Thünemann[a,*]

Associated Data

Supplementary Materials

Abstract

Go to:

This article reports on the characterization of four superparamagnetic iron oxide nanoparticles stabilized with dimercaptosuccinic acid, which are suitable candidates for reference materials for magnetic

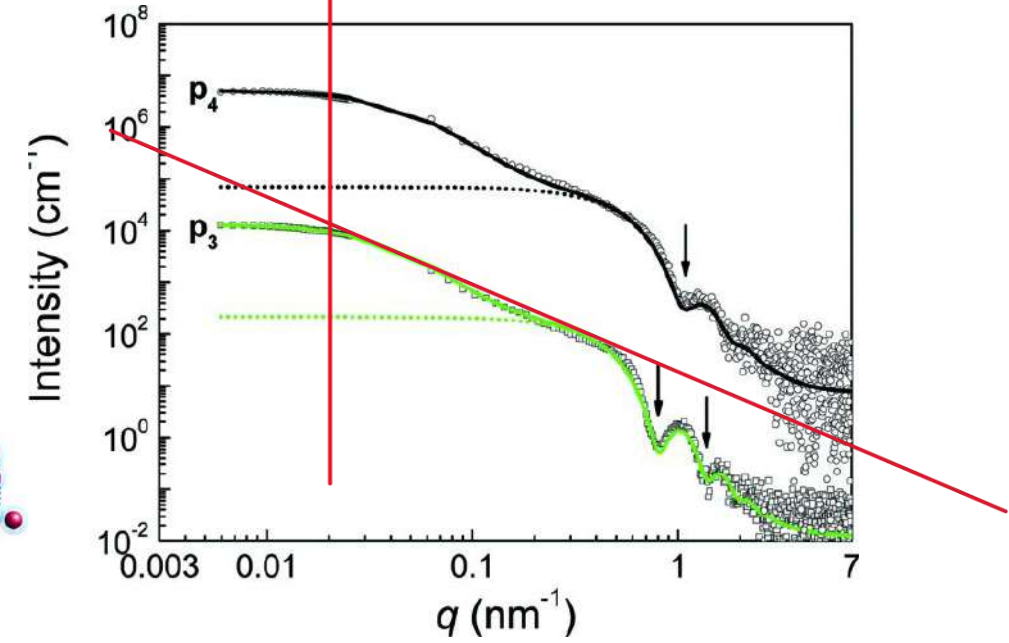

SAXS Instrumentation

Optimization of the scattering intensity

$I_{mesured} = I(q)ste^{-\mu(E,z_i)t}$ scattered intensity: dependence with sample thickness

s t: Irradiated volume
- s: beam cross section area
- t: sample thickness

$I_0/I_t = e^{-\mu(E,z_i)t}$ sample attenuation
- μ: lineal absorption coefficient
- E: photon energy
- z_i: atomic number of element i

$I_{measured} = I(q)ste^{-\mu t}$

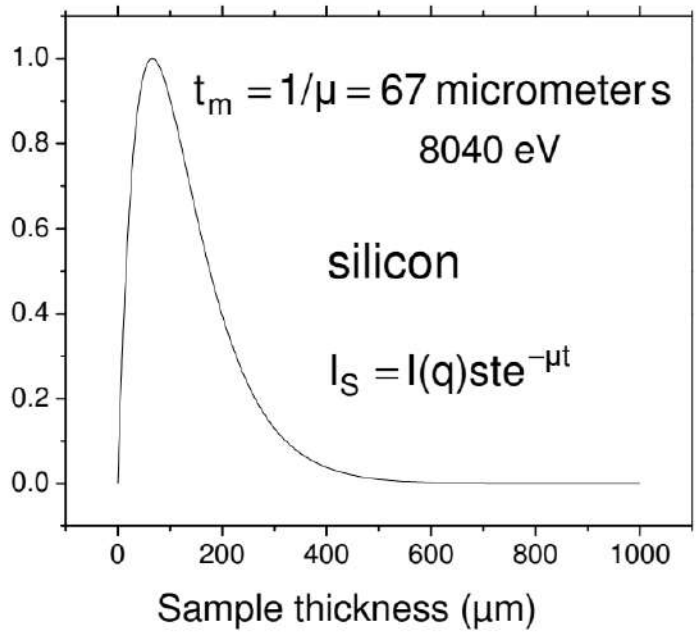

SAXS facility at INIFTA

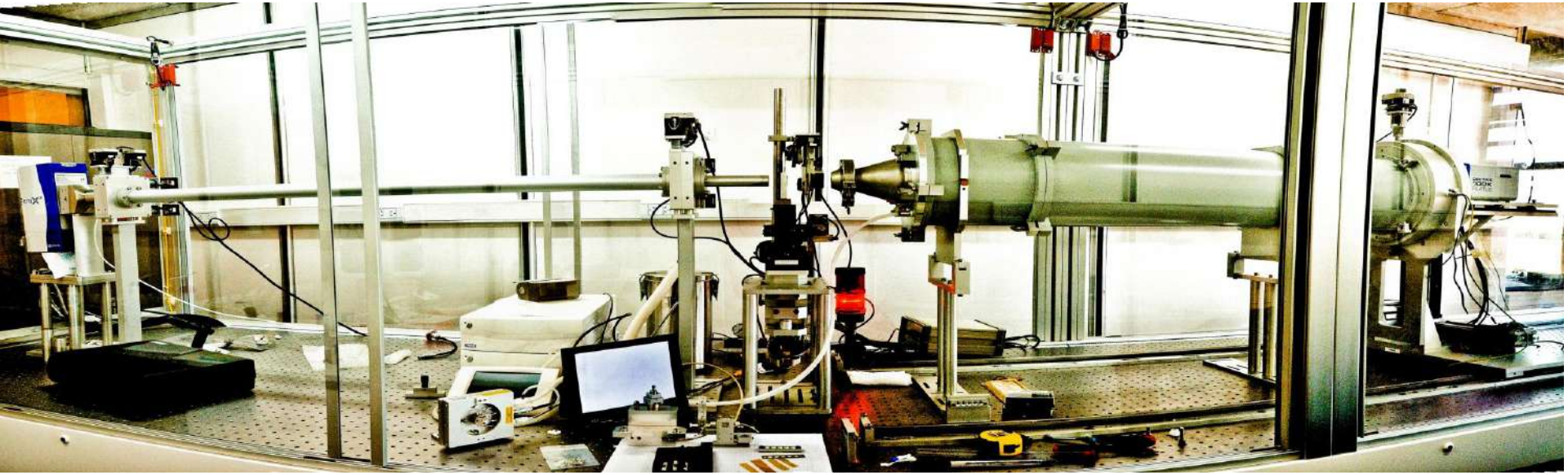

.X-ray source and collimation

Cu microsource λ=0.154 nm

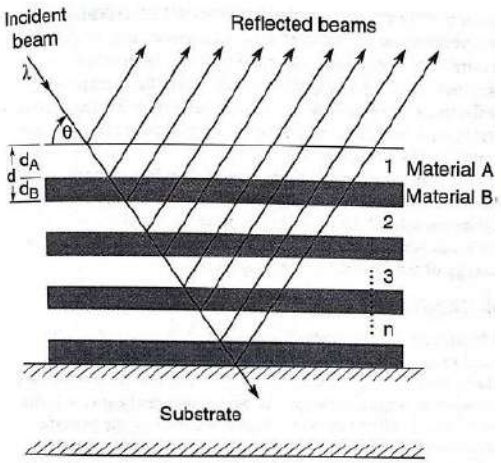

$2d \sin\theta = k\lambda$

Parallel beam collimation

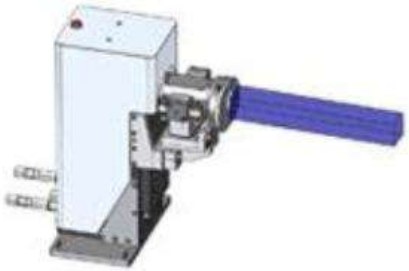

Paraboloid of revolution

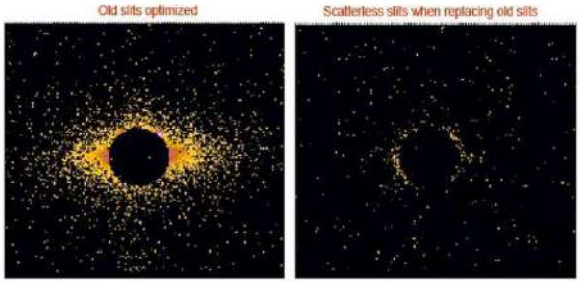

Figure 1 : Comparison of the background scattering close to the beamstopper between our previous setup and the scatterless slits. The images are ROIs taken on a Pilatus 100k detector (Dectris)

Line beam lab sources

Advantage: high flux for a lab source.

Disadvantage: the need to remove the effect of the beam profile from the data (desmearing). Primarily low-q data are affected.

Beam shape measurement is needed for desmearing.

$$I_{0S}(h)=\int_{-\infty}^{+\infty}\int_{-\infty}^{+\infty} W_z(z)W_y(y)I_0[((h-y)^2+z^2)^{\frac{1}{2}}]dydz$$

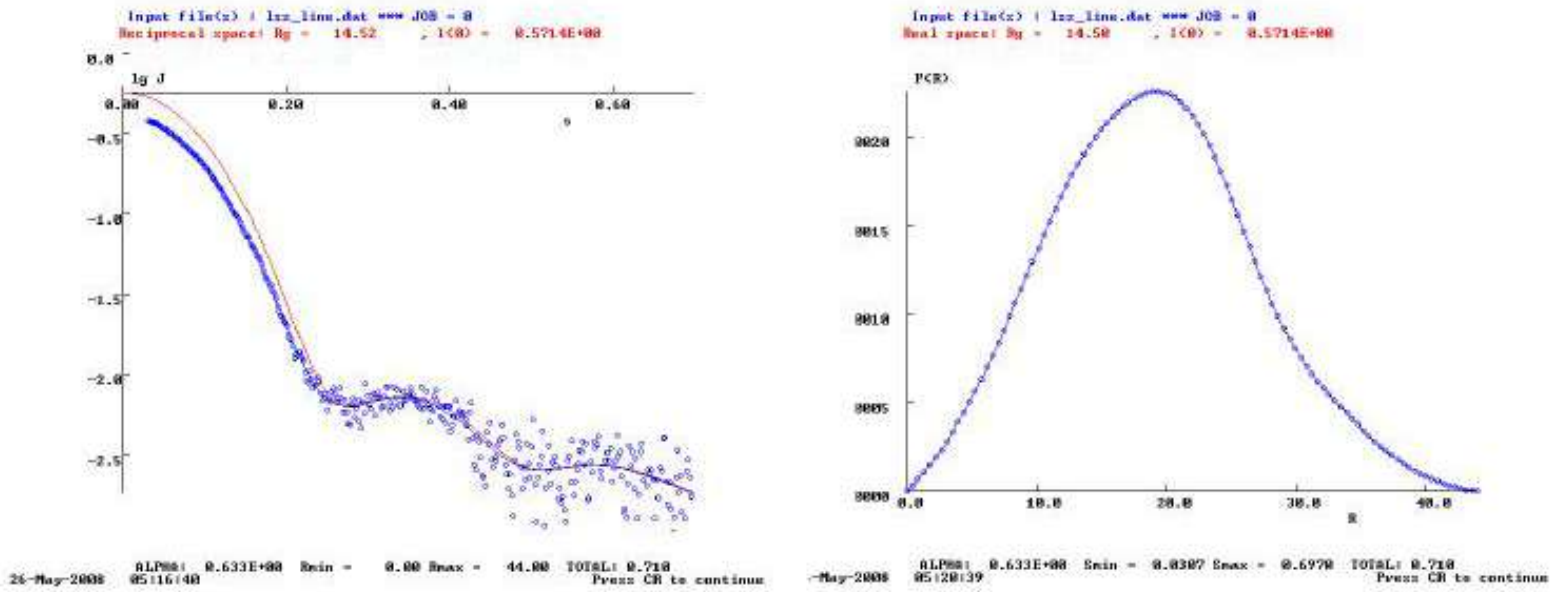

Feigin, L., Svergun, D. (1987) Structure Analysis by Small-angle X-ray and Neutron Scattering (Chapter 9). Plenum Press.

Lake, J. (1966) An iterative method for slit-correcting small-angle X-ray data. Acta Cryst. 23, 191-194.

Sample holders and sample environments

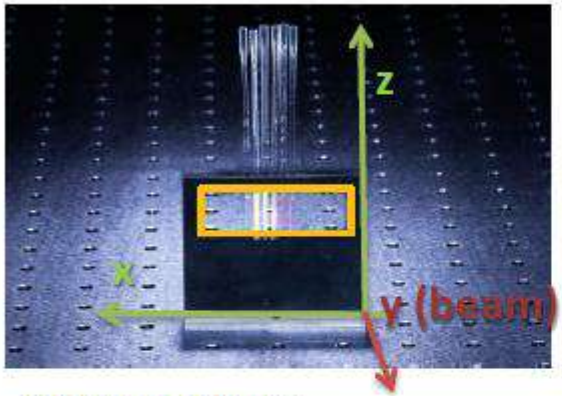

Multicapillary

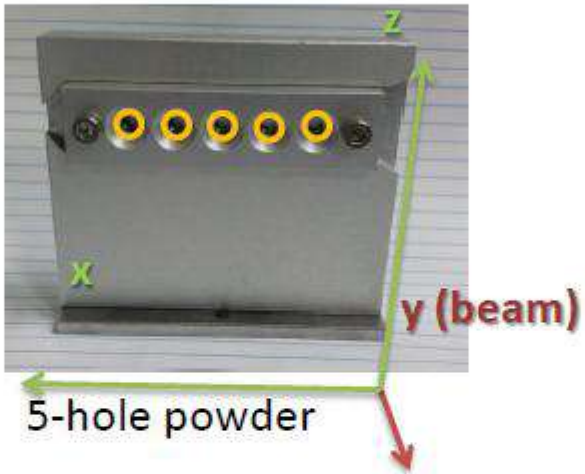

5-hole powder

Flow-through

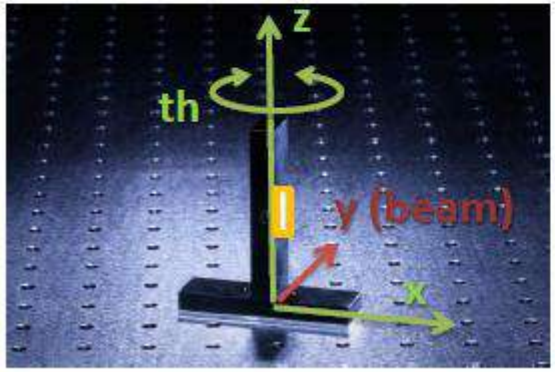

GiSAXS

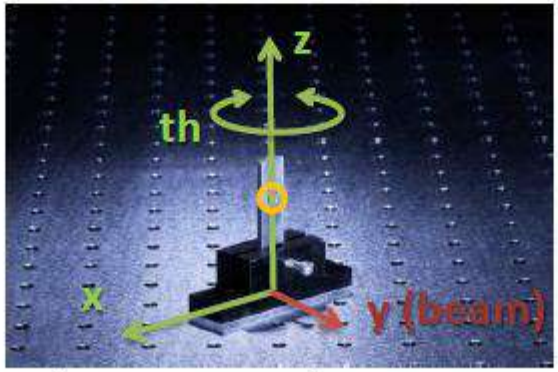

Alignment tool

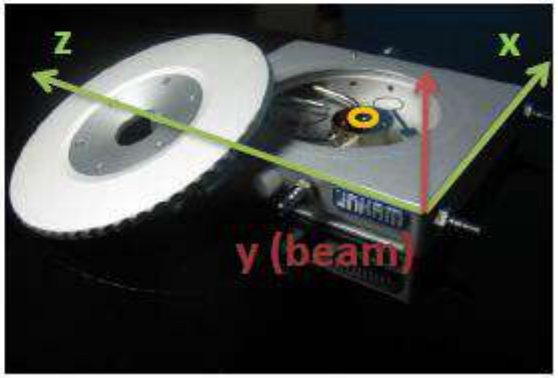

Linkam temperature

.Sample holders

The sample holder platform is coupled to motors that allow the samples to be moved around the plane perpendicular to the beam direction (axial and equatorial) and rotated relative to the axial axis.

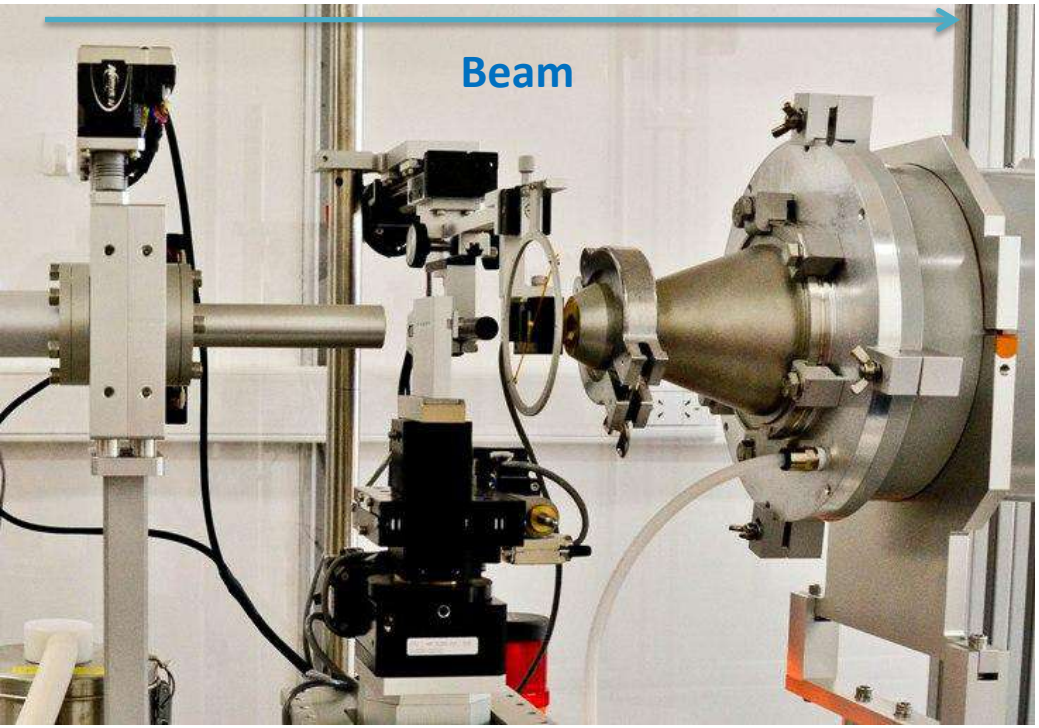

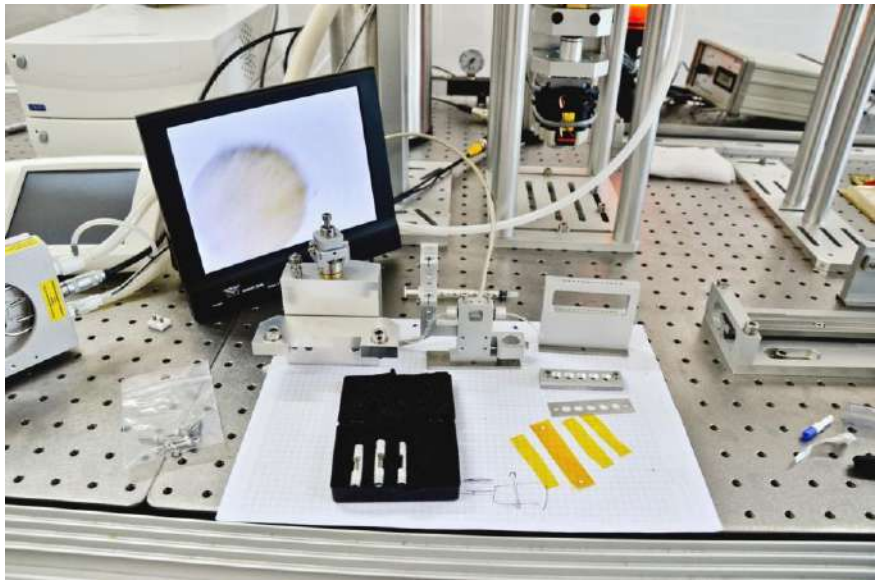

The experimental arrangement allows a wide range of options.

It's a very flexible device and easy to use.

All parts move along the optical bench.

.Temperature control

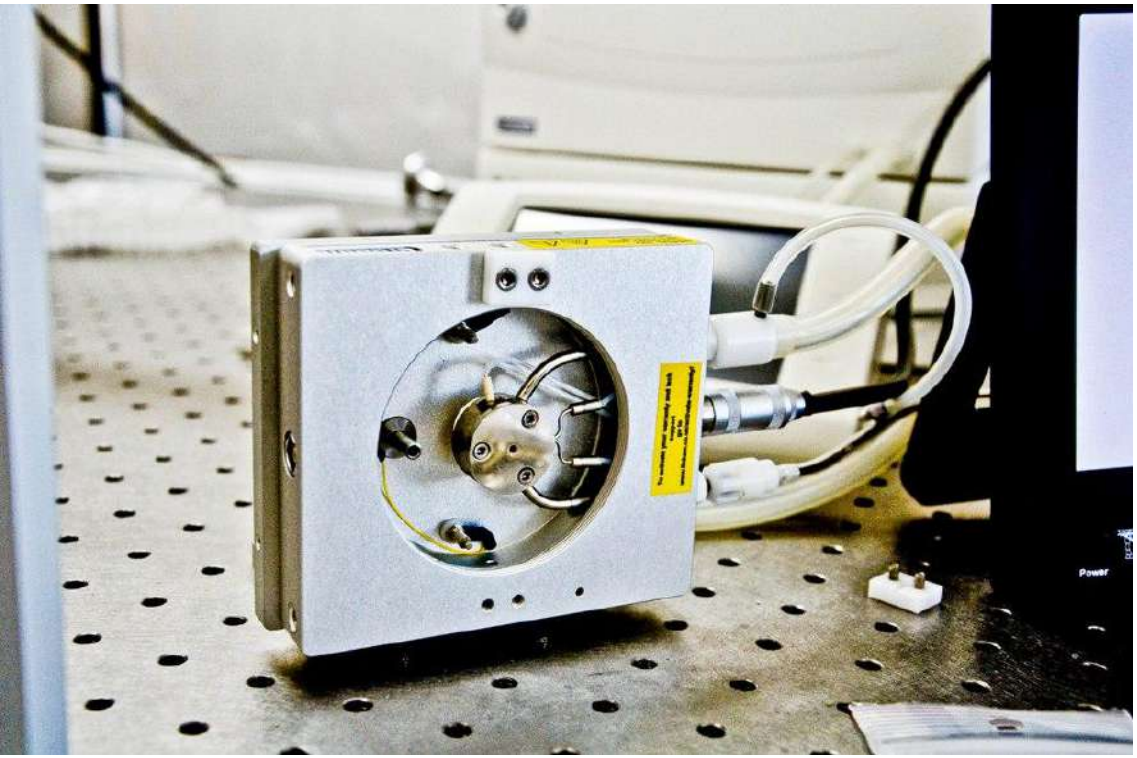

Allows to perform conentional SAXS and GISAXS.

Range between -50 C to 350 C

Max rate 40 C/min

The module can be controlled externally through a touch screen or through the command line of the computer that is fully coupled to the experimental setup.

•Sample distances and detector

Distances:

WAXS : 9 mm

SAXS: 500 mm; 1500 mm; 2500 mm

Detector

Pilatus 100K

Low noise
Dimensióon = 486x195 pixels
Pixels size = 0.172 mm x 0.172 mm

Wide linear dinamic range

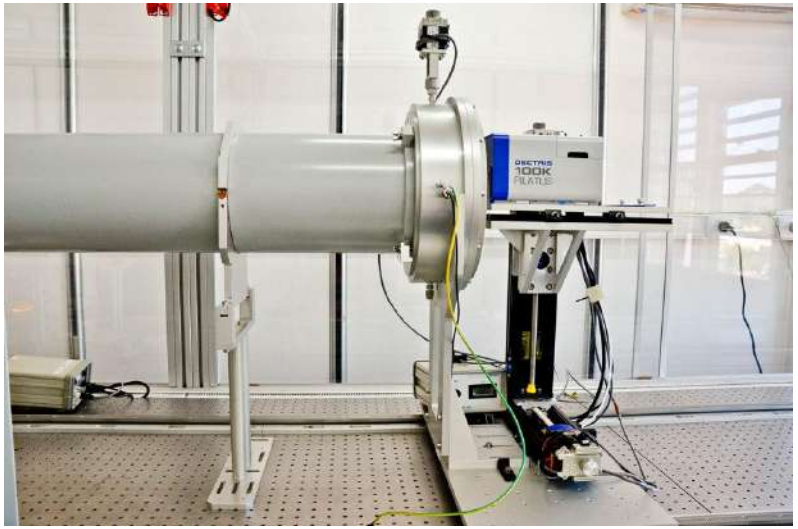

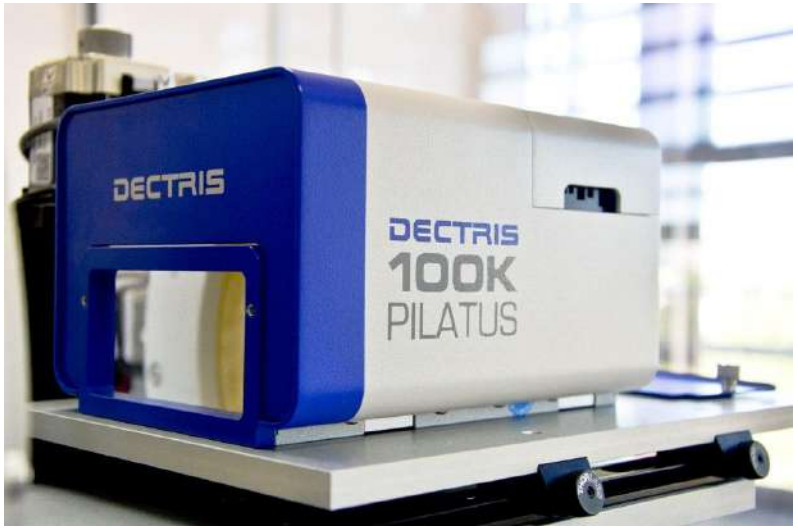

Q-range (aprox.) as function of SD distance

Beam on geometrical center of detector and beamstop

SD [mm]	Pipe Sections	q_{min} [nm^{-1}]	q^*_{max} [nm^{-1}]	Characteristic Dimension [nm]
2485		0.042	2.21	from 2.8 to 150
1190		0.085	4.58	from 1.4 to 73
538		0.18	9.8	from 0.64 to 34
360		0.27	14.2	from 0.44 to 23

Cu radiation

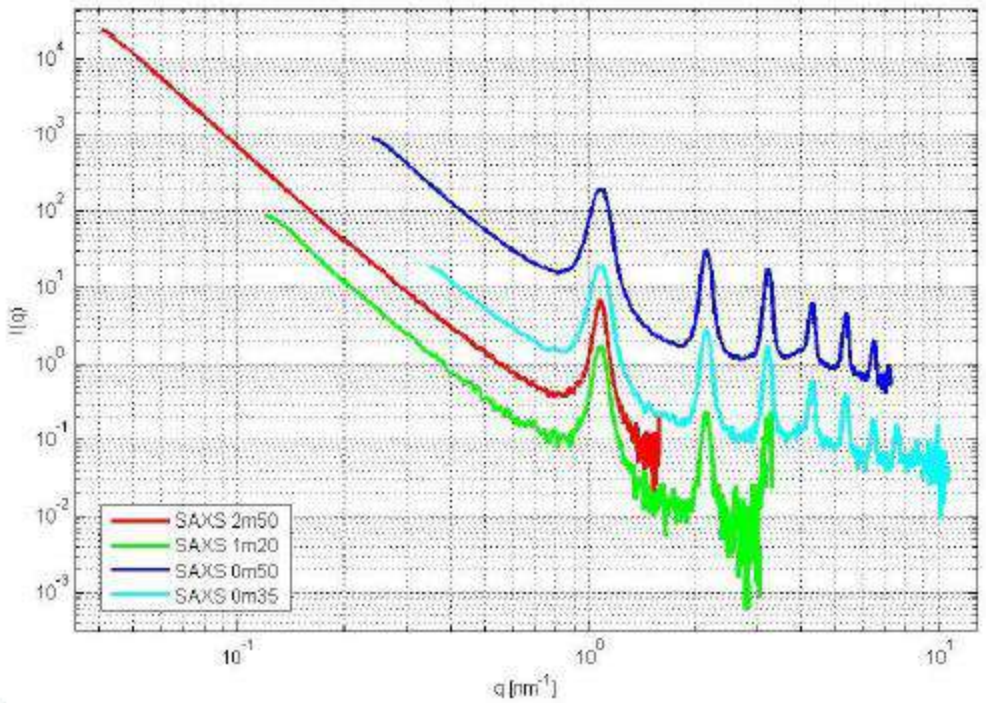

X-ray detector types

Multi-wire gas filled proportional detector (Gabriel type, 1D or 2D) detects individual ionization events by X-rays of the filler gas (CO_2/Ar). They have the lowest noise of all types, wide dynamic range limited by high local count rate, their main limitation (max ~50000/sec global or ~100/sec local). Their spatial resolution is limited (100-500 μm). They work best for lower flux sources (lab-based and synchrotrons such as SSRL).

Imaging plates are suitable for lab-based sources. They exhibit very high linear dynamic range (~5 orders of magnitude) and good spatial resolution (50 um). Not suitable for synchrotron sources.

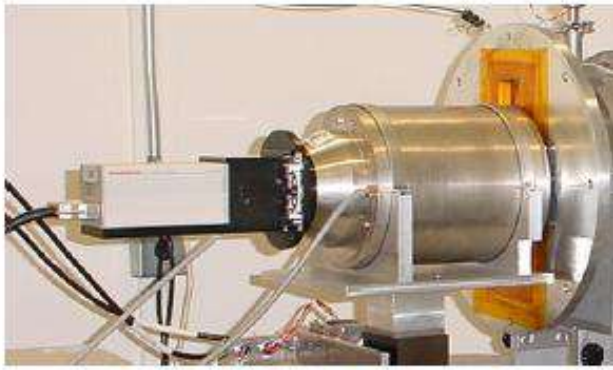

Image intensified CCD detectors (Hamamatsu): high sensitivity, large area, very rapid data acquisition. Since their count rate is unlimited, they are suitable for all synchrotron sources.

Fiber optic tape CCD detector (Mar): unlimited count rate, small pixel size (50-80 mm), low image distortion, rapid data collection. Suitable for all synchrotron sources

Detectors are periodically calibrated by long data collections of known profiles. This can be done with either ^{55}Fe radioactive source or with scattering by a glassy carbon standard samples previously calibrated using neutron scattering.

.Virtual detector

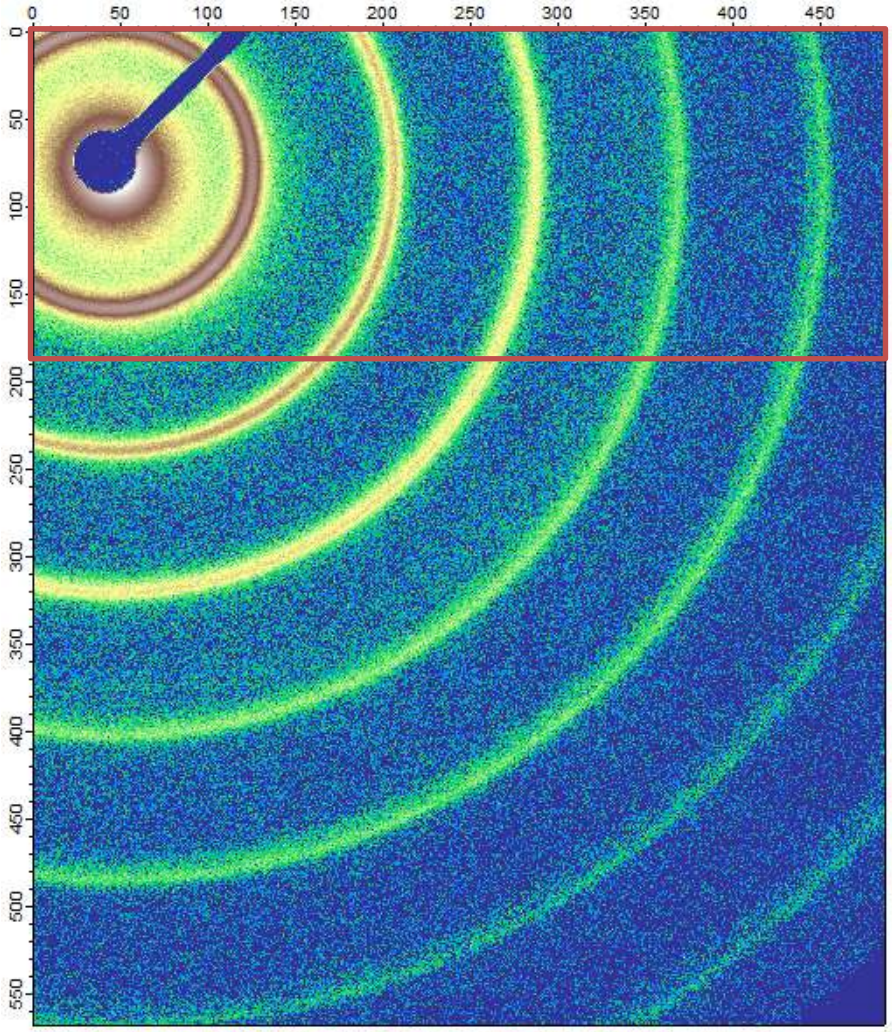

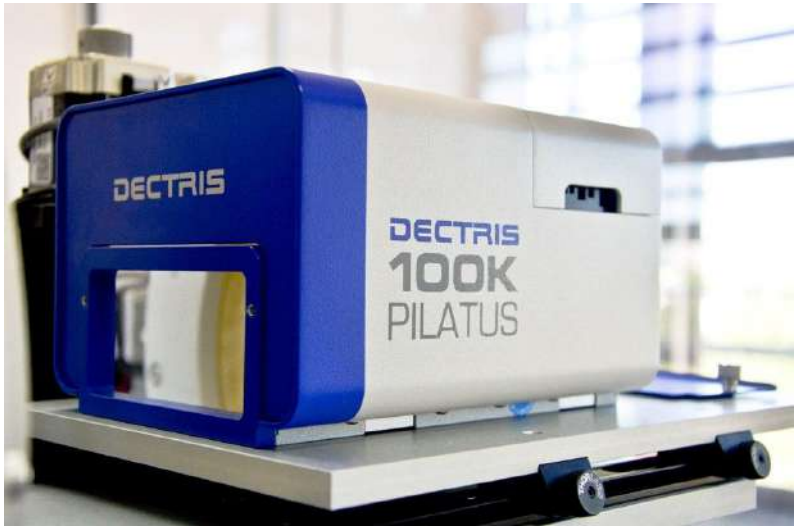

Count rate monitors

Accurate subtraction for the buffer scattering from the sample requires calibrations by the photon fluxes during the two measurements. This is accomplished by measuring beam intensity upstream and downstream from the sample.

The **incident intensity** (upstream) measurement is typically done with either ionization chambers or NaI scintillation detectors pointing towards a transparent scattering material (such as Kapton foil) in the beam. Ionization chamber measurements are limited by the drift of the dark current and NaI by the radiation damage/variable energy deposition to Kapton.

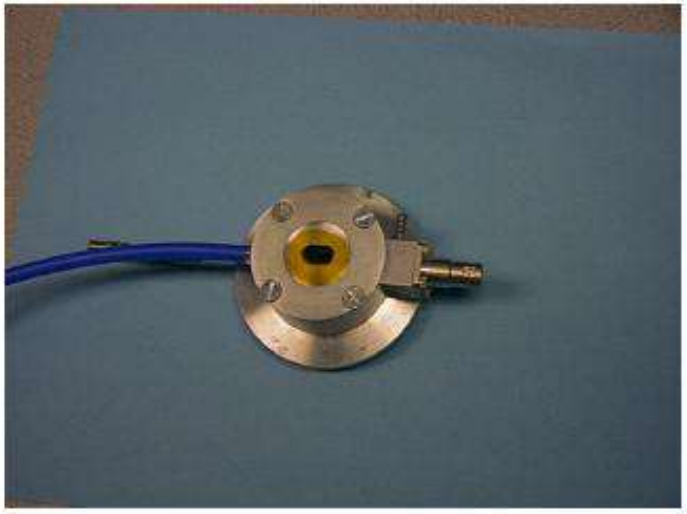

The **transmitted intensity** (downstream) measurement is done with a beamstop-mounted photodiode. Its accuracy is limited by the drift of the photodiode's dark current and the lateral drift of the beam during data collection. The transmitted intensity is affected by any changes in sample material including radiation damage and bubble formation.

The transmitted intensity measurement can also be done using a semi-transparent beam stop to get the transmitted beam intensity to a level comparable to the scattering

.Virtual detector

Acquisition

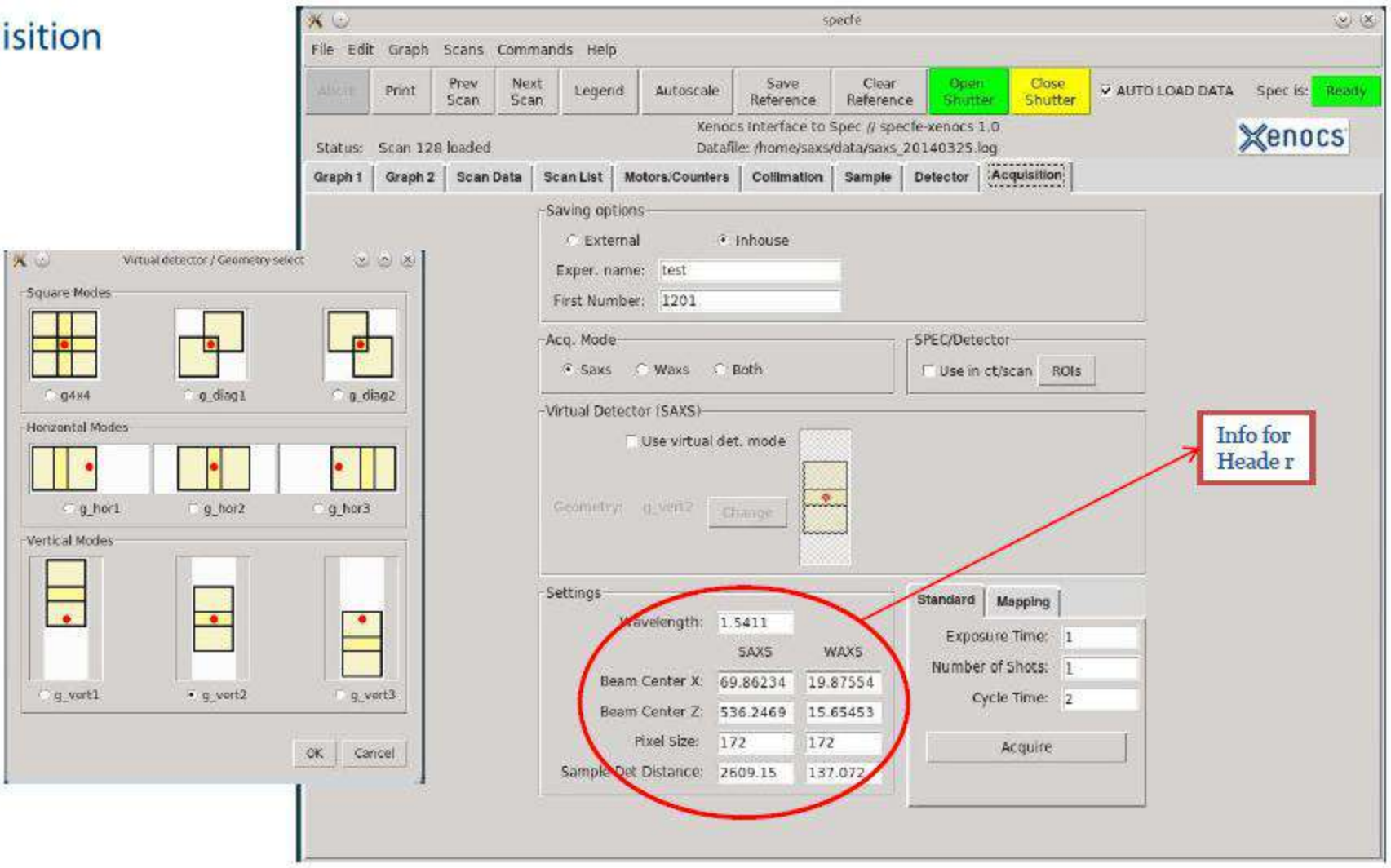

.Virtual detector

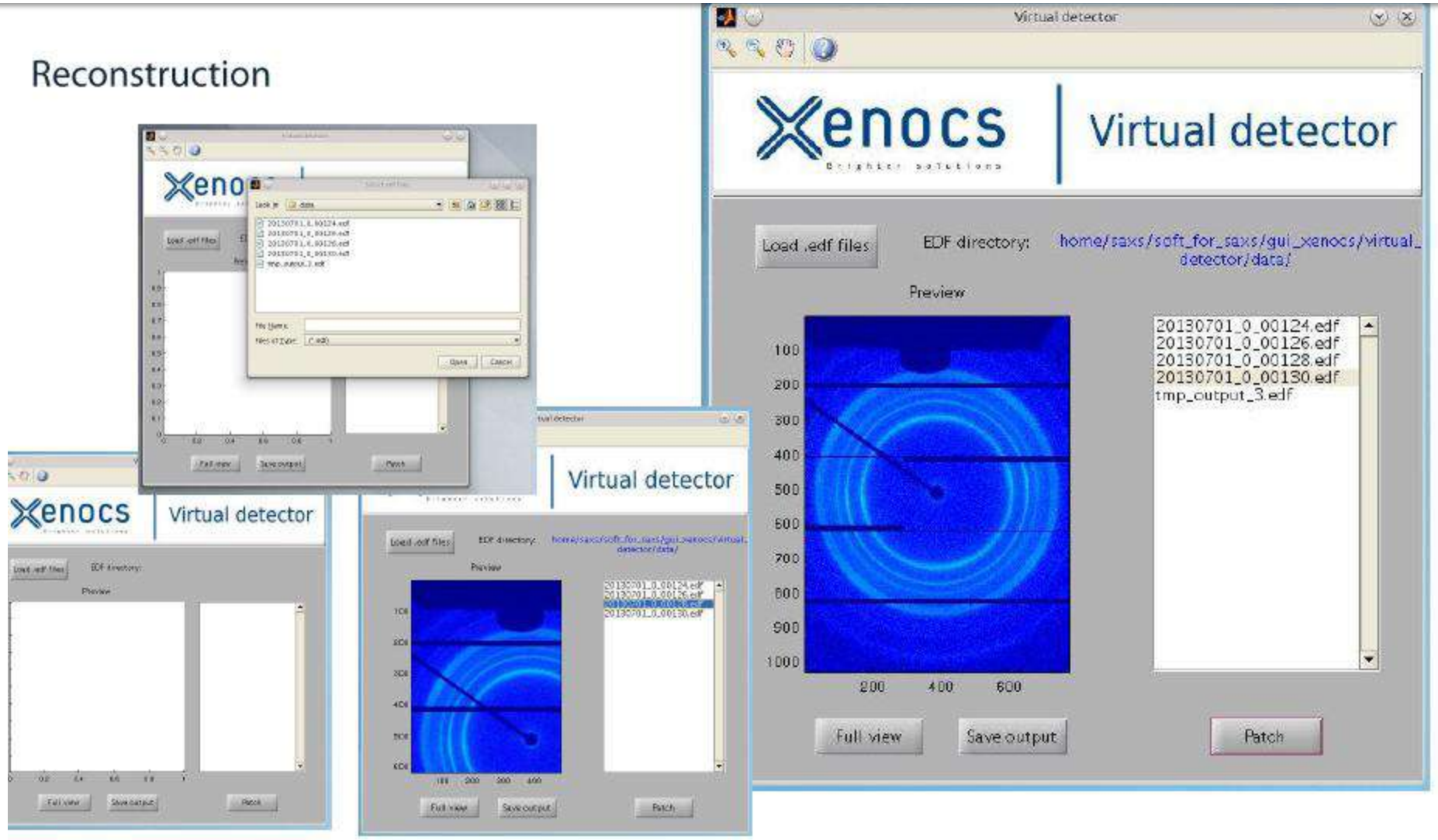

SAXS
Data processing

Reducción de datos

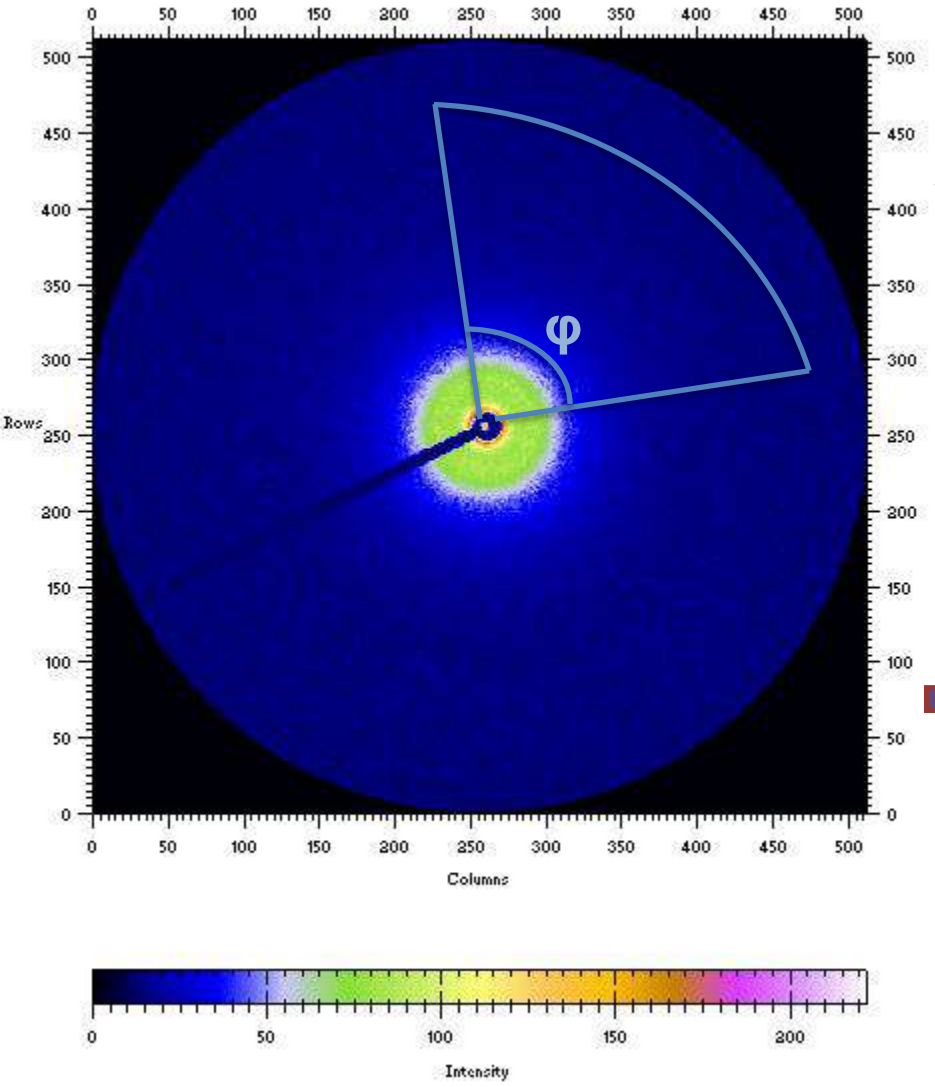

Contraste: la diferencia entre la densidad electronica del solvente y de la fase dispersa genera el fenomeno $\Delta\rho = \rho_{disperso} - \rho_{continuo}$

Vectores de onda

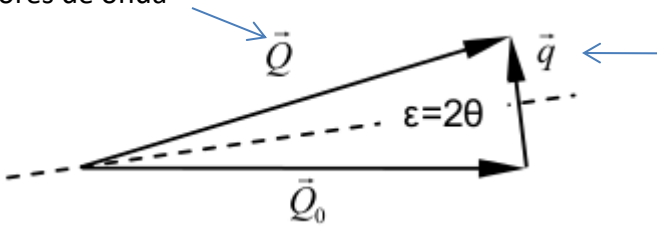

Vector de dispersion

$$\vec{P} = h\vec{Q}$$

$$|\vec{q}| = q = \frac{4\pi sen(\theta)}{\lambda}$$

Módulo del vector de dispersión

Integrando en función del angulo φ

$$\frac{d\sigma}{d\Omega} = I(q)$$

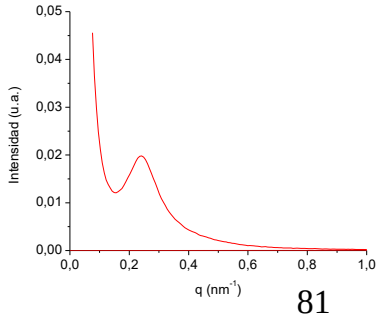

a. 2D image → 1D data conversion

1. Find beam center
2. q calibration/mapping
3. Image mask
4. Conversion

The above procedures for both SAXS & WAXS

done at synchrotron beamline station during data aqusition

Software: Mardetector v4.9 screen capture

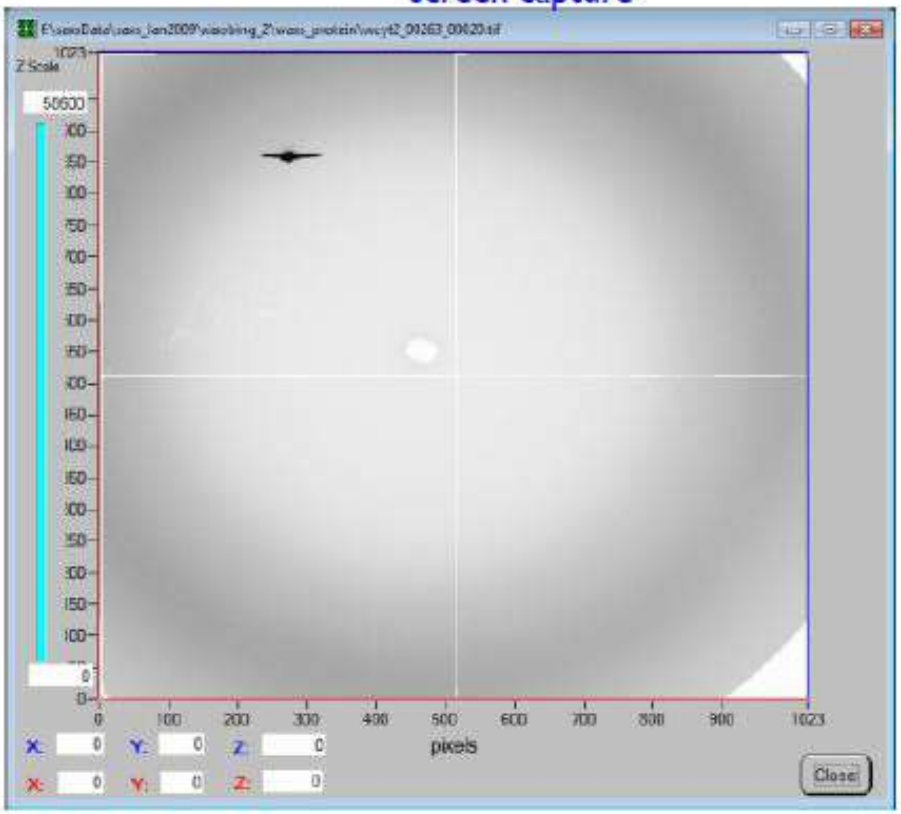

A 2D scattering image for a solution sample recorded on a home-made 2x2 CCD chips detector (gold detector) at 12-ID at Argonne

Find beam center

Software: Mardetector v4.9
D. Tiede (Argonne) & X. Zuo

Initial: off beam center

Along the four directions, peak positions do not overlap well

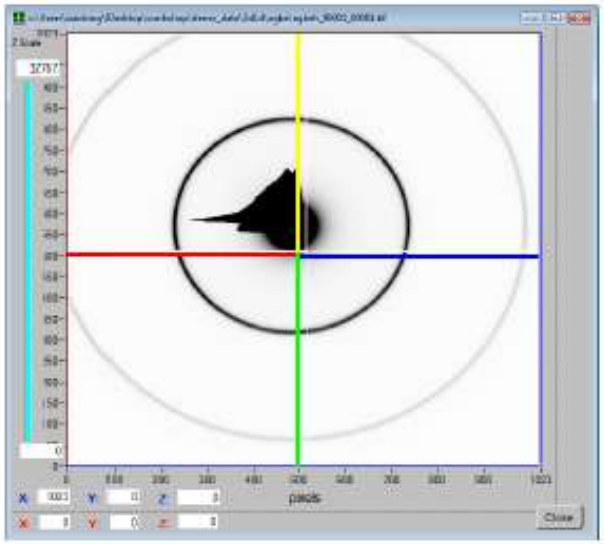

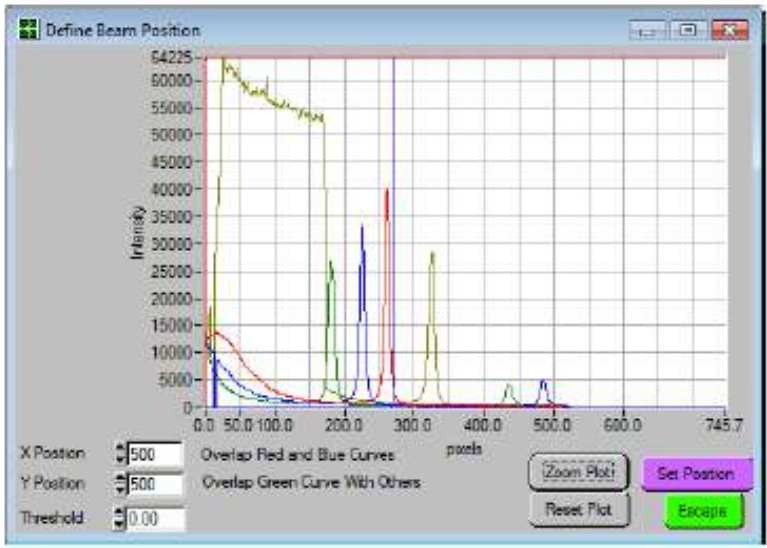

At beam center

Peak positions overlap well

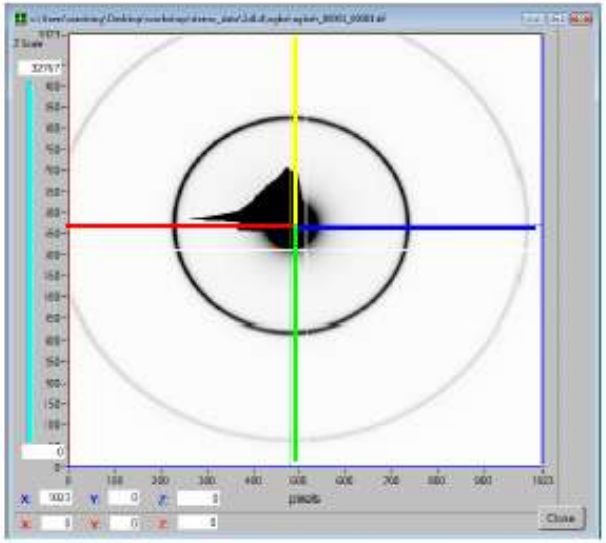

Scattering image of silver behenate

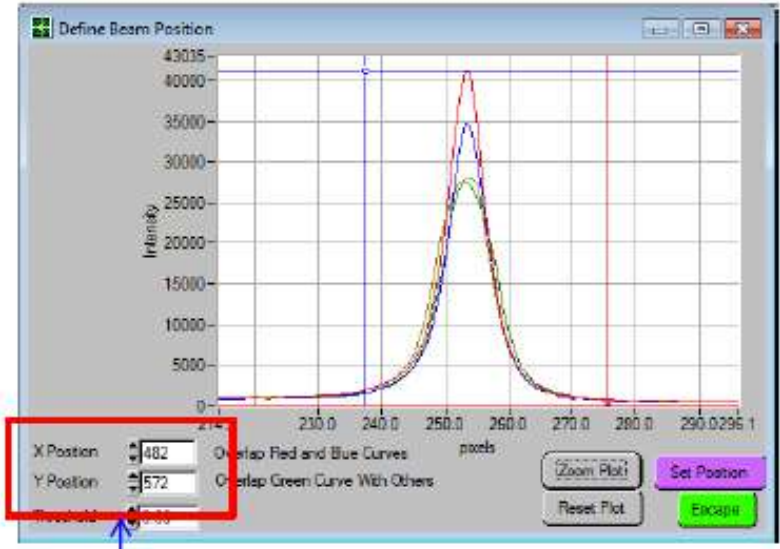

position of beam center on detector

q-calibrants and sample-to-detector distance

Primary q-calibrant standards in X-ray scattering:

standards	d-spacing (Å)	First harmonic peak ($Å^{-1}$)
Silver behenate (IUCr standard, most popular)	58.380	0.1076 0.1076 x N (N≤10, Nth peak)
Cholesterol Myristate	51.1	0.1230
Wet Rat Tail Collagen	650-670	~0.01
Anatase (TiO_2)	3.51	1.790

Using q-calibrant to determine sample-to-detector distance:

$$q = (4\pi / \lambda)\sin\theta$$

$$2\theta = \mathrm{atan}(r / d)$$

d: sample-to-detector distance

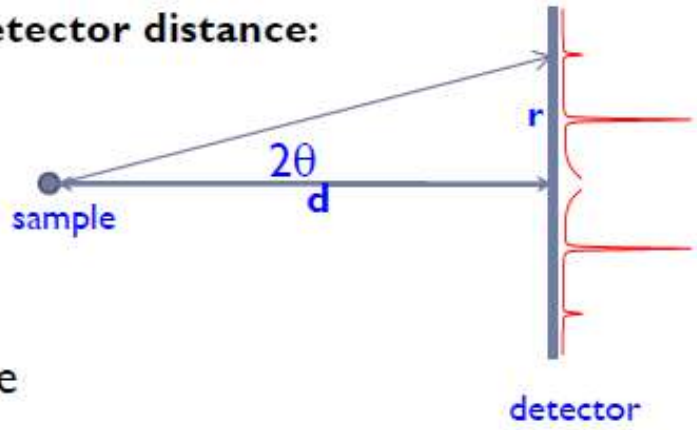

q value calibration/mapping

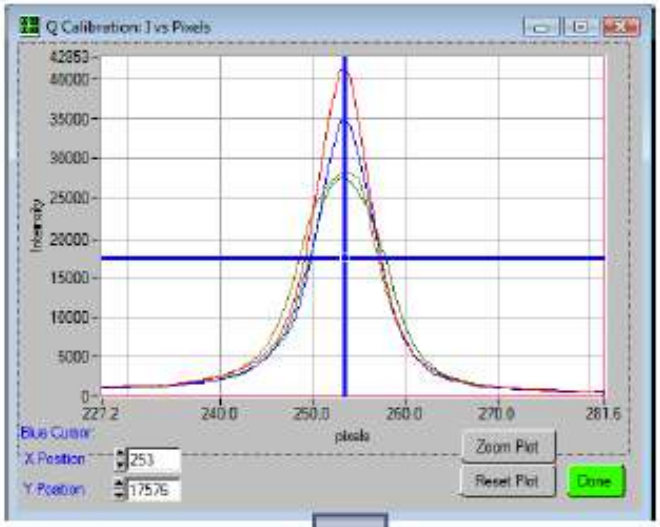

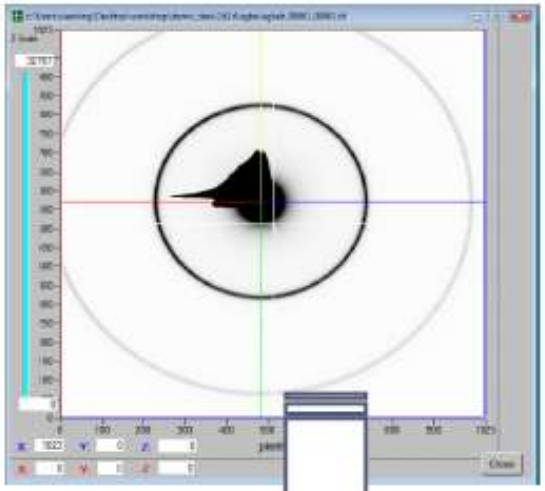

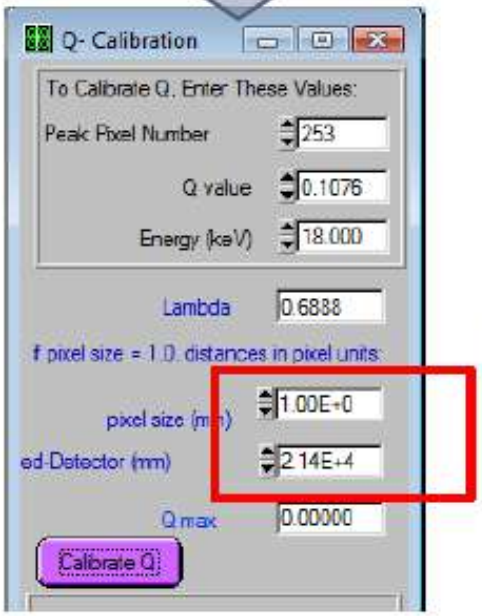

Sample-to-detector distance

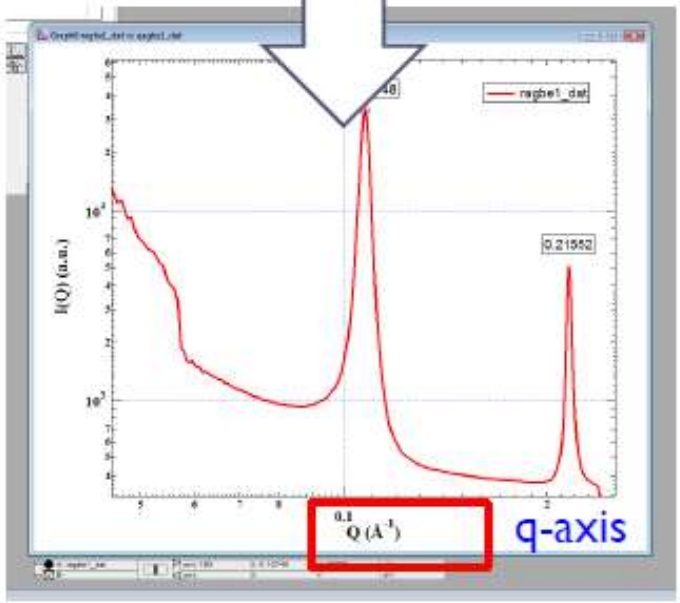

Every time sample-to-detector distance is changed, q-mapping need to redo.

Image Mask and zinger removal

Mask:

- detector responses nonlinearly beyond a threshold,
  - Gold detector at 12-ID: 44k
  - Marccd165: 65k
- High intensity at low q could be due to too long exposure time, diffraction from slits, fluorescence from beam stop, etc
- High intensity spots at higher q could come form diffraction of front mica window
- Mask out nonlinear pixels

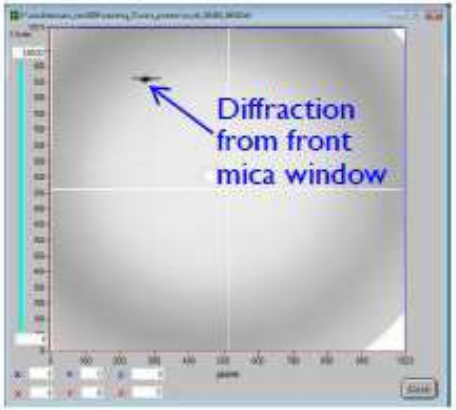

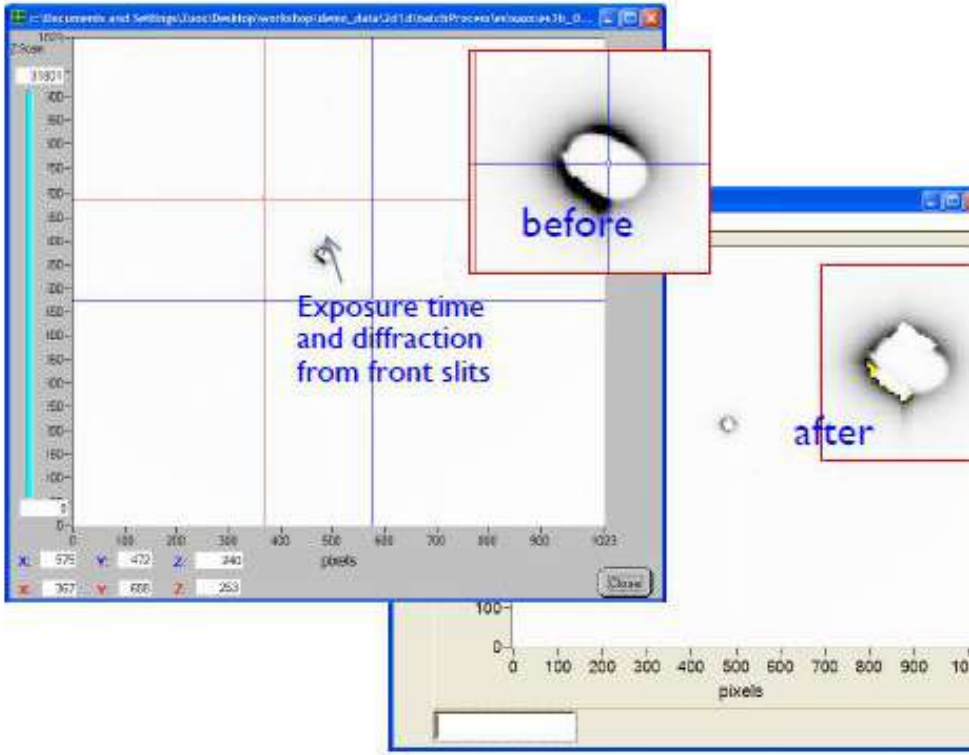

Zinger removal:

- Zinger: spots with intensity much higher than those of neighbor pixels
- Comes from diffractions, electronic noises, etc
- ignored if $|I(x,y)-I_{ave}|>6\sigma$

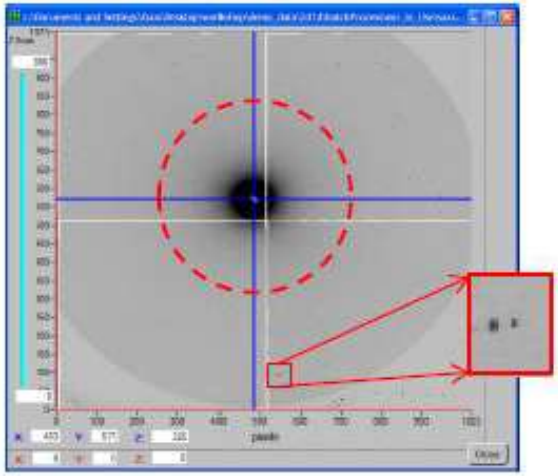

2D→1D data conversion

Data conversion flow chart:

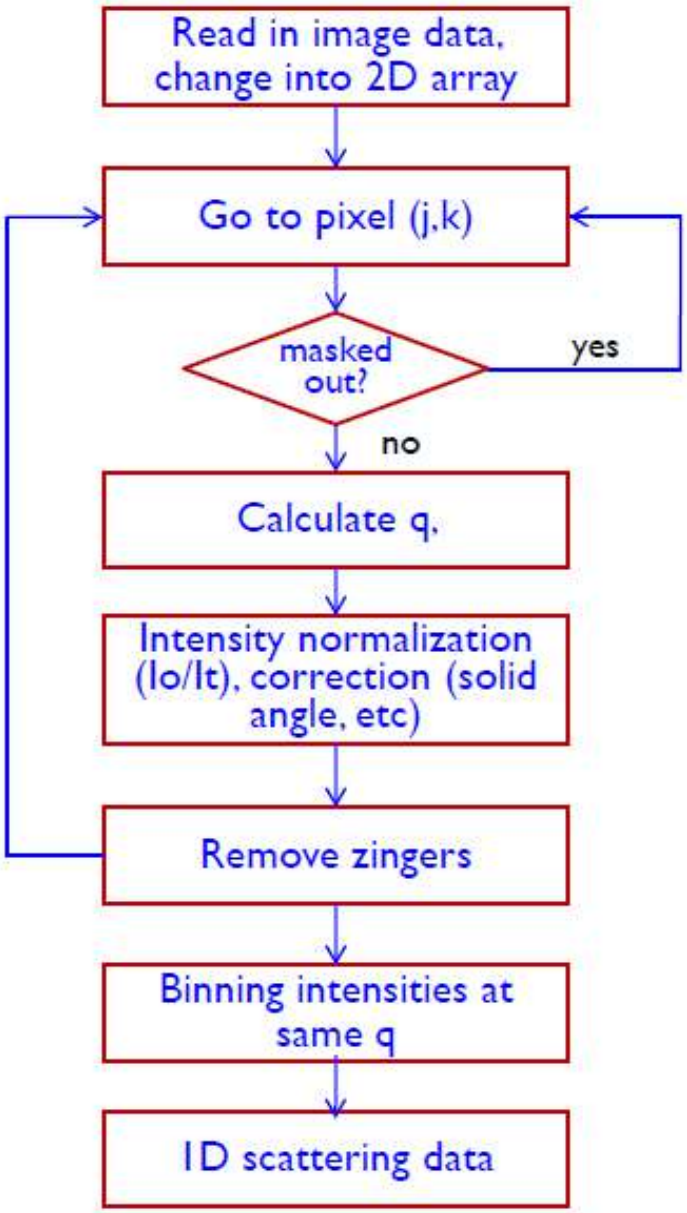

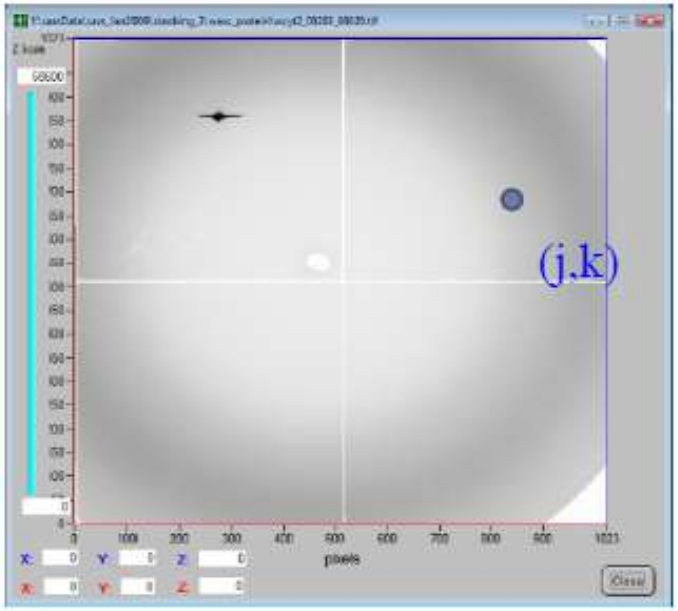

Image data structure:
1D (1kX1k) unsigned integer

X-ray detectors at 12-ID:
gold CCD detector: home-made, 2x2 CCD chips, square, data size 1024X1024
marCCD165 detector: round, 1024X1024

Software

Fit2D

http://www.esrf.eu/computing/scientific/FIT2D/

SASFit

http://kur.web.psi.ch/sans1/SANSSoft/sasfit.html

ATSAS

http://www.embl-hamburg.de/biosaxs/software.html

Igor Routines

http://usaxs.xor.aps.anl.gov/staff/ilavsky/irena.html

Etc....

SAXS + GI

GISAXS

SAXS (transmission)

both allow us to study very small objects (nanometer scale range)

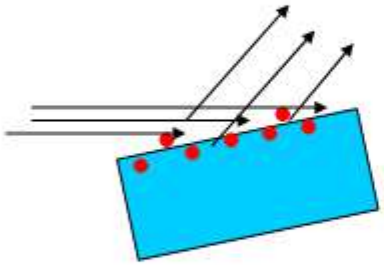

small information depth is required (5 to few hundred of nanometers from top surface)

incidence and/or exit angles of the radiation must be comparable to the critical angle α_c

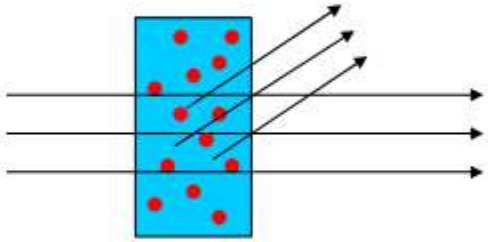

information is obtained over the entire irradiated volume sample

incidence normal to the sample surface

Why GISAXS?

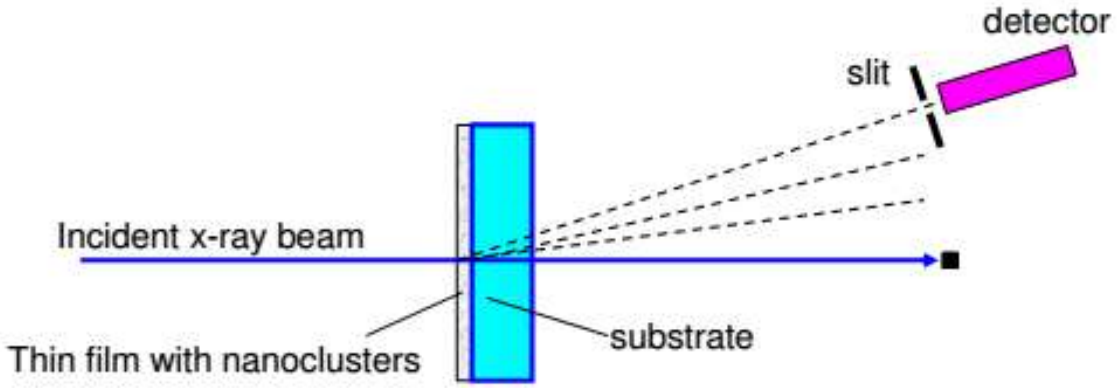

Limitations:

- *low signal-to-background ratio*
- *low signal from thin layer film (SAXS Intensity ∝ irradiated volume of the sample)*
- *substrate absorption*
- *modification of the thin layer consequence of substrate thinning processes*
- *sometimes thinning is not possible*

Optimization of the scattering intensity

$I_{mesured} = I(q)ste^{-\mu(E,z_i)t}$ scattered intensity: dependence with sample thickness

s t: Irradiated volume
- s: beam cross section area
- t: sample thickness

$I_0/I_t = e^{-\mu(E,z_i)t}$ sample attenuation
- μ: lineal absorption coefficient
- E: photon energy
- z_i: atomic number of element i

$I_{measured} = I(q)ste^{-\mu t}$

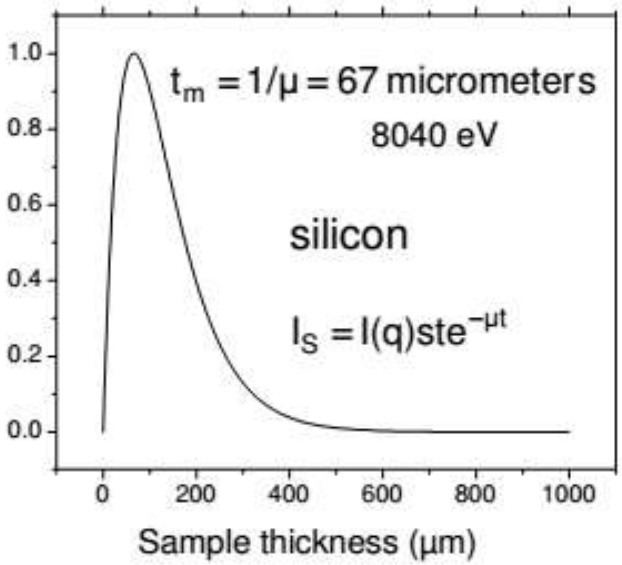

Typical experimental setup

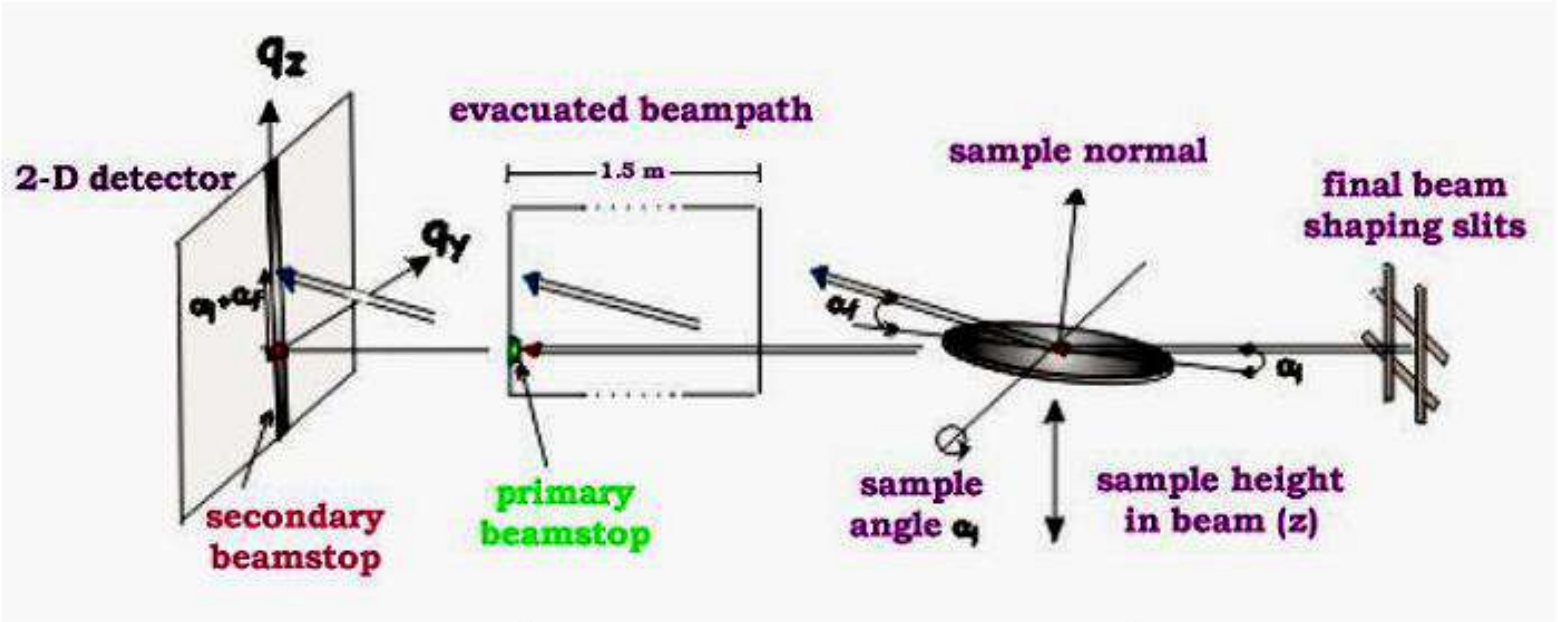

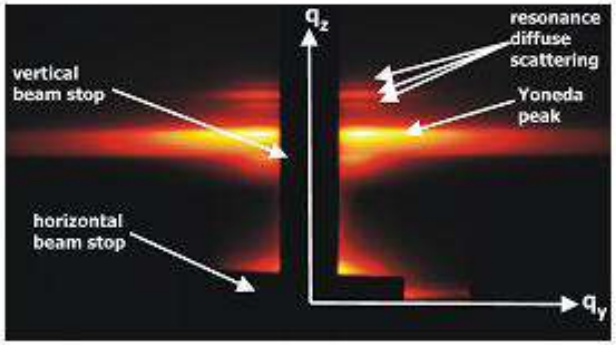

Geometry and some theoretical considerations

(Grazing Incidence Small Angle X-ray Scattering)

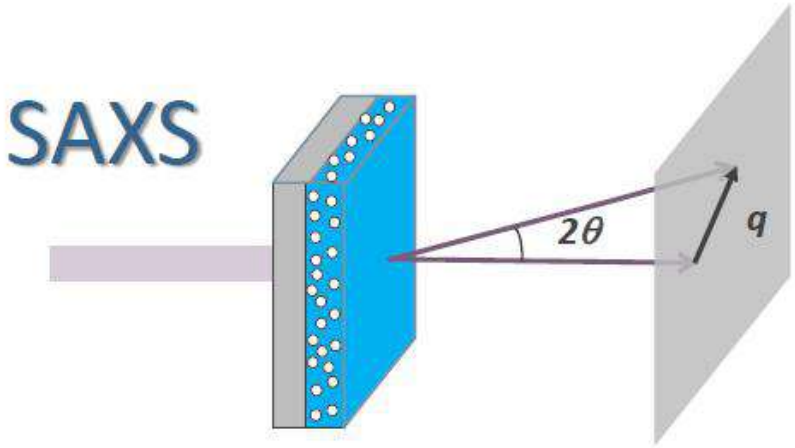

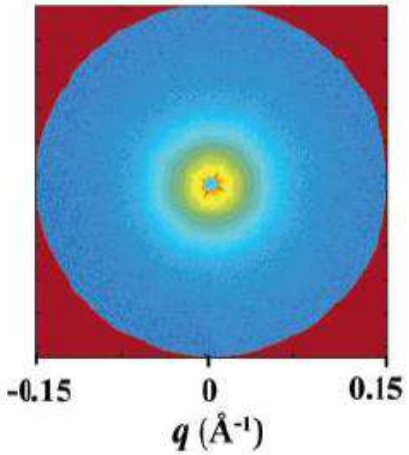

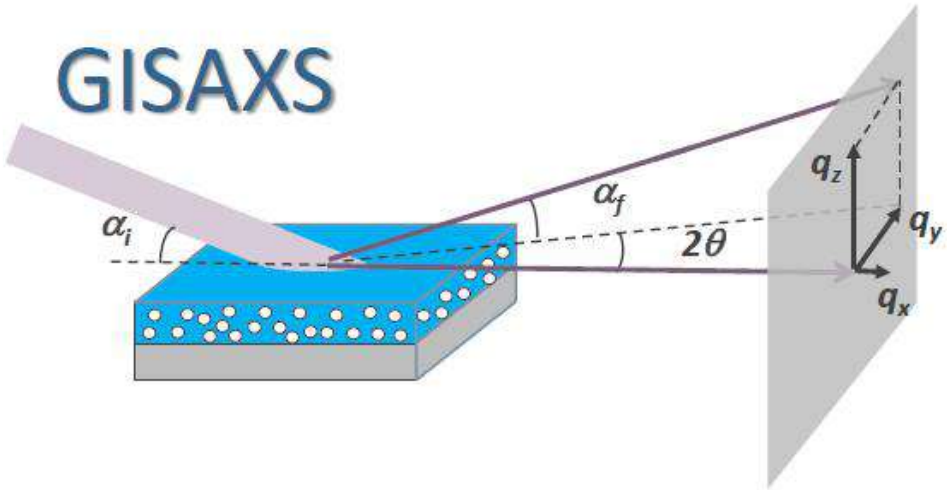

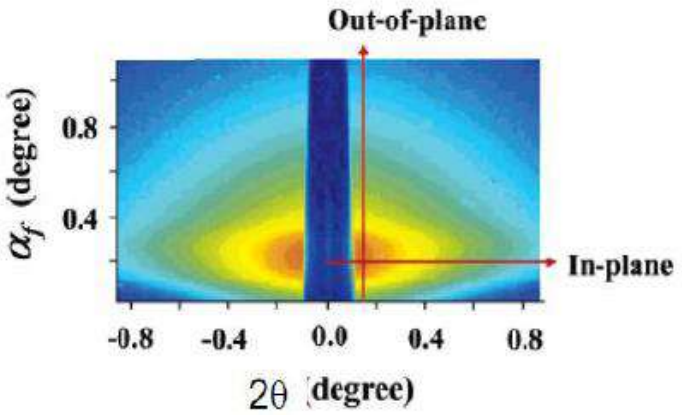

Grazing-incidence x-ray scattering (GIXS) geometry

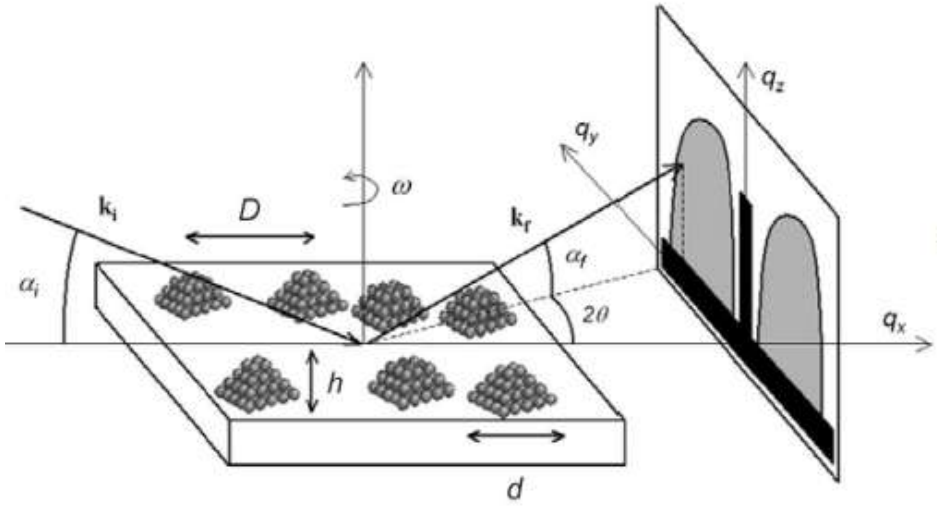

Wave vector transfer in sample reference frame:

$$q = \begin{pmatrix} q_x \\ q_y \\ q_z \end{pmatrix} = \frac{2\pi}{\lambda} \begin{pmatrix} \cos(\alpha_f)\cos(2\theta) - \cos(\alpha_i) \\ \cos(\alpha_f)\sin(2\theta) \\ \sin(\alpha_f) + \sin(\alpha_i) \end{pmatrix}$$

True q (for the scattering/diffraction) will be different due to reflection and refraction effects.

Reflection and refraction

Index of refraction

$n \geq 1$

$$n = 1 - \delta + i\beta$$

$$n \approx 1 - \frac{\lambda^2}{2\pi} r_e \rho + i \frac{\lambda}{4\pi} \mu$$

$$0 < \mathrm{Real}[n] \leq 1$$

Light

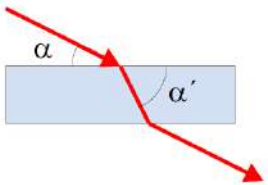

X-rays

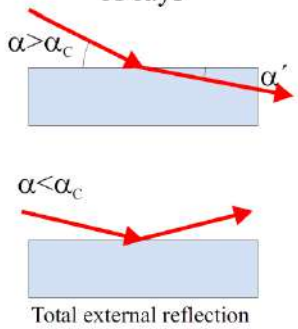

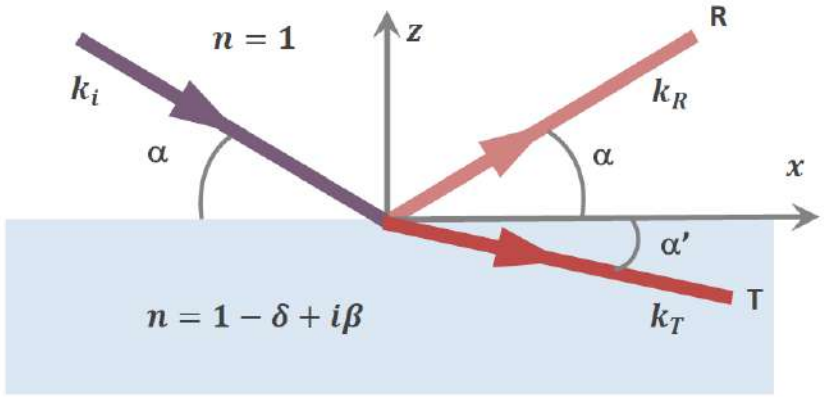

Snell's law: $\cos\alpha = n\cos\alpha'$

Critical angle for total external reflection (α'=0): $\alpha_c = \cos^{-1} n \approx \sqrt{2\delta}$

Typical $\delta \sim 10^{-5}$, so $\alpha_c \sim 0.1° - 0.5°$

Wave vector transfer for reflected beam $q_z = 2k\sin(\alpha)$

Evanescent wave and penetration depth

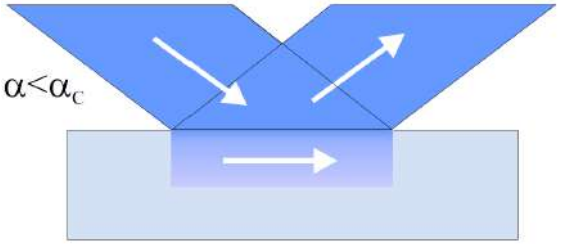

Penetration depth on Si surface with λ=1.54A

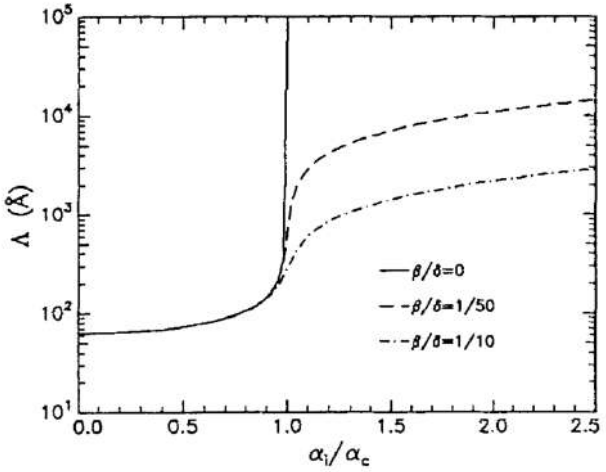

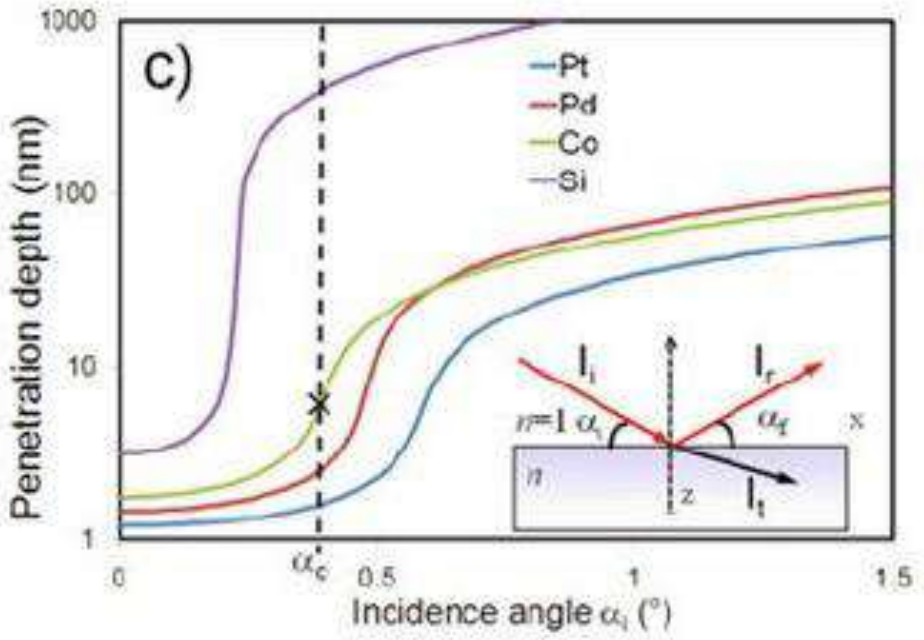

Supported nano-objects

$$\left(\frac{d\sigma}{d\Omega}\right)_{\text{diff}} = r_e^2 |\Delta\rho|^2 \left|\mathcal{F}\left(q_{||}, k_z^i, k_z^f\right)\right|^2$$

$$\mathcal{F}\left(q_{||}, k_z^i, k_z^f\right) = F\left(q_{||}, q_z^1\right) + r(\alpha_f) F\left(q_{||}, q_z^2\right) + r(\alpha_i) F\left(q_{||}, q_z^3\right) + r(\alpha_i) r(\alpha_f) F\left(q_{||}, q_z^4\right)$$

Born approximation

1

$q_z^1 = k_z^f - k_z^i$

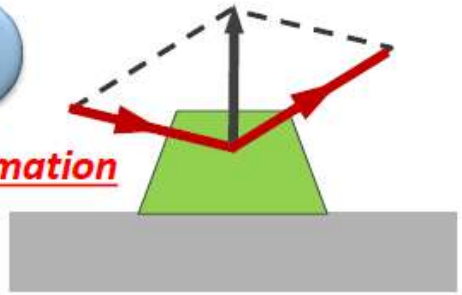

2

$q_z^2 = -k_z^f - k_z^i$

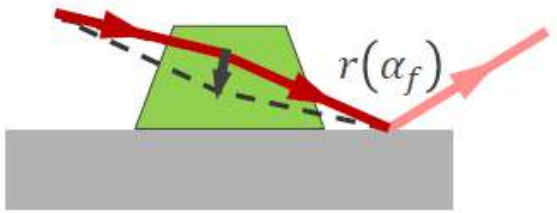

3

$q_z^3 = k_z^f + k_z^i$

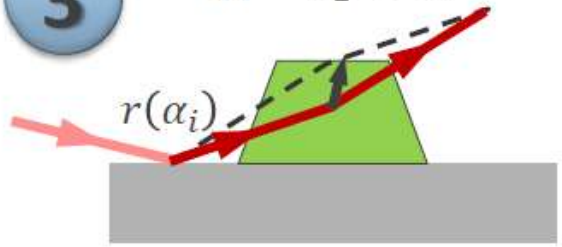

4

$q_z^4 = -k_z^f + k_z^i$

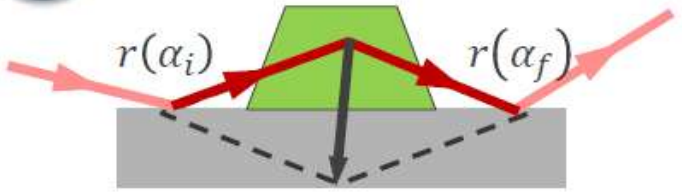

Supported nano-objects

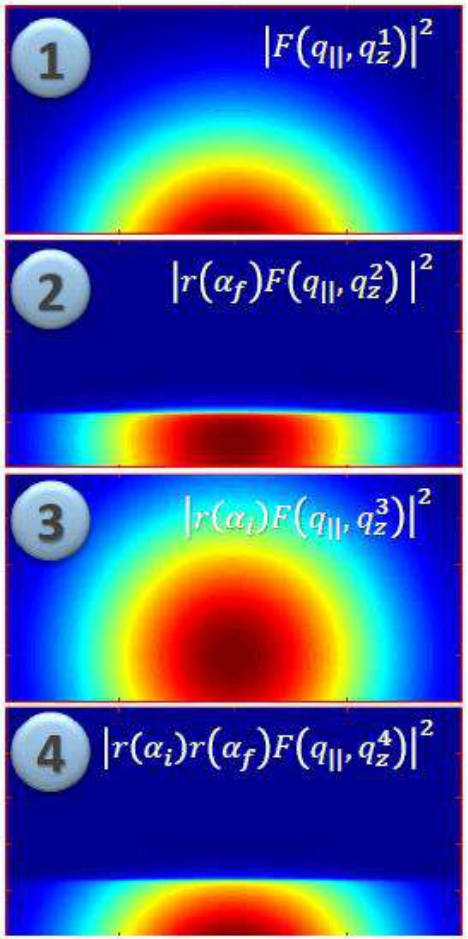

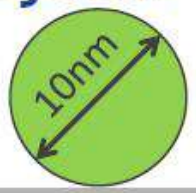

E=7.35 keV

Si substrate

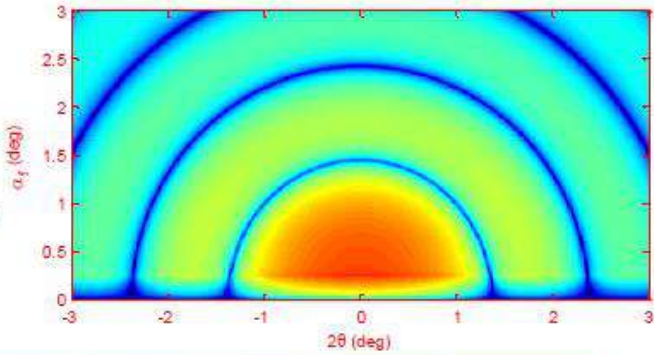

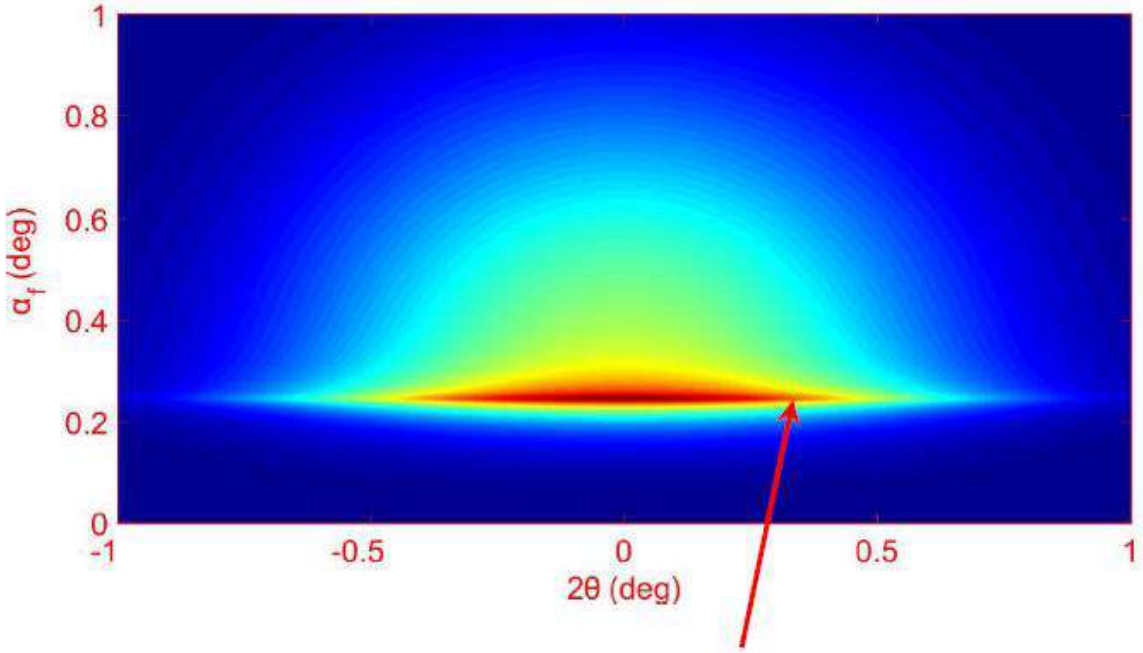

$\alpha_f = \alpha_c$ of silicon: Yoneda peak

Buried structures

$$\psi(\boldsymbol{r},\boldsymbol{k}) = e^{i\boldsymbol{k}_{||}\cdot\boldsymbol{r}_{||}} \begin{cases} e^{-ik_{z,1}z} + R_1 e^{ik_{z,1}z} & \text{for } z > 0 \\ T_2 e^{-ik_{z,2}z} + R_2 e^{ik_{z,2}z} & \text{for } -d < z < 0 \\ T_3 e^{-ik_{z,3}z} & \text{for } z < -d \end{cases}$$

$$\mathcal{F}(q_{||}, k^i_{z,1}, k^f_{z,1}) = T_2(k^f_{z,2})T_2(k^i_{z,2})F(q_{||}, q^1_{z,2}) + R_2(k^f_{z,2})T_2(k^i_{z,2})F(q_{||}, q^2_{z,2}) + T_2(k^f_{z,2})R_2(k^i_{z,2})F(q_{||}, q^3_{z,2}) + R_2(k^f_{z,2})R_2(k^i_{z,2})F(q_{||}, q^4_{z,2})$$

1

$$q^1_{z,2} = k^f_{z,2} - k^i_{z.2}$$

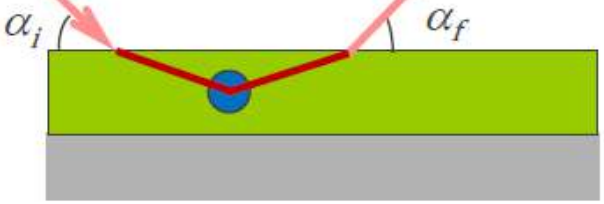

2

$$q^2_{z,2} = -k^f_{z,2} - k^i_{z.2}$$

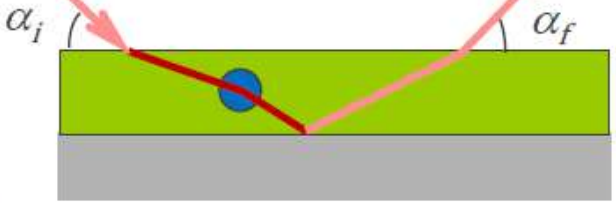

3

$$q^3_{z,2} = k^f_{z,2} + k^i_{z.2}$$

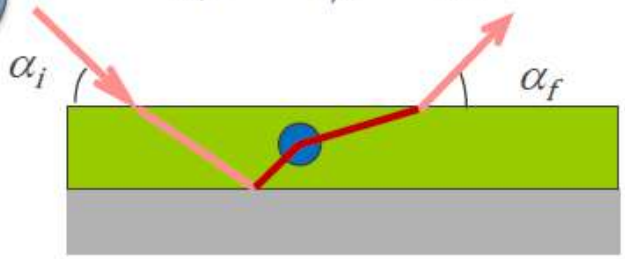

4

$$q^4_{z,2} = -k^f_{z,2} + k^i_{z.2}$$

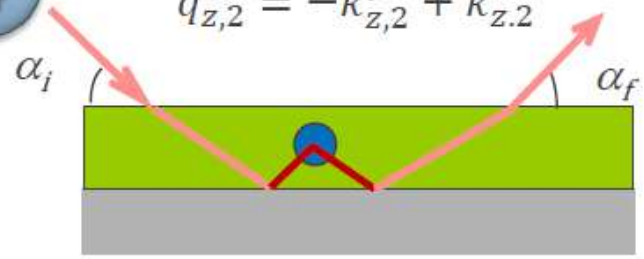

1 2 $$\alpha_f = \arcsin\sqrt{\left(\frac{q_z}{k}\right)^2 + \sin^2\alpha_i - \frac{2q_z}{k}\sqrt{n^2 - 1 + \sin^2\alpha_i}}$$

3 4 $$\alpha_f = \arcsin\sqrt{\left(\frac{q_z}{k}\right)^2 + \sin^2\alpha_i + \frac{2q_z}{k}\sqrt{n^2 - 1 + \sin^2\alpha_i}}$$

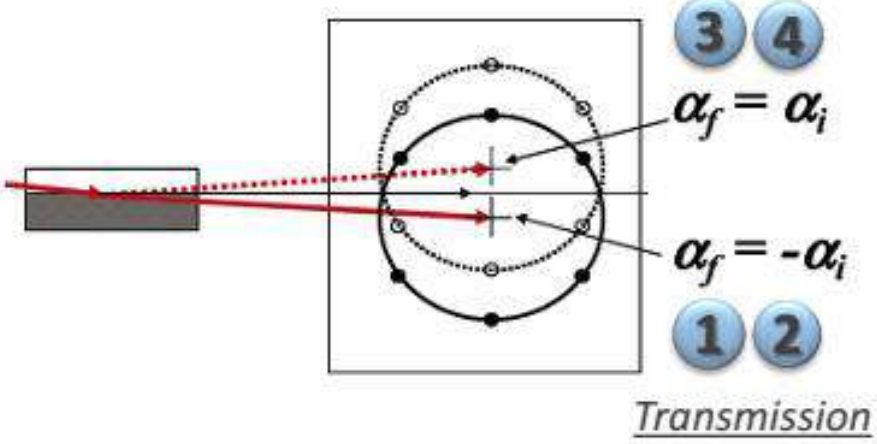

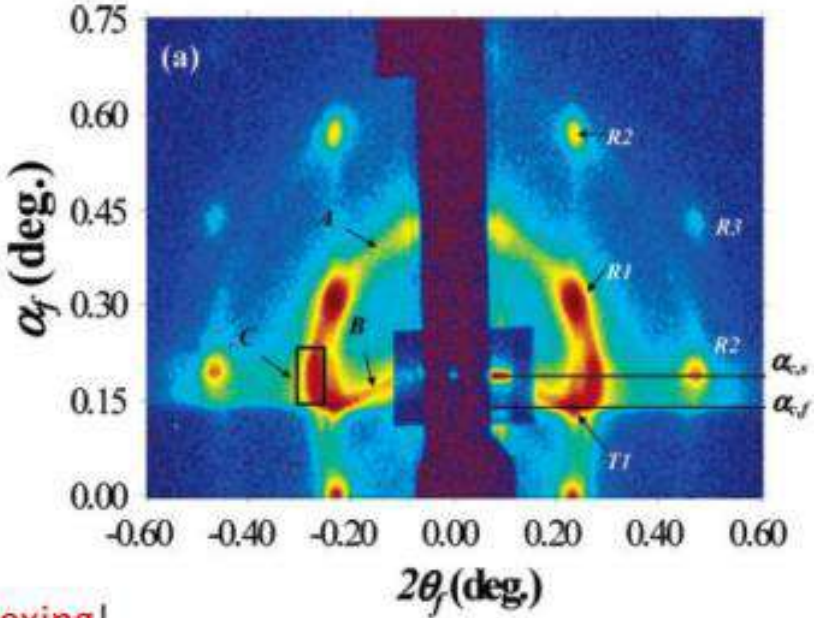

Important for substrate supported 3D structure indexing!

B. Lee et al, Macromolecules 38, 4316 (2005)

- DWBA fundamental (single rough interface)
  - Sinha, et al., Phys. Rev. B 38, 2297 (1988)
- Multiple rough interfaces
  - Holy et al., Phys. Rev. B 47, 15896 (1993); 49, 10668 (1994)
- Supported nano-objects
  - Rauscher et al, J. Appl. Phys. 86, 6763 (1999) (IsGISAXS)
  - Lazzari, J. Appl. Cryst. 35, 406 (2001)
- Nanostructures in supported single layer film
  - Lee et al.,, Macromolecules 38, 3395 and 4311 (2005)
  - Tate et al., J. Phys, Chem. B 110, 9882 (2006)
- Depth-dependence structures in films
  - Babonneau et al., Phys. Rev. B 80, 155446 (2009)
  - Jiang, et al., Phys. Rev. B 84, 075440 (2011)
- Some GISAXS analysis softwares
  - IsGISAXS, FitGISAXS, BornAgain, HipGISAXS

Data analysis

- Qualitative interpretation
- Line cuts
- Modeling and fitting

Qualitative interpretation

- GISAXS makes this more complicated:
  - Refraction shifts and distorts reciprocal-space
  - Reflection leads to two sets of peaks

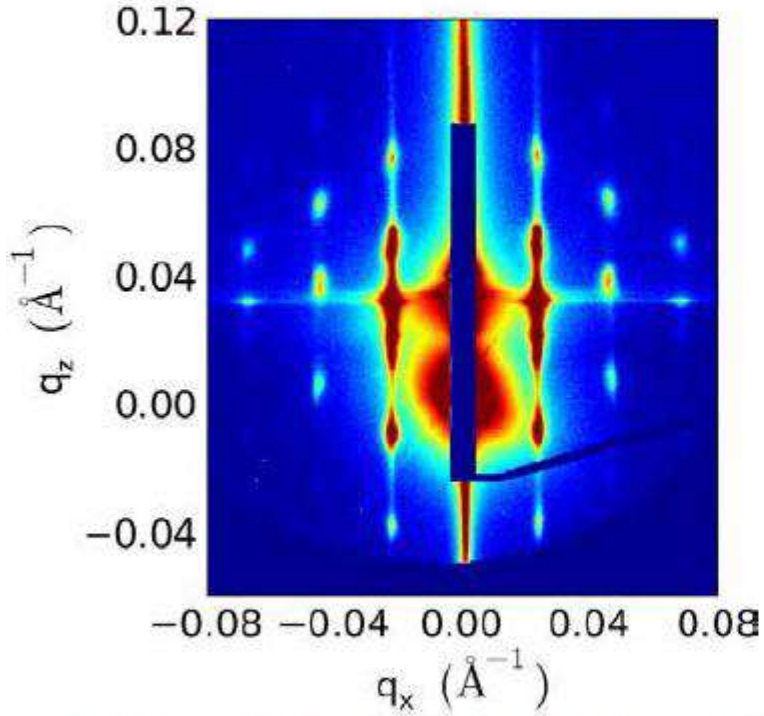

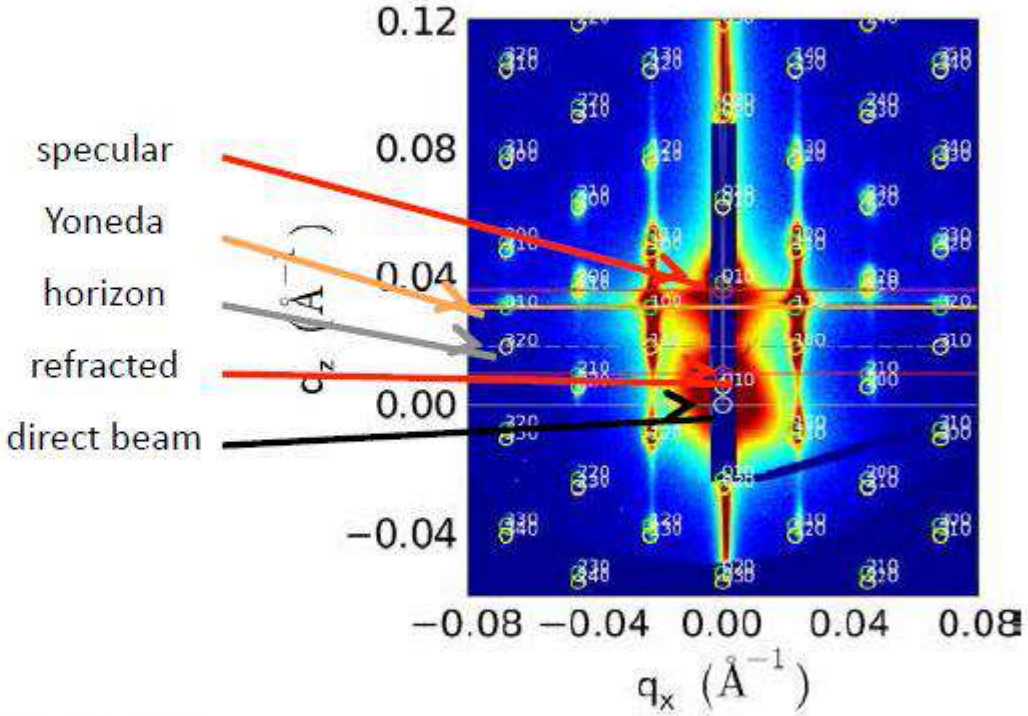

- You can use DWBA to predict peak positions
- So, you can index all the peaks, …

Singh *ACS Nano* **2012**, 17, 10335

- Block-copolymer cylinder phase

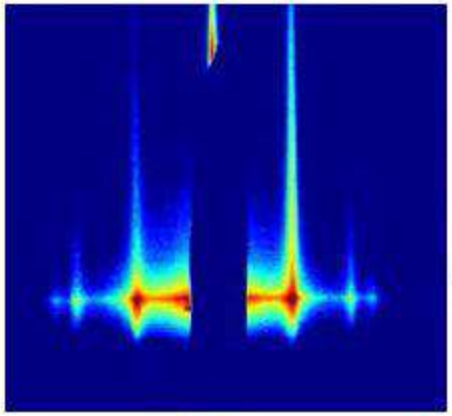

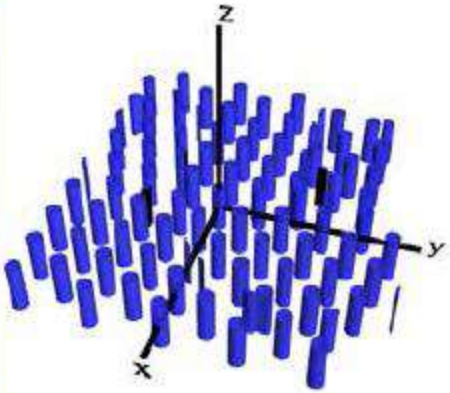

Note two rings

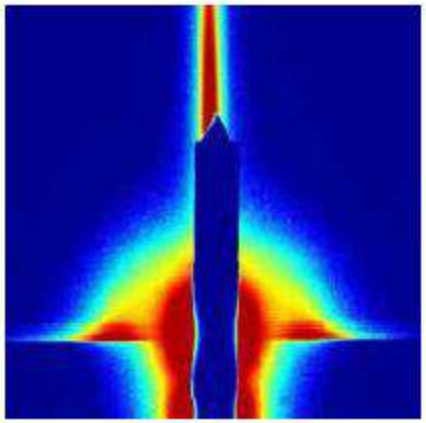

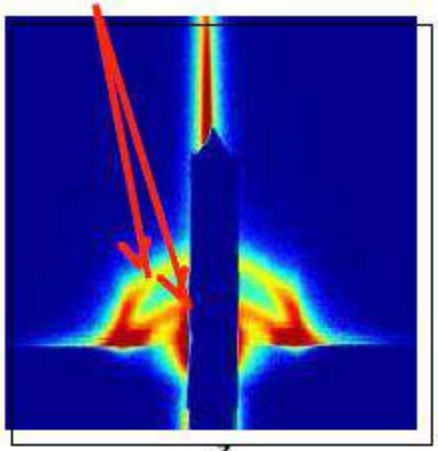

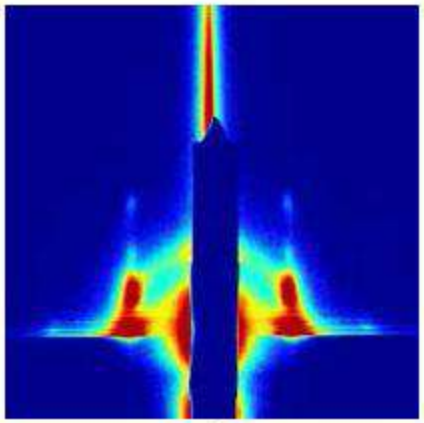

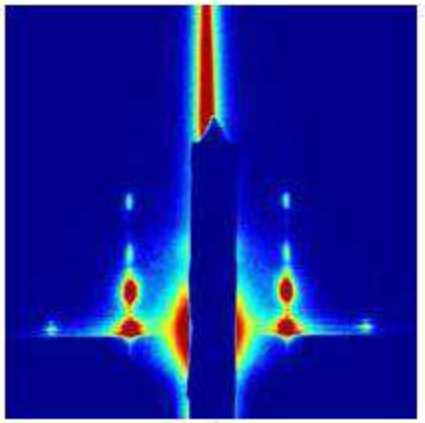

Disordered

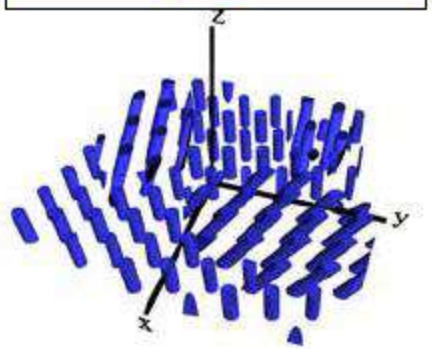

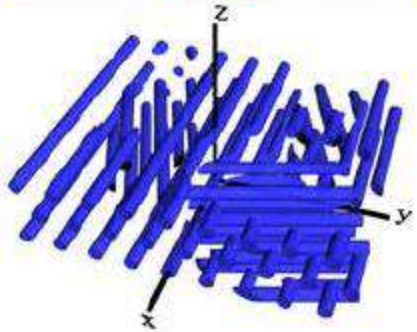

- Diffuse scattering comes from disorder, roughness…
- Halo usually means amorphous, sharp rings means good order (crystal?)
- Intensity along ring tells orientation
- Peaks becomes speckled as the grain size becomes very large
- An array of distinct peaks means crystal is well-oriented w.r.t. substrate
- If the peaks appear/disappear when you rotate, you may have a single crystal

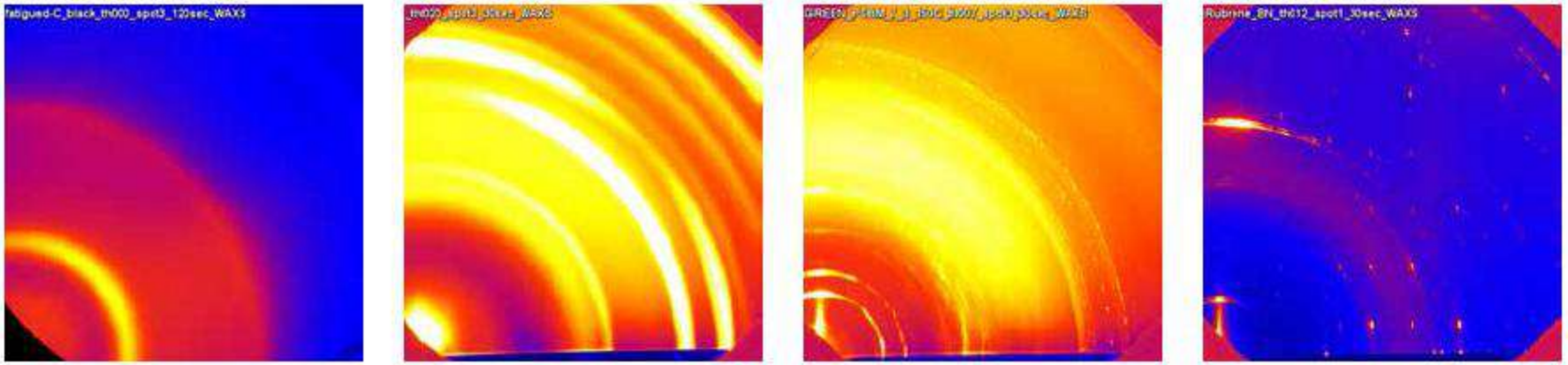

Line cuts

- Calibration converts from pixel to *q*
  - Detector distance
  - X-ray energy
  - Beam position
  - Detector orientation/tilt
- Adjust intensity
  - Beam flux and measurement time
  - Polarization, pixel acceptance, …
- Linecuts:
  - 1D radial average
  - Radial (in-plane, out-of-plane, other)
  - "Straight" (qz or qr,)
  - Along an arc
- Binning:
  - Average multiple pixels to improve SNR
  - Don't smear-out real features! (e.g. peak width)
  - Account for background!

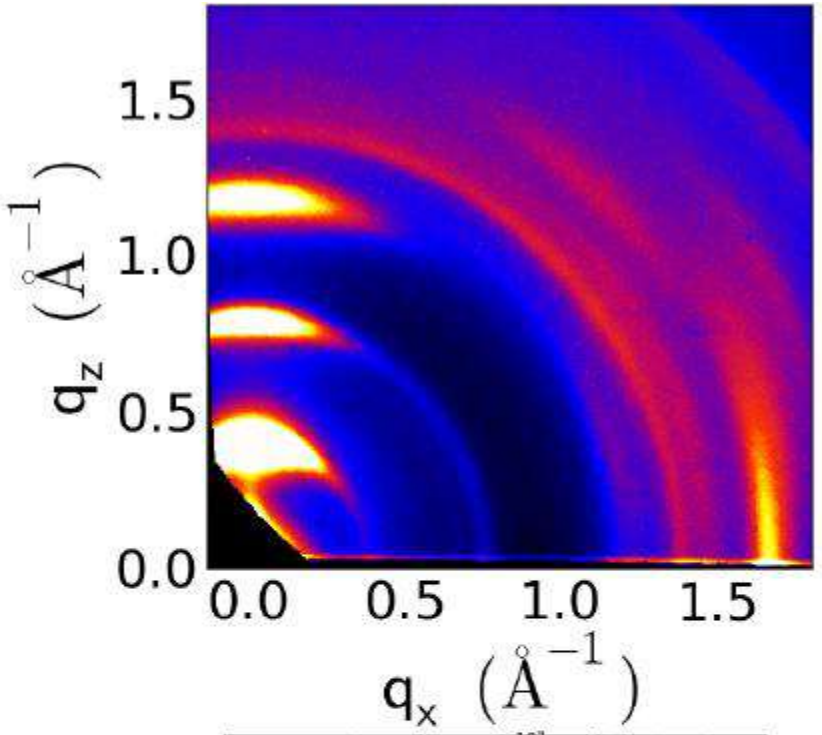

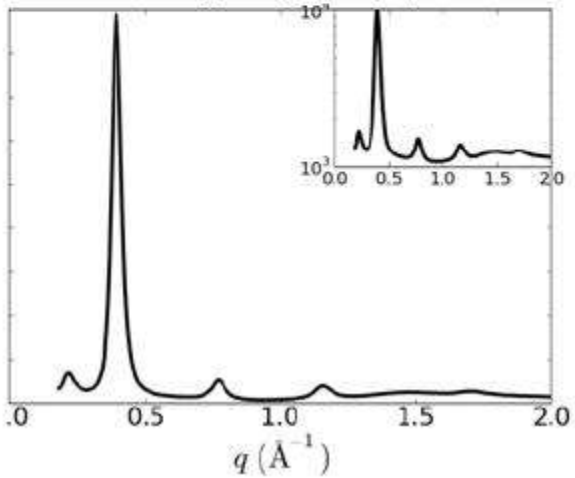

General interpretation of GISAXS data

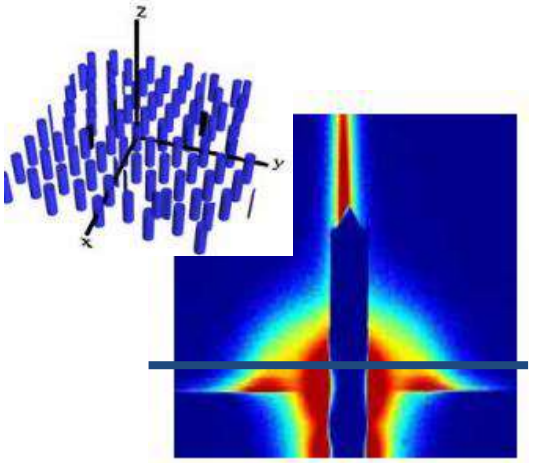

- Nanostructure morphology
  - Form factor *F*: size, shape, facet etc.
  - Structure factor *S*: inter-particle correlation
- General rule: scattering intensity $I \sim |F|^2 S$ (for both SAXS and GISAXS)
- Separation of form factor and structure factor
  - Diluted or disordered systems, the inter-particle correlation is weak, i.e., the interference function is nearly one
  - Concentrated system, particles are strongly correlated at small q values.
  - Quick analysis is not accurate.
  - To help model the data, experimentally one needs to measure
    - away from the origin of the reciprocal space, i.e. high q
    - over several orders of magnitude in q (with clean background)

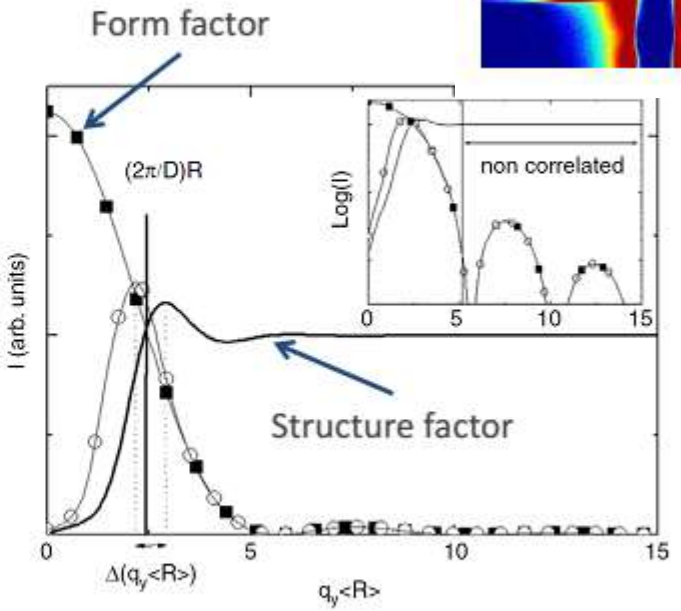

In-plane linecut (q_y) for disordered vertical cylinders on a substrate

$$\left(\frac{d\sigma}{d\Omega}\right) \propto \left\langle \left| \sum_{r_j} f_j(\boldsymbol{Q}) e^{i\boldsymbol{Q}\cdot\boldsymbol{r}} \right|^2 \left| \sum_{R_n} e^{i\boldsymbol{Q}\cdot\boldsymbol{R}_n} \right|^2 \right\rangle = \langle |F(\boldsymbol{Q})|^2 \rangle S(\boldsymbol{Q})$$

- F is the form factor; S is the structure factor to describe the statistical position correlation between particles.

Dilute nanoparticles

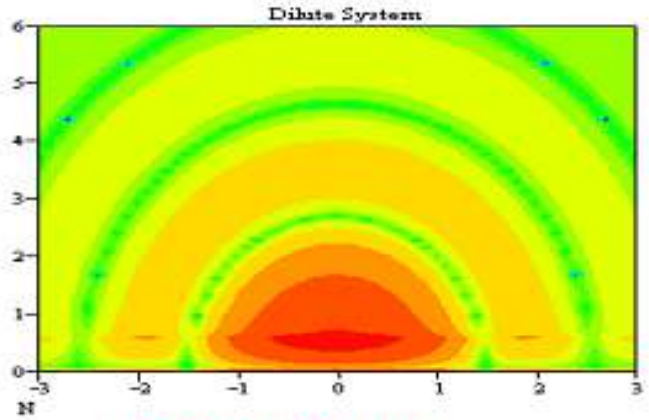

Byeongdu Lee

2D monolayer of nanoparticles

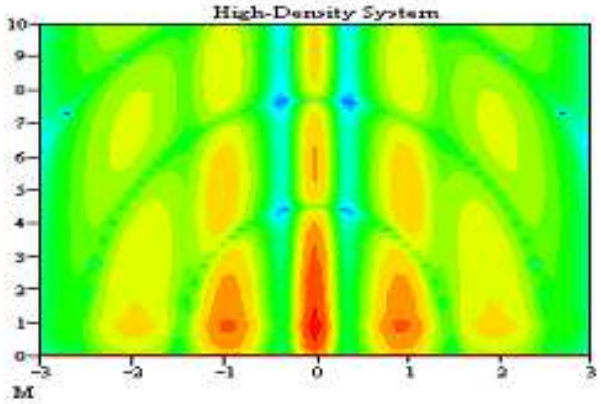

Zhang Jiang

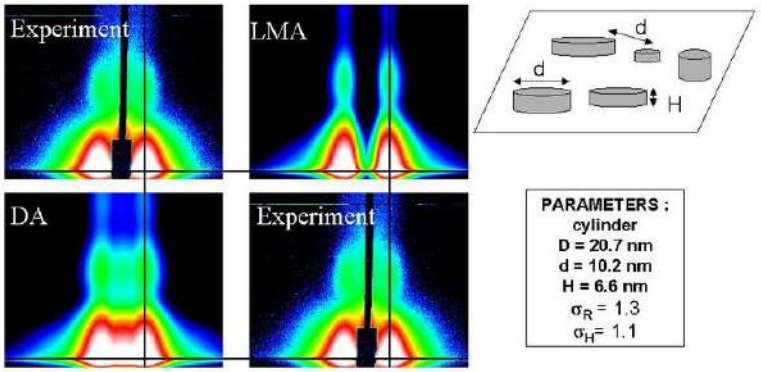

Fig. 2 : Simulation of a GISAXS pattern obtained for a 3nm thick deposit of Pd on MgO(100)@700K. The layer is simulated by a disordered set of cylindrical islands with a log-normal size distributions. The obtained parameters are given in the right panel and compare well with ex situ transmission electron microscopy experiments .

The same procedure was applied to different cuts along the vertical direction

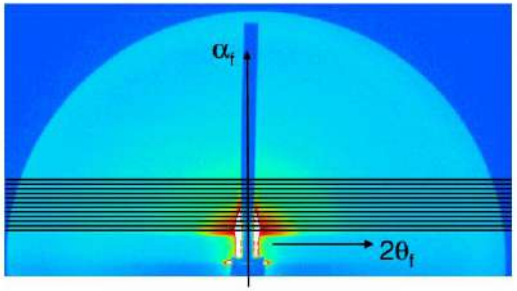

The lines correspond to horizontal cuts along which the scattering profiles are obtained

Experimental GISAXS curves

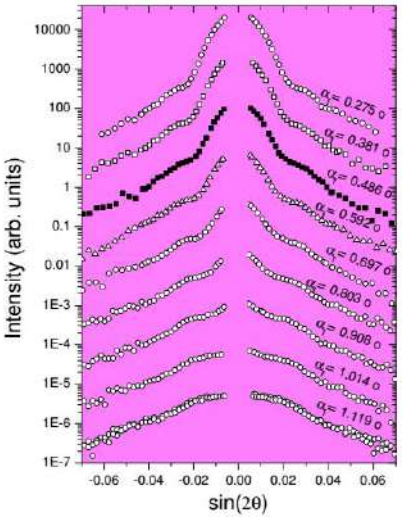

Tabulated Form Factors:

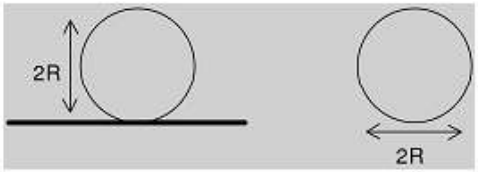

sphere

$$F_{fsp}(\mathbf{q}, R) = 4\pi R^3 \frac{\sin(qR) - qR\cos(qR)}{(qR)^3} \exp(-iq_z R)$$

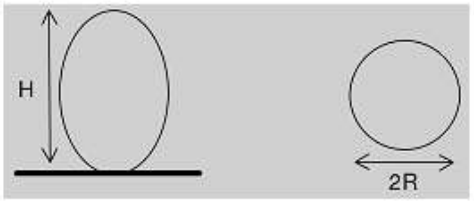

prolate spheroid

$$F_{fsph}(\mathbf{q}, R, H) = \exp(-iq_z H/2) \int_0^{H/2} 4\pi R_z^2 \frac{J_1(q_\parallel R_z)}{q_\parallel R_z} \cos(q_z z)\, dz$$

$$q_\parallel = \sqrt{q_x^2 + q_y^2},\ R_z = R\sqrt{1 - 4\frac{z^2}{H^2}}$$

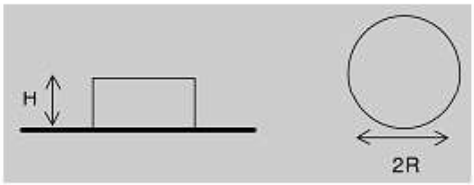

cylinder

$$F_{cy}(\mathbf{q}, R, H) = 2\pi R^2 H \frac{J_1(q_\parallel R)}{q_\parallel R} \mathrm{sinc}(q_z H/2) \exp(-iq_z H/2)$$

$$q_\parallel = \sqrt{q_x^2 + q_y^2}$$

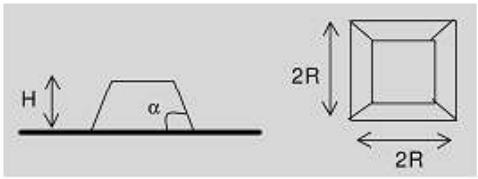

pyramid

$$F_{py}(\mathbf{q}, R, H, \alpha) = \int_0^H 4R_z^2 \mathrm{sinc}(q_x R_z)\mathrm{sinc}(q_y R_z) \exp(-iq_z z)\, dz$$

$$R_z = R - z/\tan(\alpha)$$

$$H/R < \tan(\alpha)$$

tetrahedron

$$F_{te}(\mathbf{q}, R, H, \alpha) =$$

$$\int_0^H \frac{2i\sqrt{3}}{q_x(q_x^2 - 3q_y^2)} [q_1 \sin(q_2 R_z/2) \exp(iq_x R_z/2) - q_2 \sin(q_1 R_z/2) \exp(-iq_x R_z/2)] \exp(-iq_z z) dz$$

$$q_1 = \sqrt{3}q_y - q_x,\ q_2 = \sqrt{3}q_y + q_x,\ R_z = R - 2z/\sqrt{3}\tan(\alpha)$$

$$H/R < \sqrt{3}/2 \tan(\alpha)$$

The Fourier transform of the shape (electron density distribution)

$$\int \rho(\boldsymbol{r}) e^{i\boldsymbol{Q}\cdot\boldsymbol{r}} d\boldsymbol{r}$$

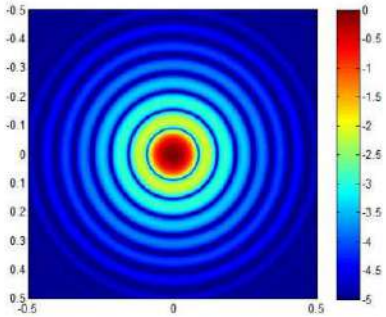

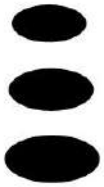

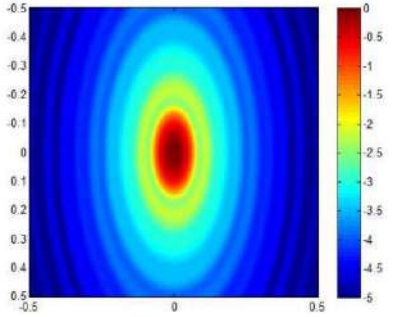

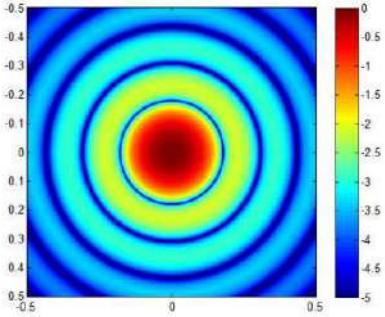

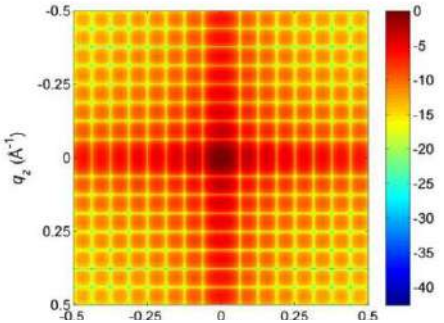

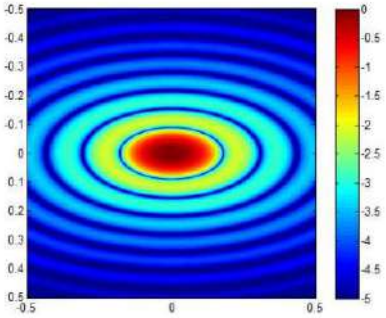

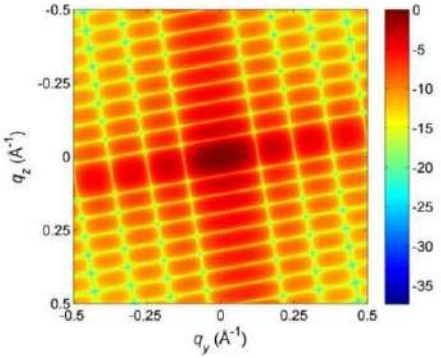

The size distribution model

- Gaussian
- Double Gaussian for the bimodal distribution.
- Log-normal
- Double Log-normal for the bimodal distribution.
- Weibull
- Schultz-Zimm function

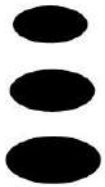

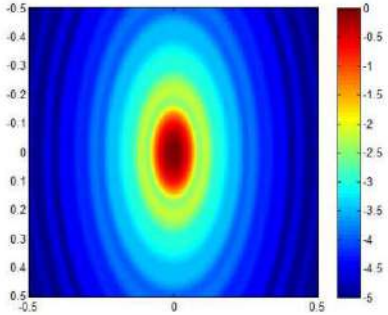

The structure factors

- Random organization: S(q) = 1
- Percus-Yevick 3D : Hard sphere potential
- Percus-Yevick 2D

- Paracrystal 1D
- Paracrystal 2D rectangular
- Paracrystal 2D hexagonal

- And many others.. See IsGISAXS manuals.

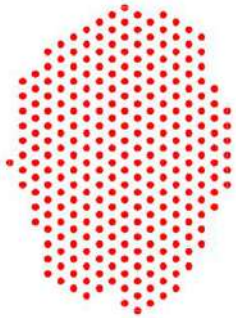

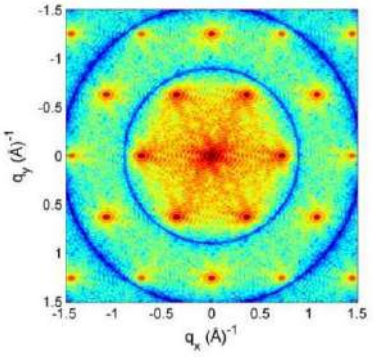

Real Time Monitoring Changes in Distance between Surfactant-coated Au Nanoparticles upon Sensing Volatile Organic Compounds (VOCs).

M.C. Dalfovo, L. J. Giovanetti, J.M. Ramallo-López, F.G. Requejo, F.J. Ibañez

Instituto de Investigaciones Fisico-Químicas Teóricas y Aplicadas (INIFTA),
FCE, UNLP – CONICET. La Plata, ARGENTINA.

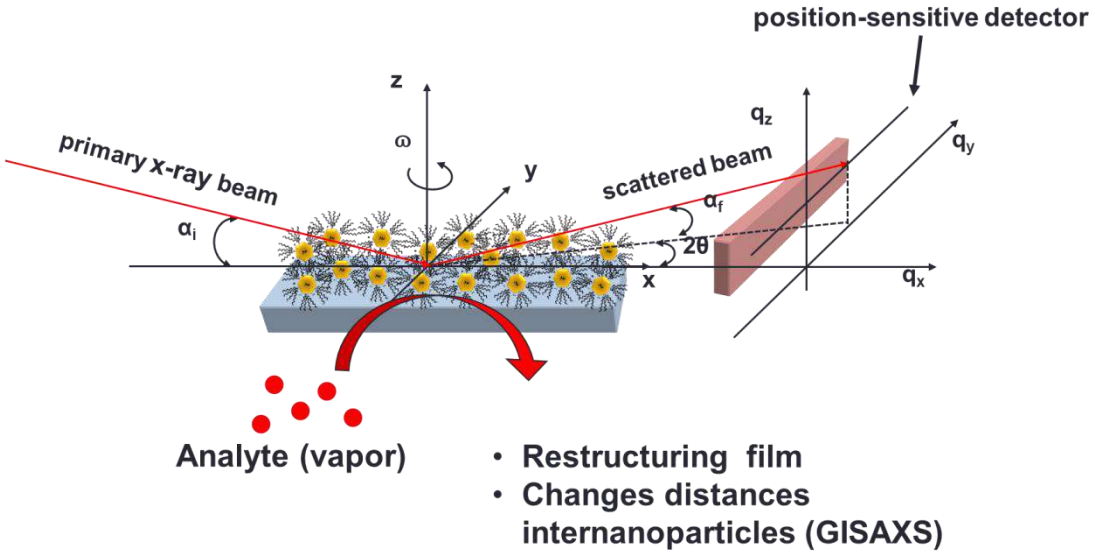

•Interest and goals: VOCs Sensors

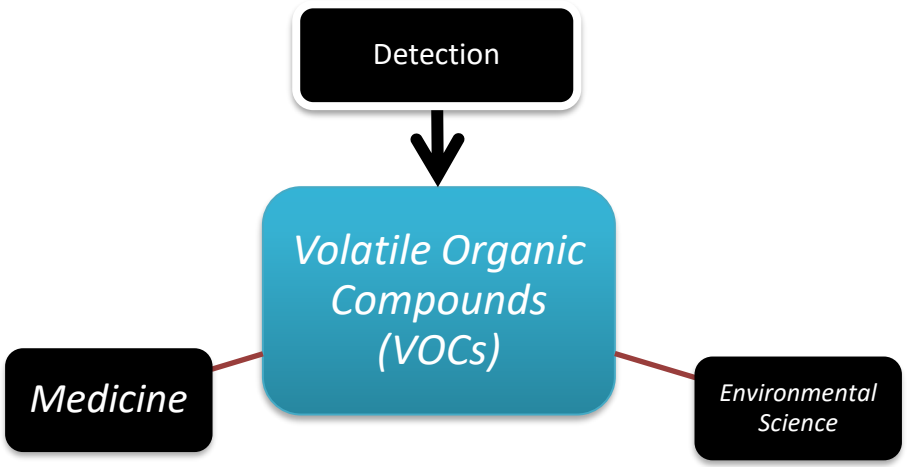

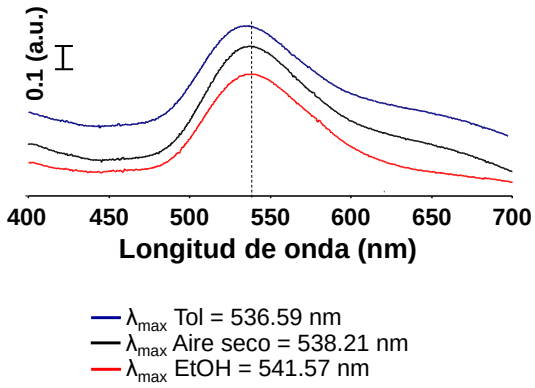

Current changes= *electron hopping*

$$\sigma_{EL} = \sigma_0 \exp[-\beta_d \delta_{edge}] \exp[-E_A/RT]$$

$$E_A \approx N_A e^2 \delta_{edge} / \varepsilon_s \varepsilon_0 R_{core} (R_{core} + \delta_{edge})$$

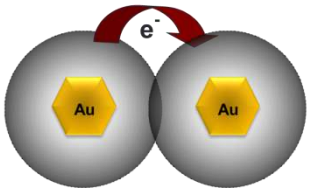

Chemiresistive sensors

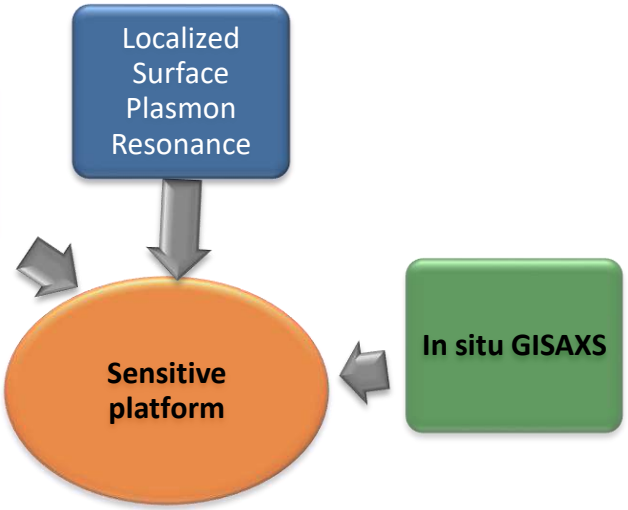

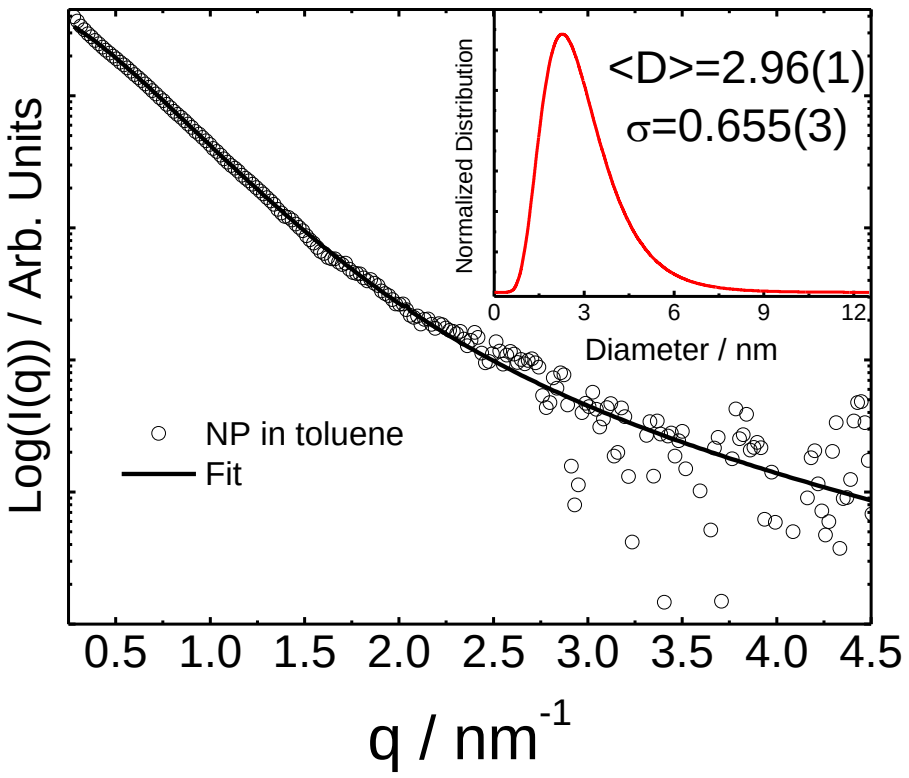

Fit assuming spherical NP with a LogNormal size distribution plus a polynomial background correction. This last contribution is associated to a possible depletion zone around the NP surface

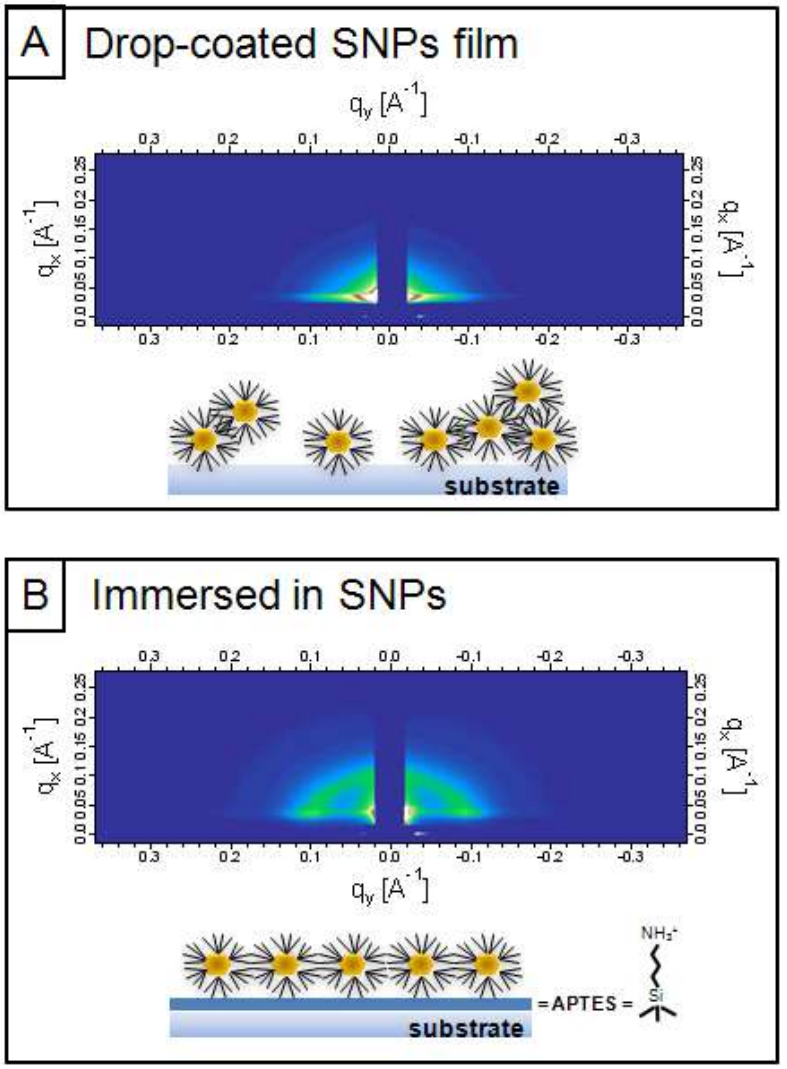

GISAXS patterns of drop-coated (a) and immersed (b) SNPs into APTES-functionalized Si substrate along with cartoons representing the outcome from film assembly.

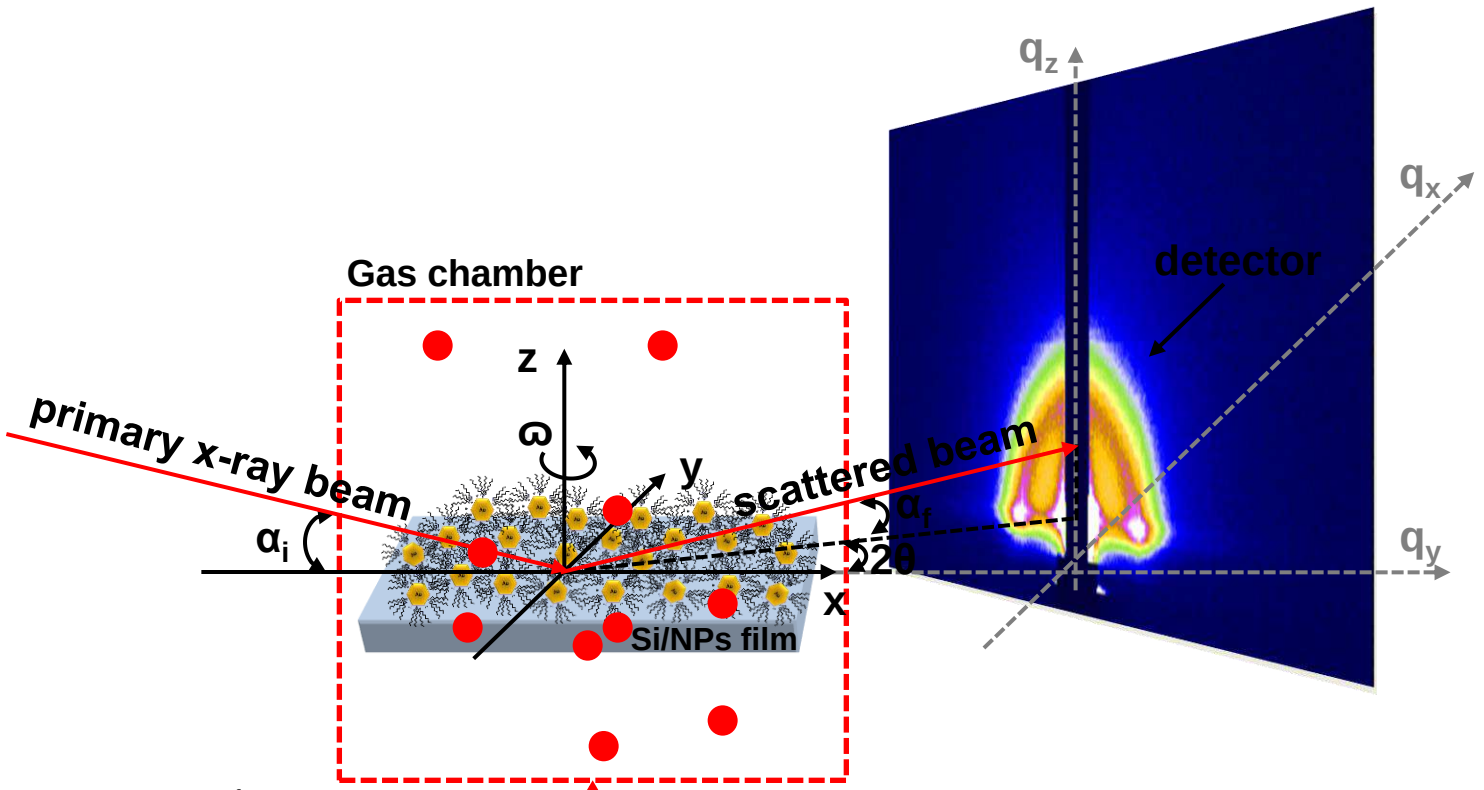

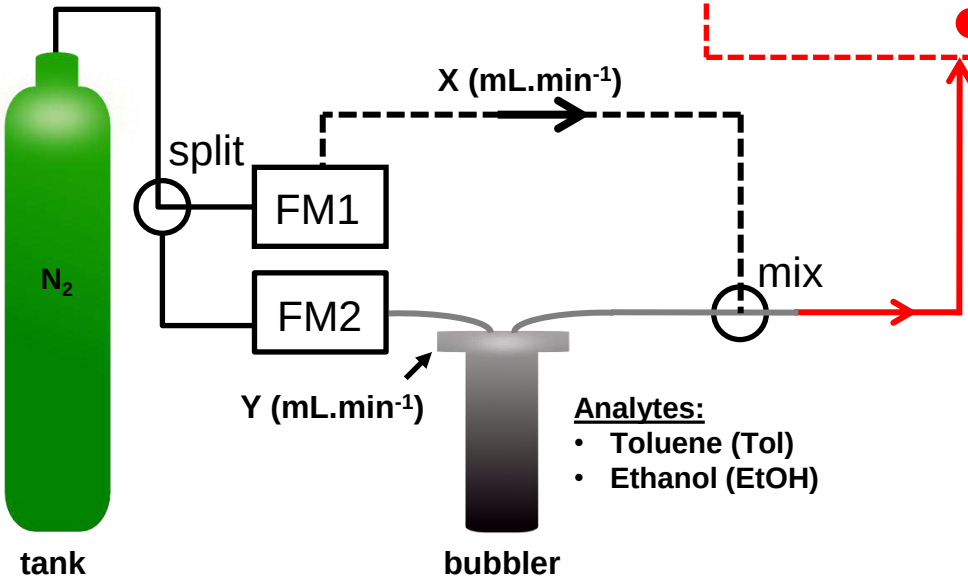

Percent vapor

$$\frac{\text{(mL.s}^{-1}\text{) FM2}}{\text{(mL.m}^{-1}\text{) FM1} + \text{(mL.m}^{-1}\text{) FM2}} = \frac{P}{P_t} \text{ X } 100$$

Sensing steps:

1 = 100% N_2 (50 cm^3/min)
2 = 20% Tol
3 = 40% Tol
4 = 80% Tol
5 = 100% Tol (50 cm^3/min)
6 = 100% Tol (100 cm^3/min)
7 = 100% Tol (200 cm^3/min)
8 = 100% Tol (500 cm^3/min)
9 = 100% N_2 (500 cm^3/min)
10 = 20% EtOH
11 = 40% EtOH
12 = 80% EtOH
13 = 100% EtOH (50 cm^3/min)
14 = 100% EtOH (100 cm^3/min)
15 = 100% EtOH (200 cm^3/min)
16 = 100% EtOH (500 cm^3/min)
17 = 100% N_2 (500 cm^3/min)

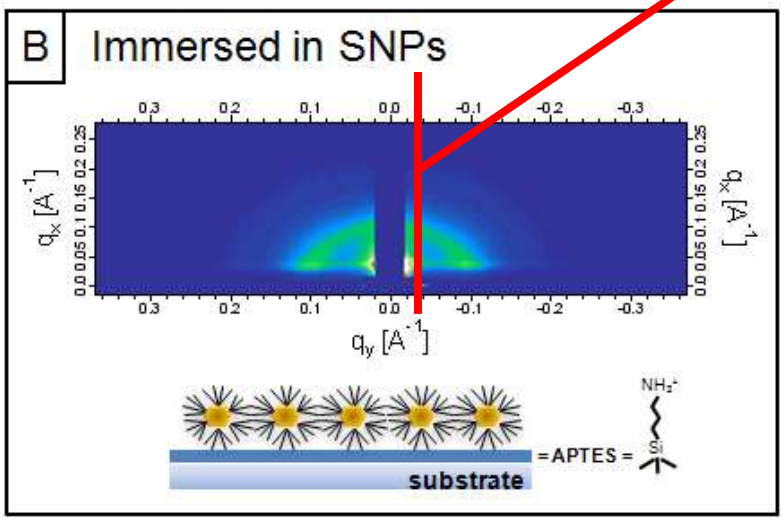

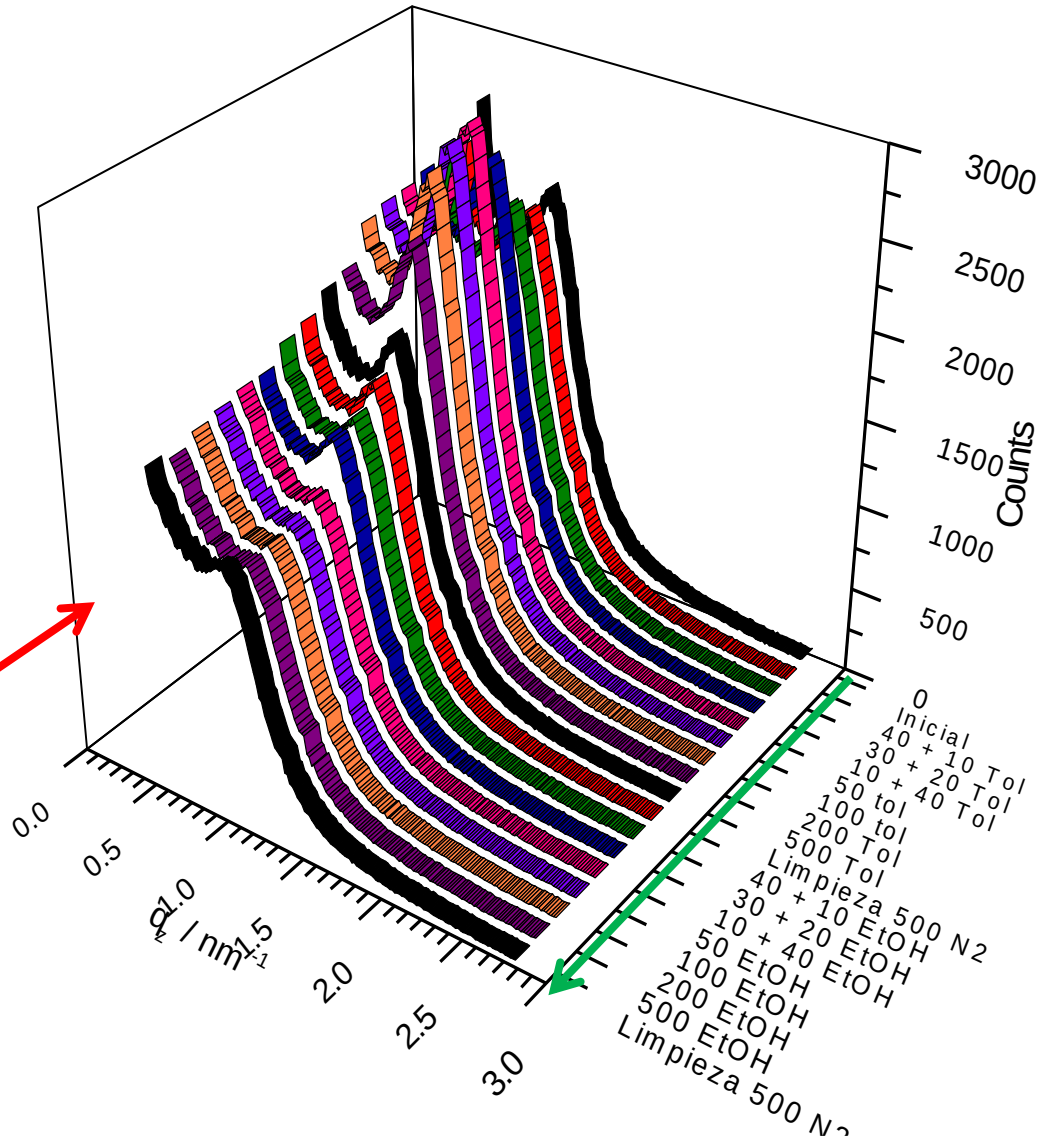

A semi-empirical structure function that describes the spatial correlation of colloidal spherical objects embedded in a homogeneous matrix, derived using the Born–Green approximation, is given by Guinier (1955):

$$S(q) = \frac{1}{1 + k \cdot \Phi(q, d)} \tag{8-28}$$

where k, called as packing factor, refers to the degree of correlation of the structure and d is the average distance between the spatially correlated nano-objects. The maximum value of k is expected for the closest packing of spheres ($k_{max} = 5.92$). The function $\Phi(q, d)$ is defined as

$$\Phi(q, d) = 3\frac{\sin(qd) - qd\cos(qd)}{(qd)^3} \tag{8-29}$$

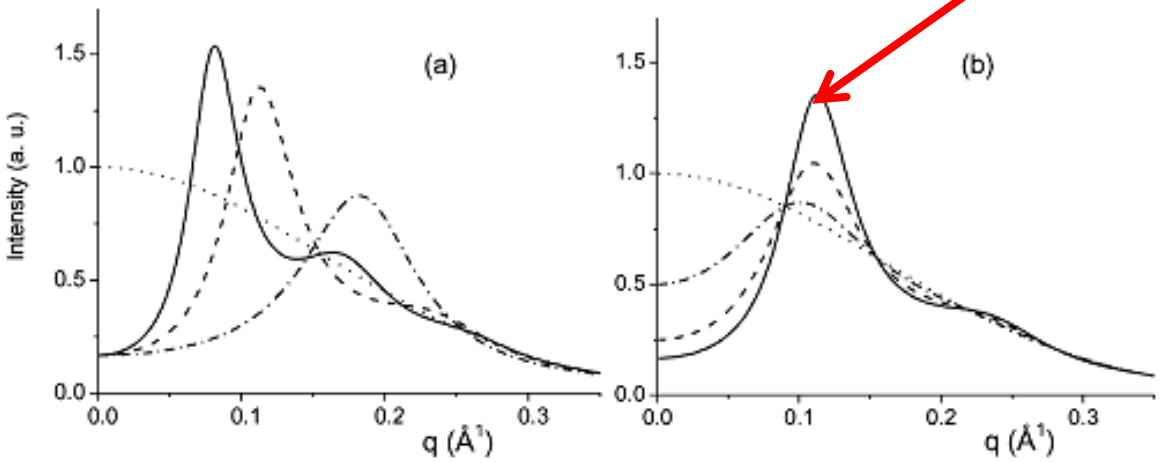

Figure 8-7. Theoretical scattering intensity curves corresponding to different two-electron density systems containing spatially correlated spheres. The spheres have all them the same radius, R = 10 Å. (a) Packing factor k = 5 and average distances d = 30 Å (-.-.-.-), d = 50 Å (-----) and d = 70 Å (——). (b) Average distance d = 50 Å and packing factor k = 1 (·-·), k = 3 (------) and k = 5 (——).

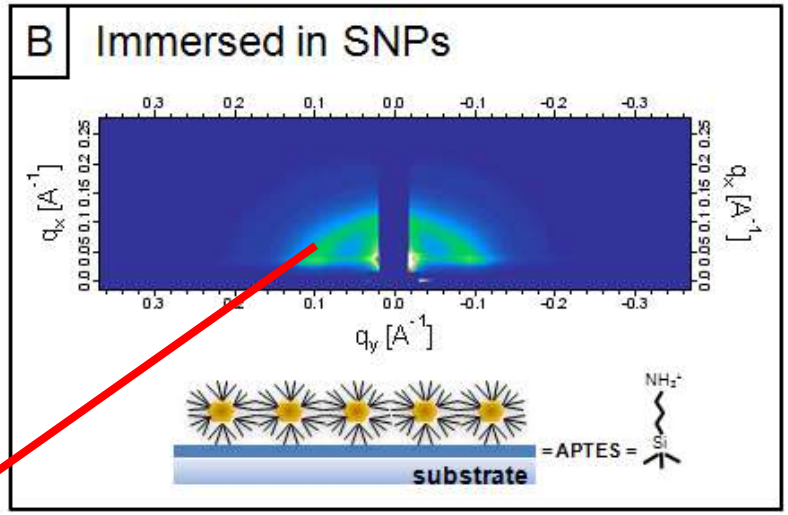

$d = 5.6 / q_{máx}$

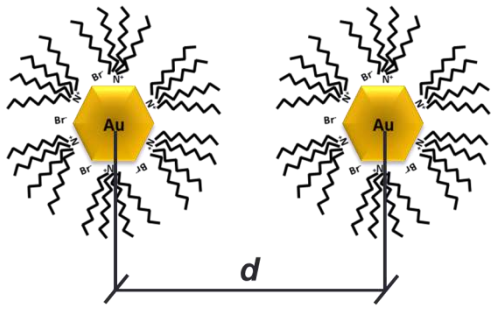

Sensing steps:

1 = 100% N_2 (50 cm^3/min)
2 = 20% Tol
3 = 40% Tol
4 = 80% Tol
5 = 100% Tol (50 cm^3/min)
6 = 100% Tol (100 cm^3/min)
7 = 100% Tol (200 cm^3/min)
8 = 100% Tol (500 cm^3/min)
9 = 100% N_2 (500 cm^3/min)
10 = 20% EtOH
11 = 40% EtOH
12 = 80% EtOH
13 = 100% EtOH (50 cm^3/min)
14 = 100% EtOH (100 cm^3/min)
15 = 100% EtOH (200 cm^3/min)
16 = 100% EtOH (500 cm^3/min)
17 = 100% N_2 (500 cm^3/min)

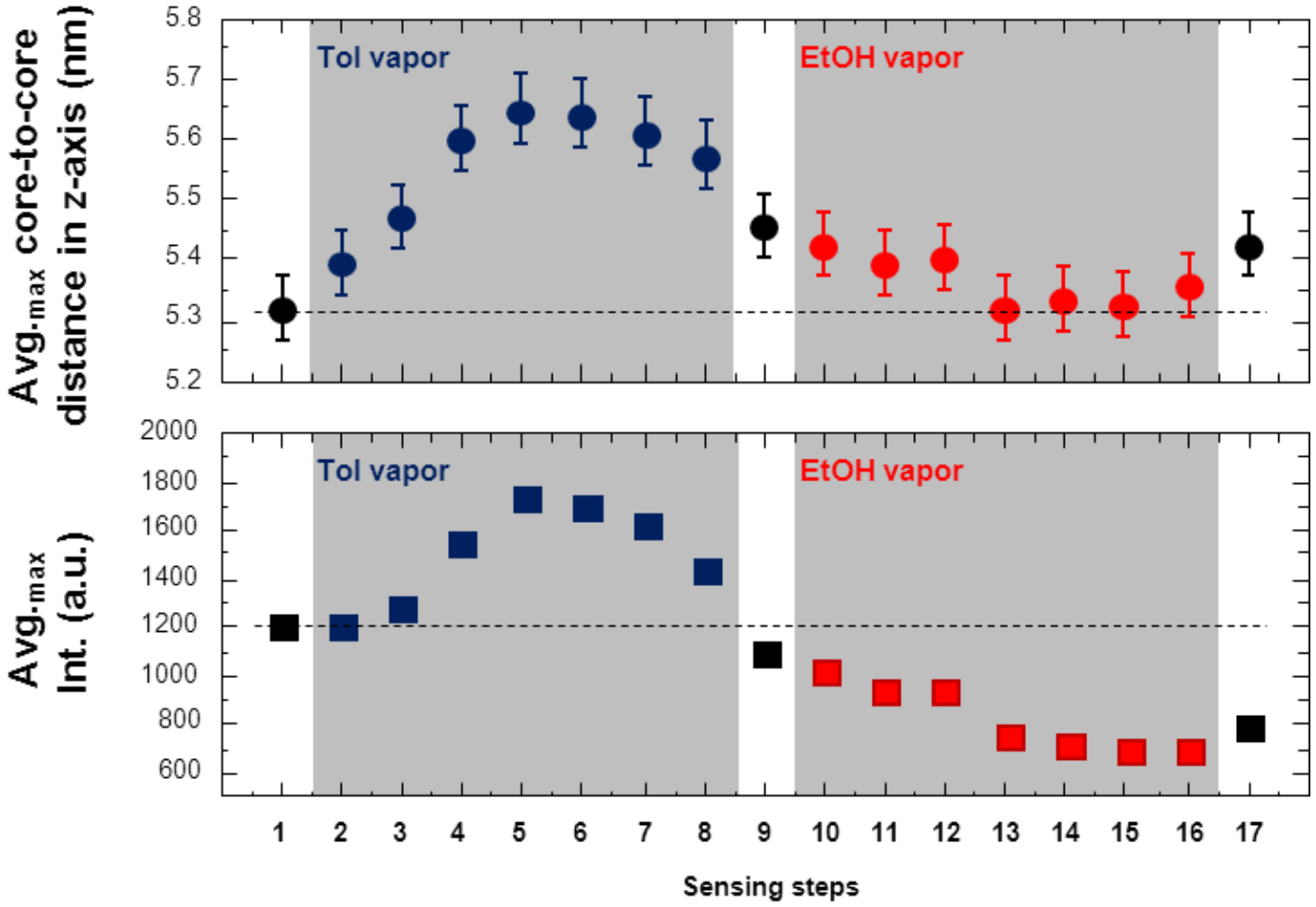

•Conclusions

- ✓ Results indicated that drop-casted films of SNP exhibited almost no correlation.
- ✓ Films assembled by immersion exhibited correlation and 6.4 nm *core-to-core* separation, which is larger distance as compared to well-assembled monolayer-protected clusters of similar size. Such large distance between SNP was attributed to excess amount of weekly coordinated TOA^+ ligands around the Au nanoparticle.
- ✓ Importantly, it was determined that inter-SNP distance came apart and slightly shrinkage, indicating film swelling and contraction in the presence of non polar (Tol) and polar (EtOH) vapors, respectively. However, in EtOH, SNP distance irreversibly decreased and film became amorphous.
- ✓ Changes in nanoparticles distance were mainly attributed to film flexibility provided by the organic alkylchains. Once TOA^+ groups were exchanged with dithiol molecules, film flexibility was lost limiting further correlations between distance and film structure.
- ✓ After NDT exchange inter-NPs distance expanded from ~3.5 to ~4.0 nm and from ~4.0 to ~5.0 nm according to GISAXS and SAXS experiments, respectively. The larger separation between metal cores was attributed to the alkanedithiols chains conformation. FT-IR showed kink defects suggesting a loop conformation around the Au cores which ultimately leads to larger SNP separation.

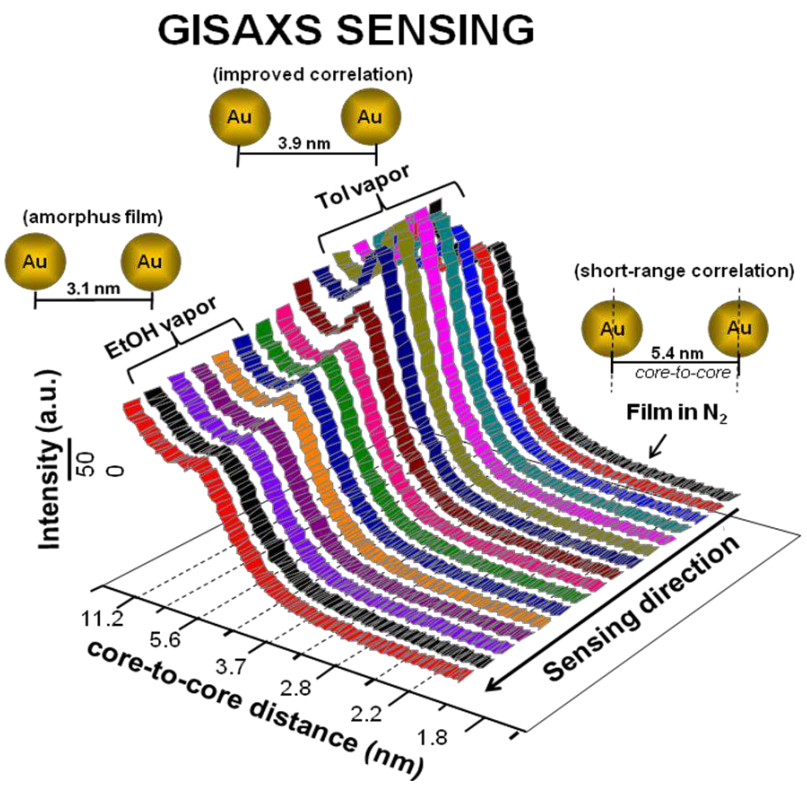

• Formation of an extended $CoSi_2$ thin nanohexagons array coherently buried in silicon single crystal

F.G. Requejo, L.J. Giovanetti, P.C. dos Santos Claro, C. Huck Iriart
Instituto de Investigaciones Fisico-Químicas Teóricas y Aplicadas (INIFTA),
FCE, UNLP – CONICET. La Plata, ARGENTINA.

G. Kellermann
Departamento de Física. Universidade Federal do Paraná, Curitiba, BRAZIL.

L.A. Montoro, A.J. Ramirez
Brazilian Nanotechnology National Laboratory (LME-LNNano), Campinas, BRAZIL.

A. F. Craievich.
Instituto de Física, Universidade de São Paulo SP, BRAZIL.

•Interest and goals: epitaxial $CoSi_2$

SEM images of shape-controlled pits grown at 865 ° C for 30 min using 30-40 nm Au NPs as catalyst. Square, triangle, and wire-shaped pits are fabricated on substrates of Si (100), Si (111), and Si (110), respectively. (d-f) Magnified SEM images of individual pits. The inset in panel A shows Au NPs on substrate before pits growth, and the scale bar corresponds to 200 nm.

H. Wang et al., ACS Nano

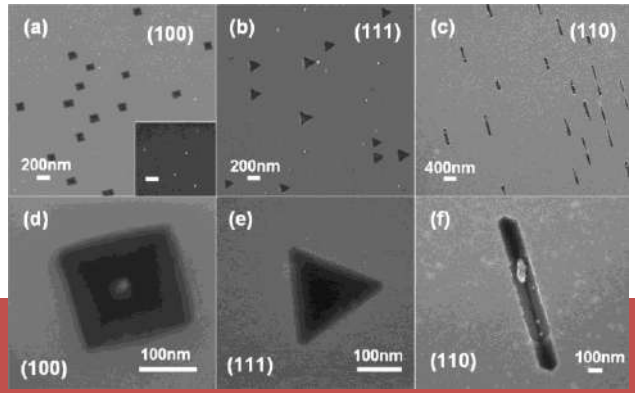

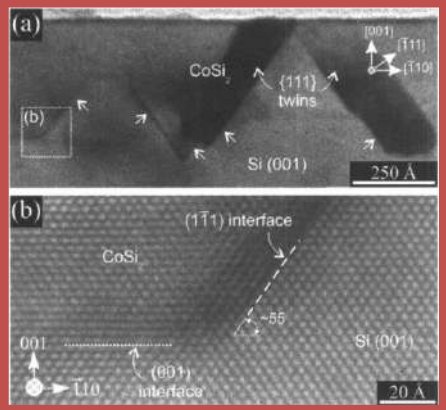

(a) Bright-field XTEM micrograph, along the (110) zone axis, from the interface region of a RDE $CoSi_2$(001) layer. (b) HR-XTEM micrograph of the area highlighted in sad.

Lim et al., J. Appl. Phys. 97 (2005) 044909

Bright field cross-sectional TEM images of buried structures of cobalt disilicide formed in Si(100) matrix by 400 keV Co^+ ion implantation at 875 K substrate temperature with total dose of implanted ions of $7.8 \cdot 10^{15}$ ions/cm^2 or 3% of critical dose, and postimplant annealed at 1275 K during various times: (A) as implanted, (B) 30 s, (C) 1 min, (D) 3 min, (E) 5 min, (F) 10 min.

O. Hul'ko et al., Surface Science 547 (2003) 219

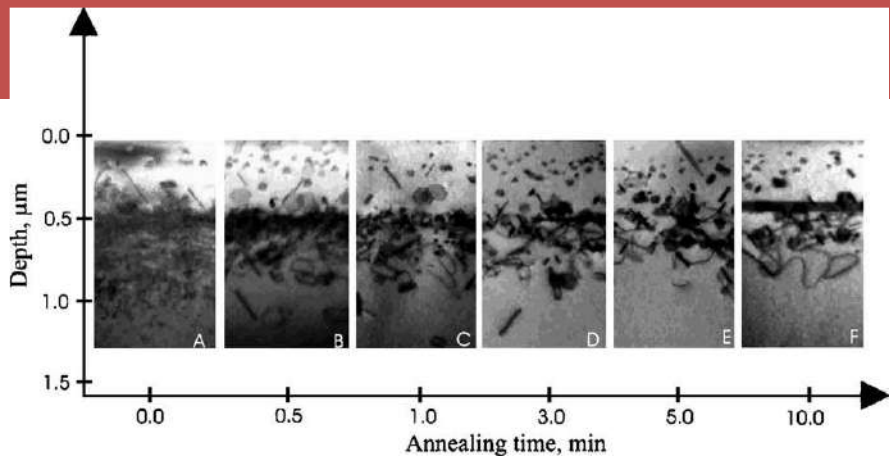

•Description of the samples

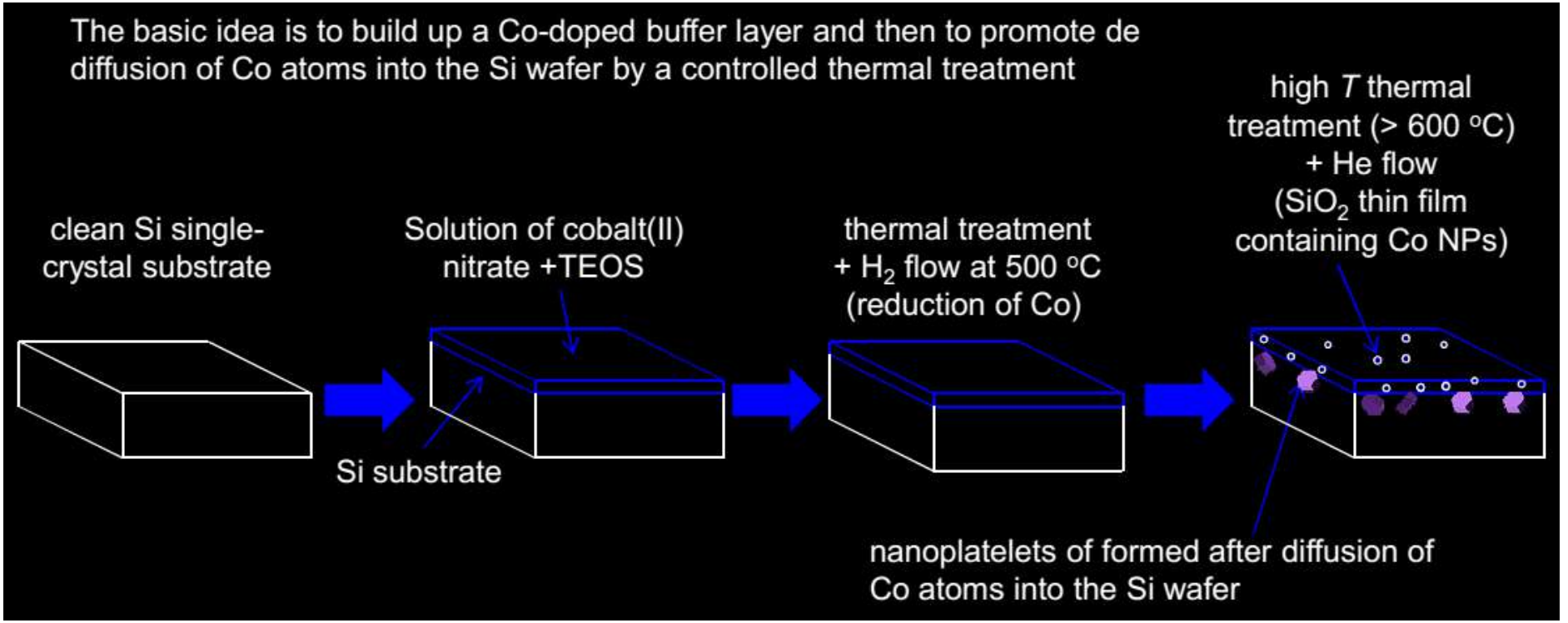

The initial step of our preparation procedure was to deposit a Co-doped SiO_2 thin film onto a Si(110) flat substrate. The basic idea was to build up a Co-doped buffer layer and then to promote de diffusion of Co atoms into the Si wafer by a controlled thermal treatment.

Results: GISAXS (extended order)

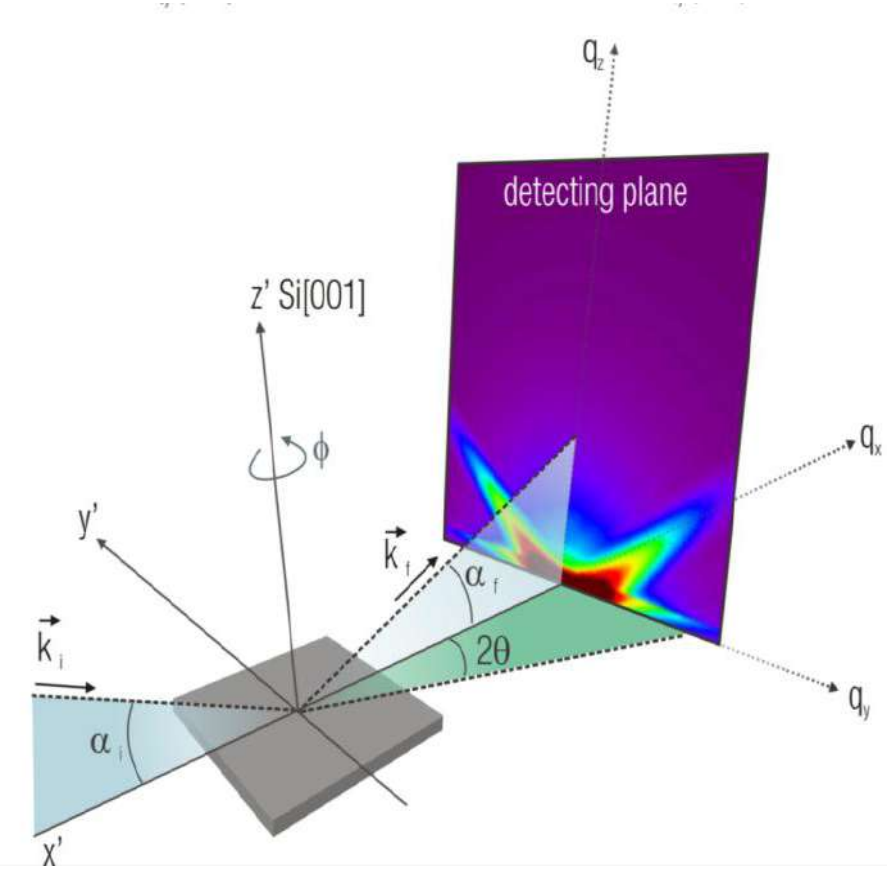

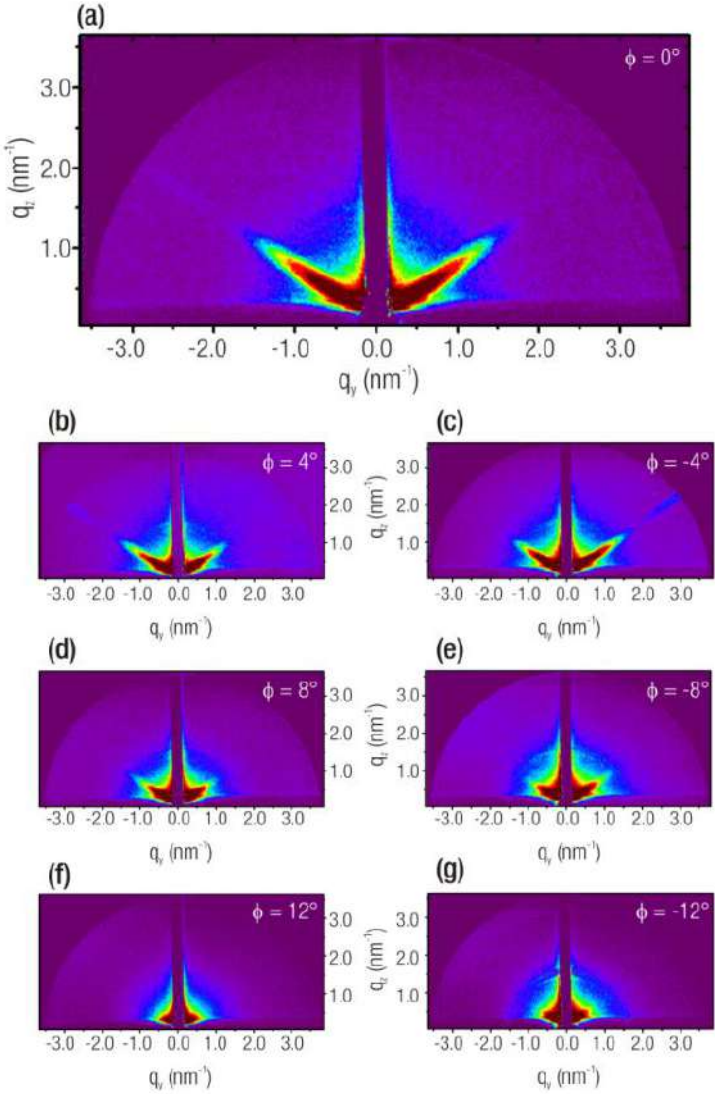

Experimental 2D-GISAXS images taken for different azimuthal angles: (a) $\phi = 0$ °, (b) $\phi = 4$ °, (c) $\phi = -4$ °, (d) $\phi = 8$ °, (e) $\phi = -8$ °, (f) $\phi = 12$ °, and (g) $\phi = -12$ °.

Appl. Phys. Lett. 100 (2012) 063116

•Results: TEM (local order)

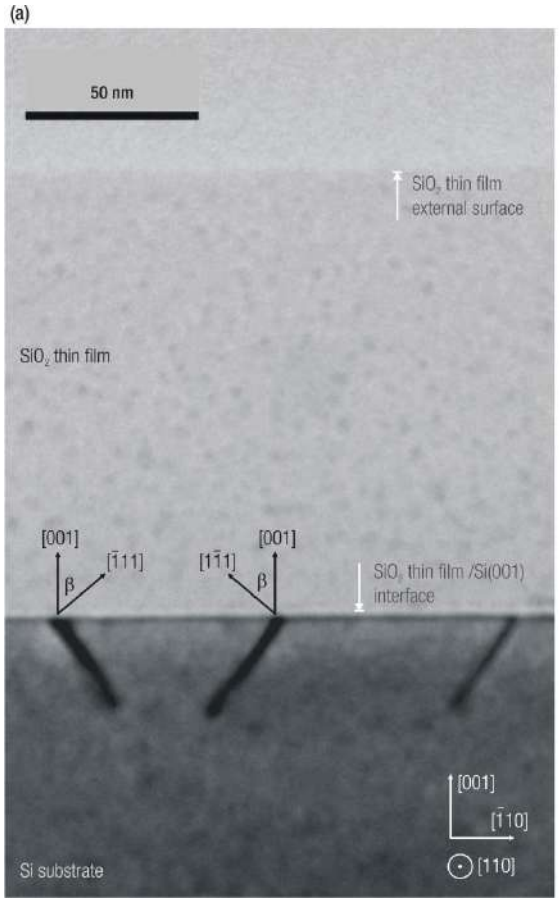

(a) TEM image corresponding to a cross-sectioned (001) silicon wafer in which a Co-doped silica (SiO_2) was deposited.

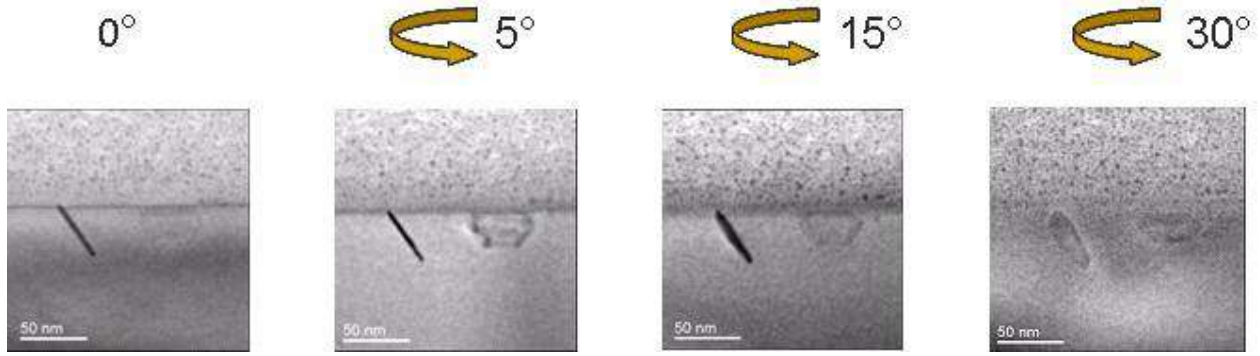

90°

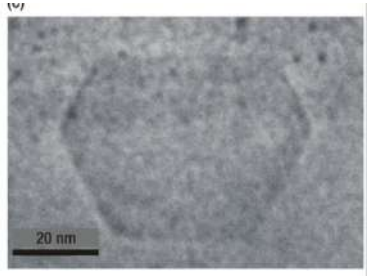

Specimen shown oriented along the large faces normal to the electron beam showing a projection of the hexagonal nanoplatelet onto the Si(110) plane.

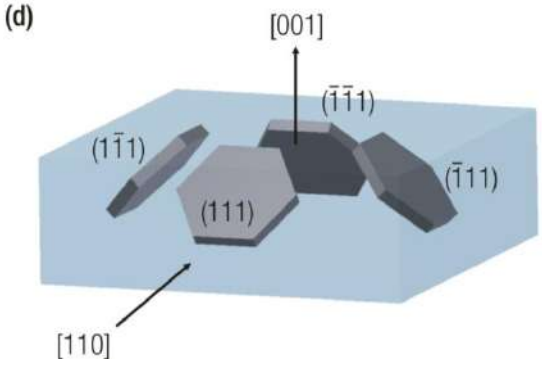

(d) Schematic display of the hexagonal $CoSi_2$ nanoplatelets with four different orientations, each of them parallel to one plane belonging to the Si{111} crystallographic form.

Appl. Phys. Lett. 100 (2012) 063116

•Results: GISAXS modeling

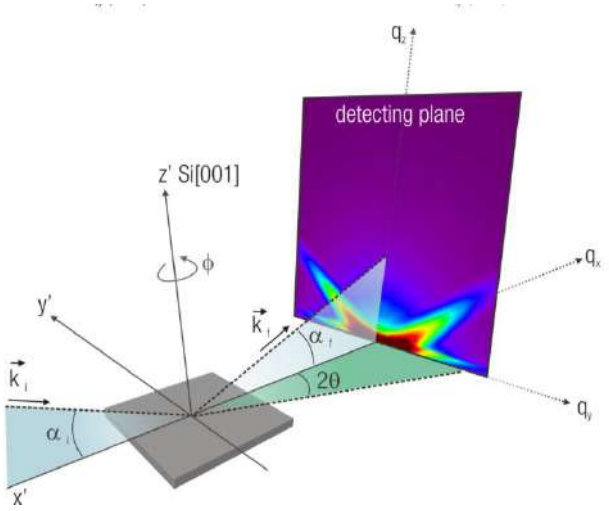

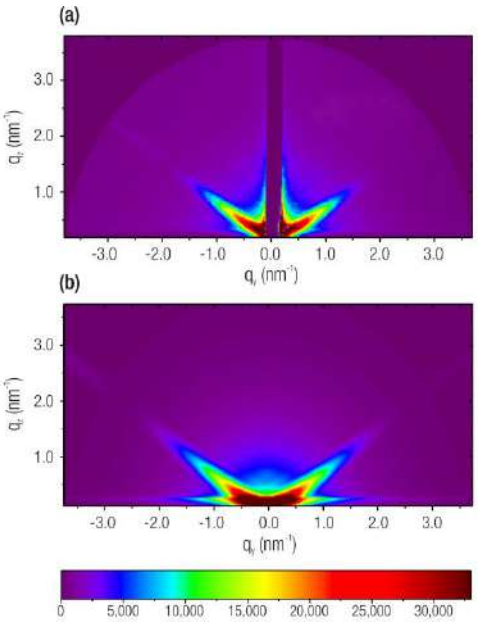

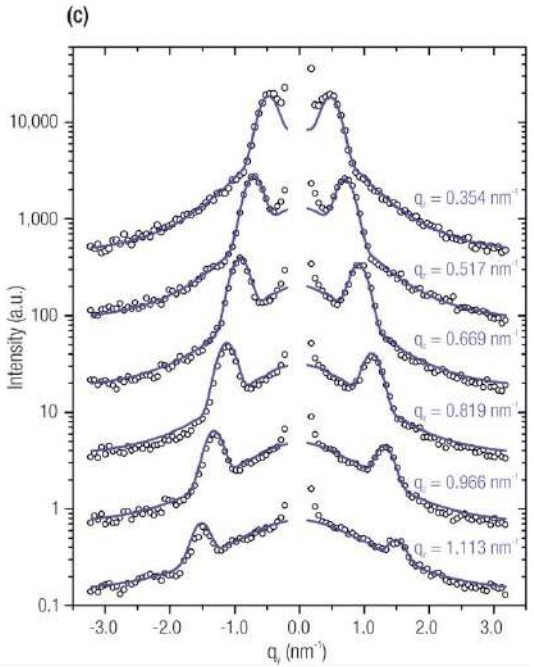

(a) Experimental 2D GISAXS pattern corresponding angle ϕ = 1.5. The vertical dark ribbon is the shadow of a stopper that avoids to the azimuthal the strong totally reflected beam reaching the imaging plate. (b) Simulated 2D GISAXS pattern for which the best fit to the experimental pattern (a) was achieved. (c) Experimental GISAXS 1D profiles (symbols) and fitted curves (continuous lines) corresponding to different constant q_z values, i.e., different horizontal GISAXS linear profiles derived from the 2D image displayed in (a).

Appl. Phys. Lett. 100 (2012) 063116

•Results: GISAXS analysis

GISAXS simulation:

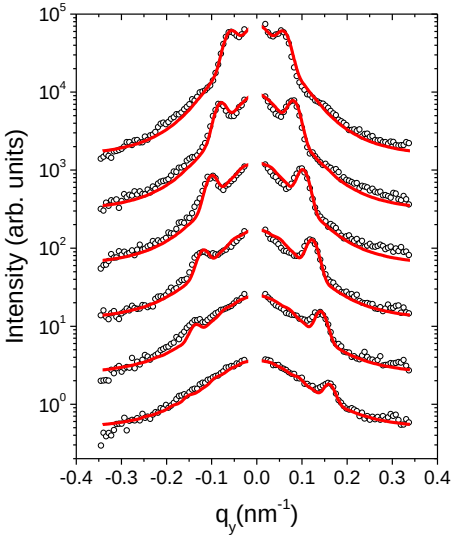

HEXAGONS:

Tilt angle = 35° (theory: 35.3°)

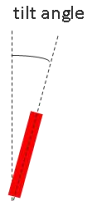

Side of the (regular) hexagon = 20 nm
(*TEM ~ 35 nm*)

Hexagon thickness = 2.5 nm
(*TEM ~3 nm*)

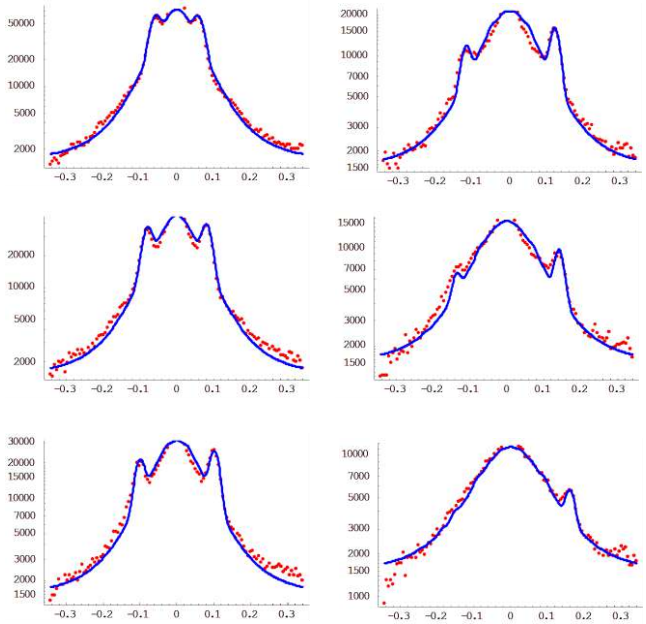

SPHERES (nanoparticles):

Size distribution: lognormal
Average radii = 0.43 nm

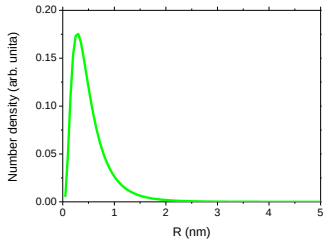

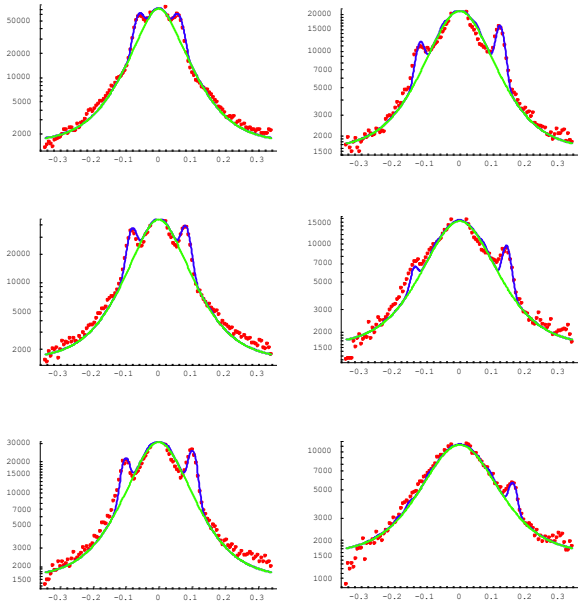

Appl. Phys. Lett. 100 (2012) 063116

•Results: GISAXS analysis

GISAXS simulation:

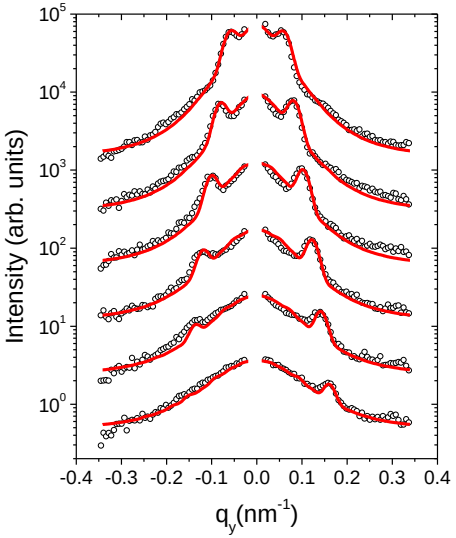

HEXAGONS:

Tilt angle = 35° (theory: 35.3°)

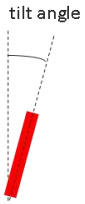

Side of the (regular) hexagon = 20 nm
(*TEM ~ 35 nm*)

Hexagon thickness = 2.5 nm
(*TEM ~3 nm*)

SPHERES (nanoparticles):

Size distribution: lognormal
Average radii = 0.43 nm

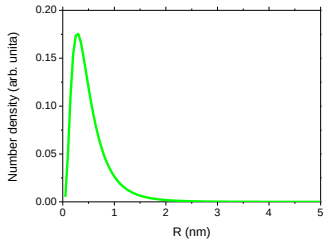

GISAXS pattern repeats every time the azimuthal angle is incremented by 90° , as is expected from the 4-fold rotational symmetry around Si[001] axis.

Diffusion angle between the Si[110] and Si[111] crystallographic directions 35.3° .

Thickness and lateral side of the $CoSi_2$ nanoplatelets buried into the Si wafer t = (2.5 ± 0.3) nm and d = (19.5 ± 0.5) nm.

Spherical **NP** embedded in the silica <R> = (0.43 ± 0.03) nm, σ_R/<R> = 0.58 ± 0.06.

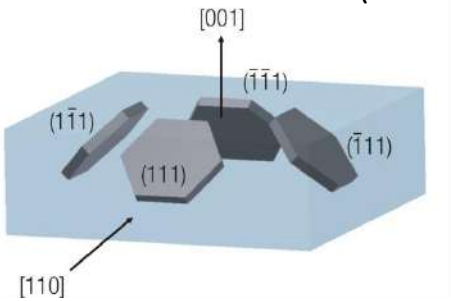

Appl. Phys. Lett. 100 (2012) 063116

•GISAXS Results: kinetic studies

Sample treatment:

•Ex-situ, before measurement: Flowing H_2 at 500 ° C for 1 hour.
•In-situ, during measurement: Heating from room temperature to 700 ° C in He atmosphere at 9 ° C/min.

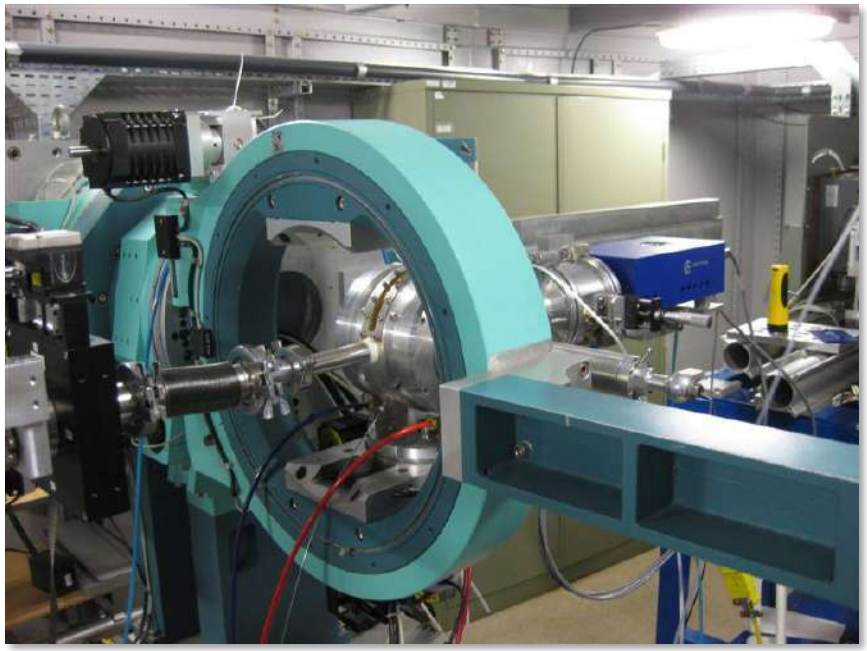

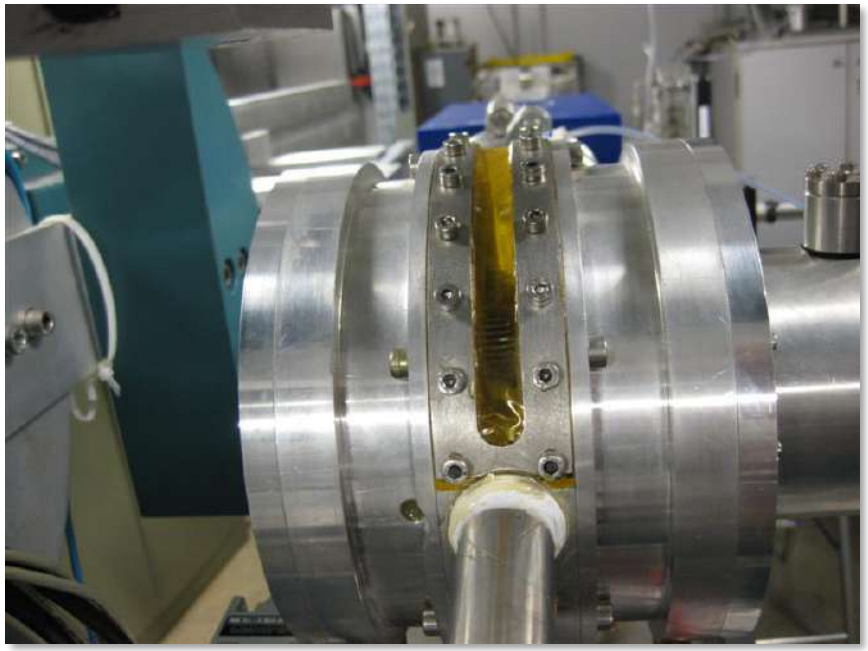

Experiment

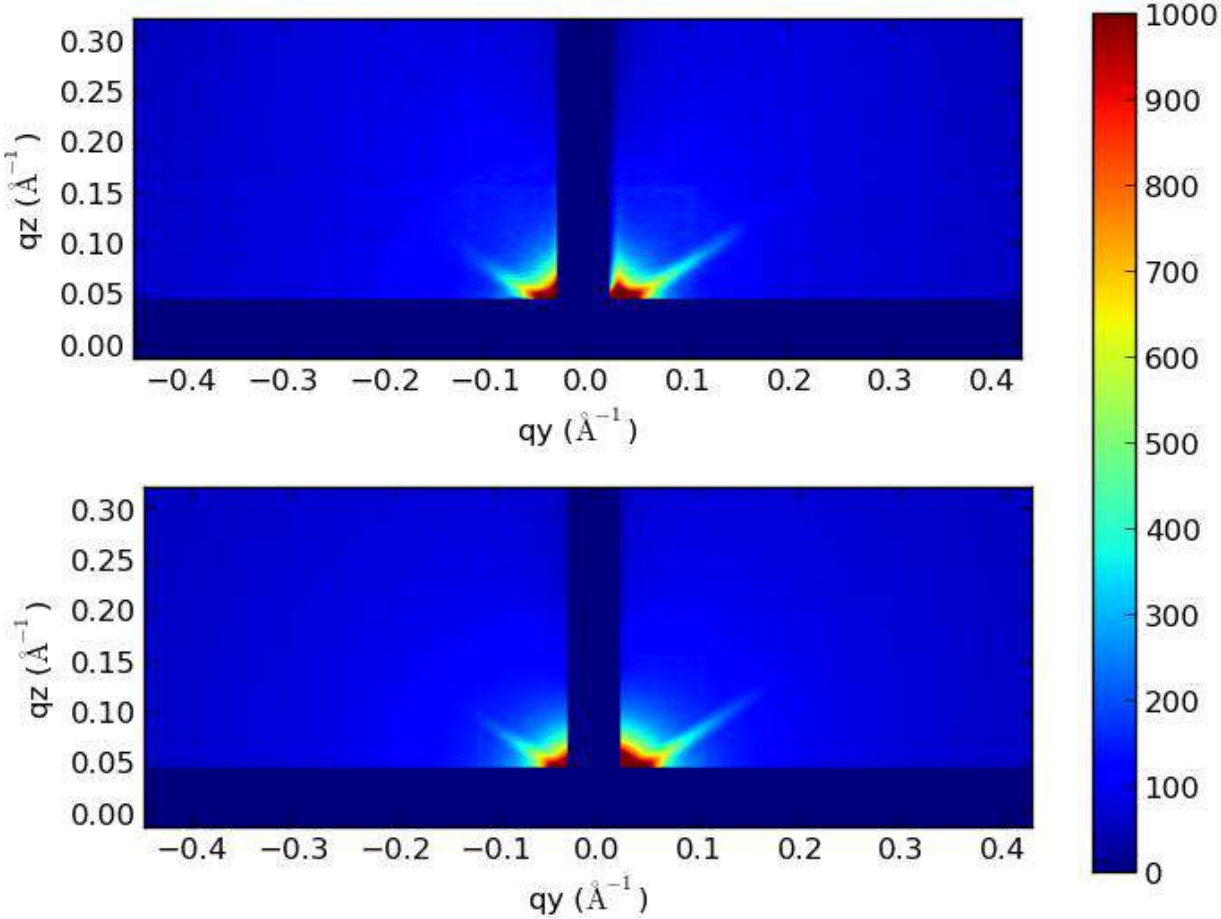

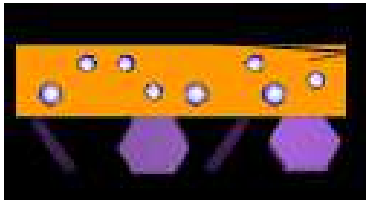

Residue

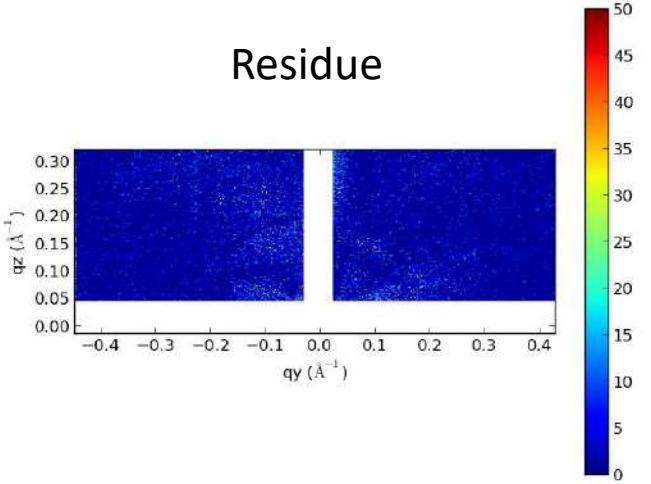

Simulation

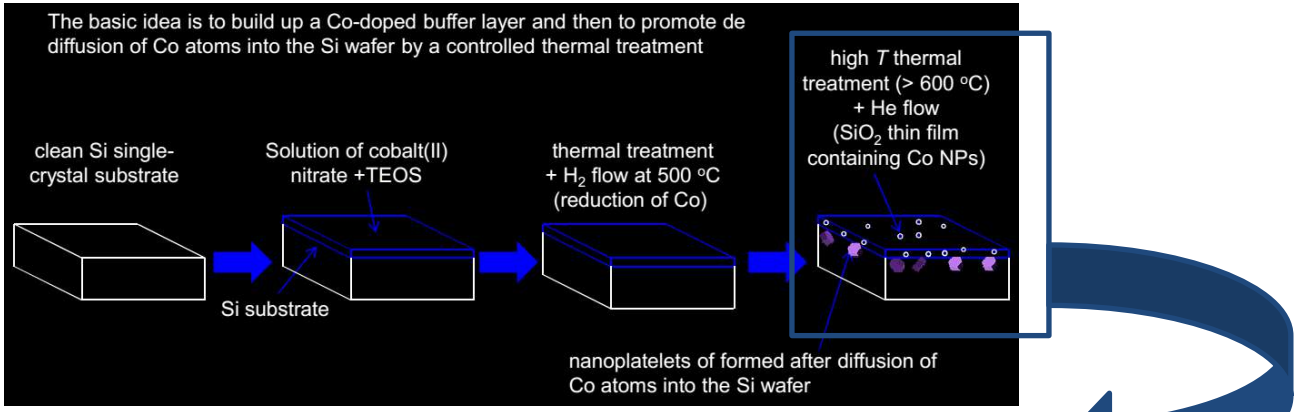

Exp

Fit

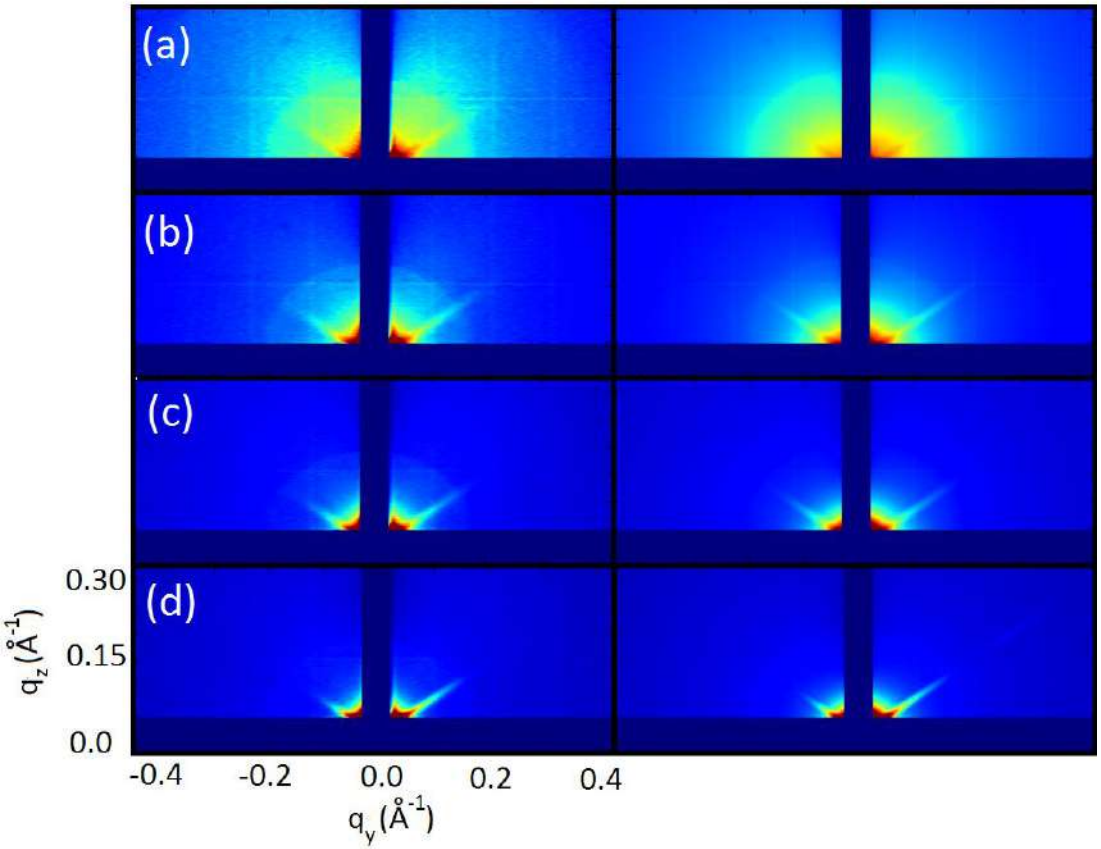

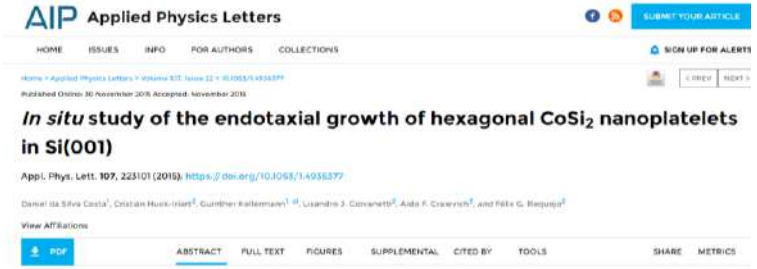
AIP Applied Physics Letters

HOME ISSUES INFO FOR AUTHORS COLLECTIONS

SUBMIT YOUR ARTICLE

SIGN UP FOR ALERTS

Published Online: 30 November 2015 Accepted: November 2015

***In situ* study of the endotaxial growth of hexagonal $CoSi_2$ nanoplatelets in Si(001)**

Appl. Phys. Lett. **107**, 223101 (2015); https://doi.org/10.1063/1.4936377

View Affiliations

PDF ABSTRACT FULL TEXT FIGURES SUPPLEMENTAL CITED BY TOOLS SHARE METRICS

$$V_{sph}^{total} \propto Q = 4\pi \int_0^\infty I(q) q^2 dq$$

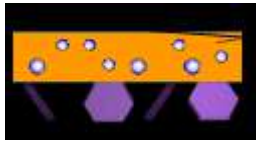

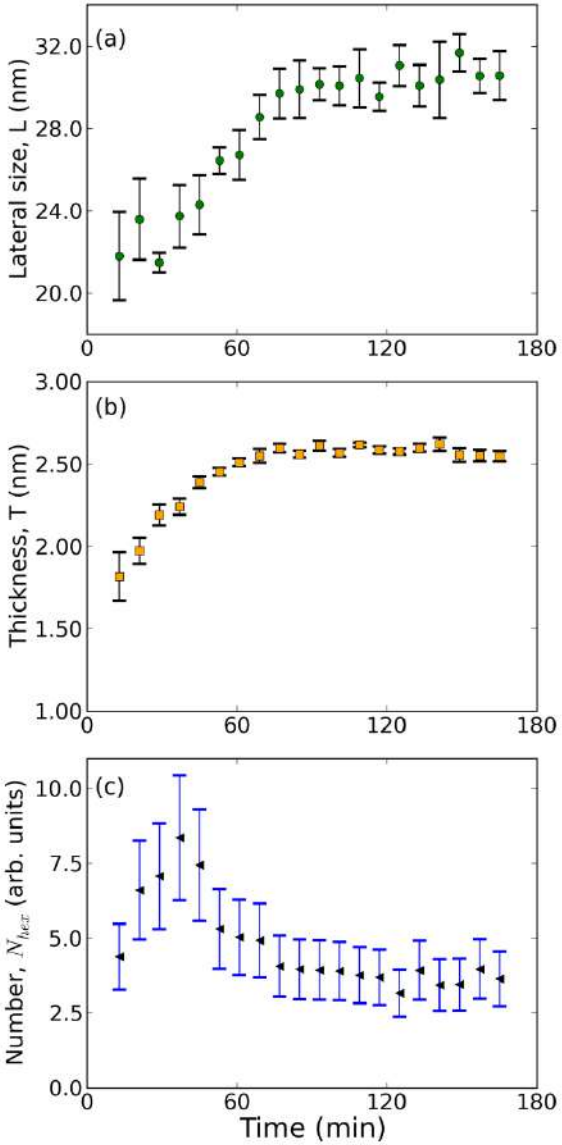

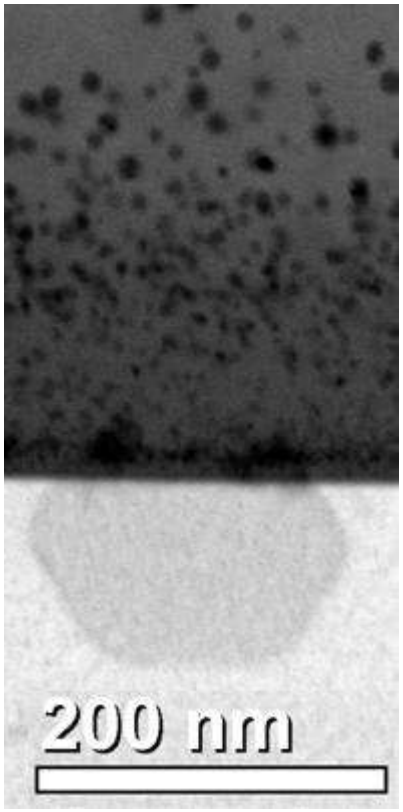

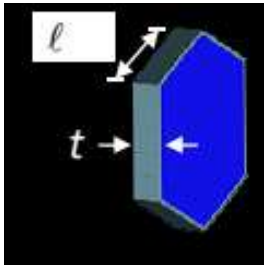

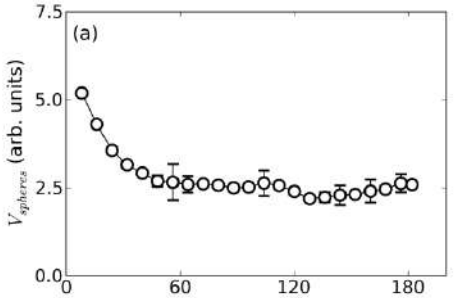

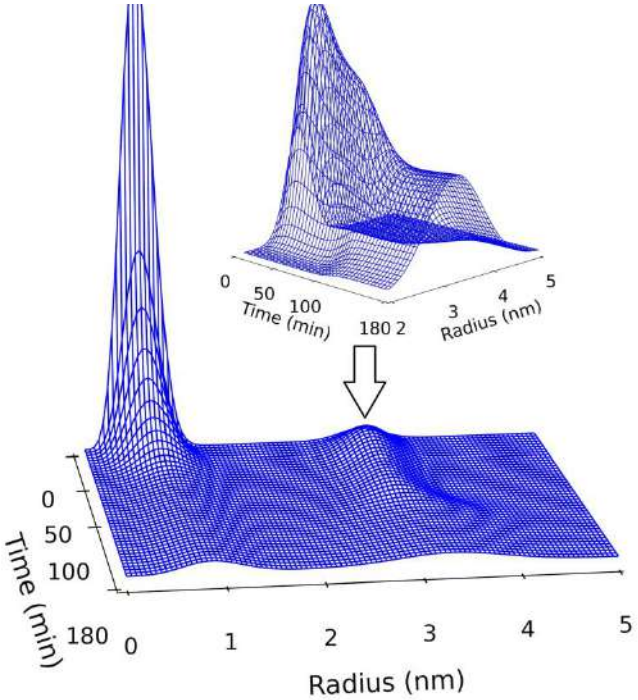

$$X_V(t) = 1 - exp(-k \cdot t^n)$$

Volume fraction

$$X_V = \frac{V_0 - V(t)}{V_0 - V_\infty}$$

[1] Melvin Avrami. Kinetics of phase change. I general theory. 7(12):1103–1112, 1939.

[2] Melvin Avrami. Kinetics of phase change. II transformation time relations for random distribution of nuclei. 8(2):212–224, 1940.

[3] Melvin Avrami. Granulation, phase change, and microstructure kinetics of phase change. III. 9(2):177–184, 1941.

[4] W. A.; Van Den Berg P. J. De Bruijn, T. J. W.; De Jong. Kinetic parameters in avrami—erofeev type reactions from isothermal and non-isothermal experiments. 45(3):315–325, 1981.

Reaction mechanism	Constant nucleation rate n	Growth of a constant number of nuclei n
one dimensional growth	2	1
two dimensional growth	3	2
three dimensional growth	4	3

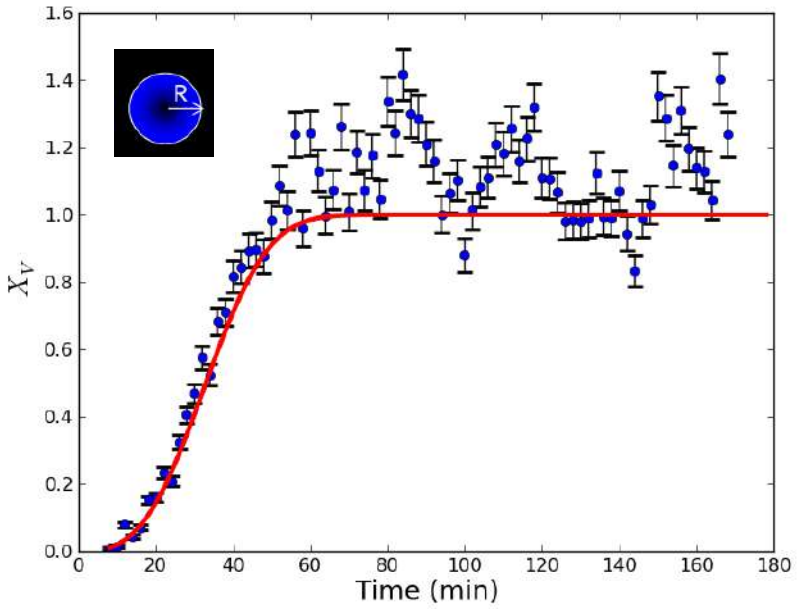

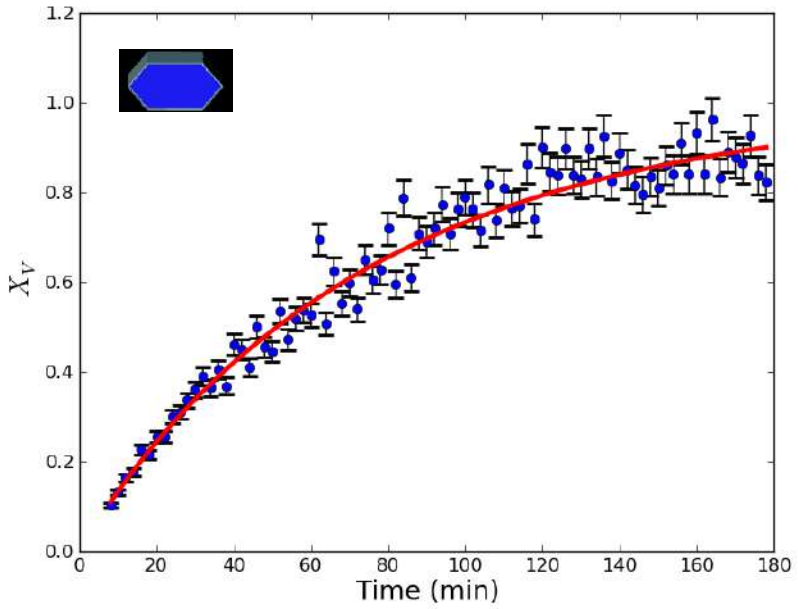

•Conclusions

- ✓ The joint use of TEM and GISAXS techniques provided complementary and essential information, both being indispensable for achieving a clear and detailed description of the studied nanostructured material.
- ✓ The process of diffusion of cobalt atoms from a cobalt-doped thin film into a Si(001) single crystalline wafer well defined thickness and lateral sizes can be achieved and well controlled.
- ✓ The buried structures exhibit four different orientations, each of them strictly parallel to one of the four planes of the Si{111} crystallographic form. The $CoSi_2$ nanohexagons are parallel only to planes of the {111} form, because the free energy of their (coherent) interface is in this case lower than in the other cases.
- ✓ Since the described process can be reproducibly achieved, it can also be considered as an original and simple alternative for the production of nanostructured materials with relevant physical properties, over a large area, which may find useful applications for developments of nano-integrated devices.
- ✓ First evidences about nanostructures growing and diffusion process are addressed by in situ GISAXS.

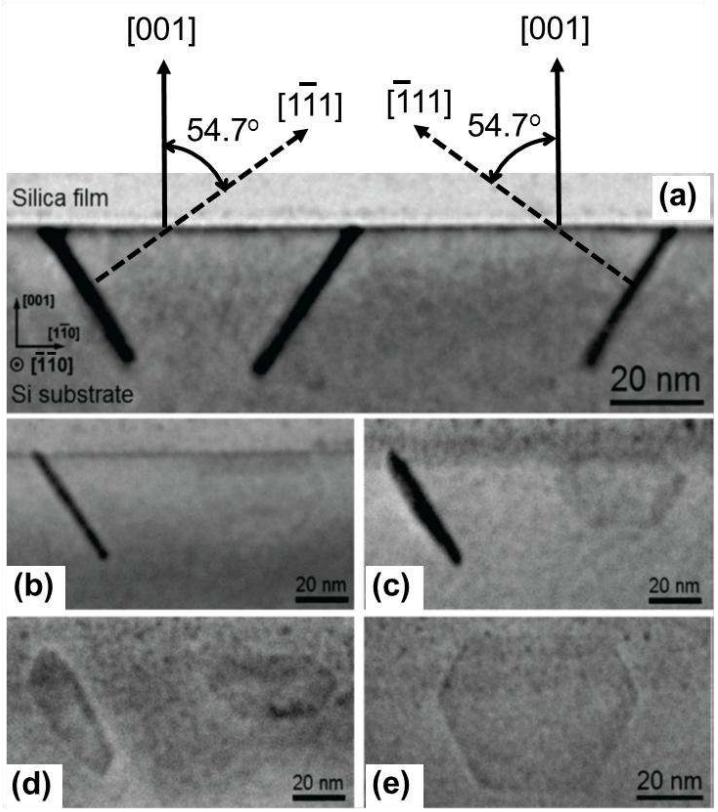

Phase change and Momentum transfer

The phase difference between two scattered X-ray beams is determined by the difference of distance they traveled before arrive the detector pixel.

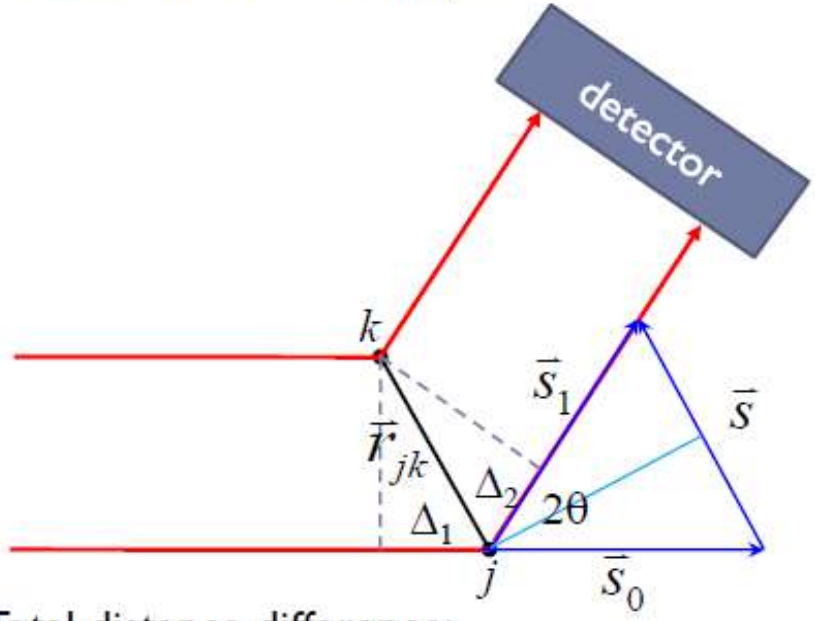

A vector $\vec{a}$ has its length $a = |\vec{a}|$ and direction (O→A).

Vector dot product:

$$\vec{a} \bullet \vec{b} = a * b \cos(\theta)$$

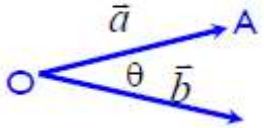

unit incident wavevector $\vec{s}_0$

unit scattering wavevector $\vec{s}_1$

wave vector change: $\vec{s}$

$$\vec{s} = \vec{s}_1 - \vec{s}_0$$

$$|\vec{s}| = 2\sin\theta$$

Total distance difference:

$$\Delta = \Delta_1 + \Delta_2 = -\vec{s}_0 \bullet \vec{r}_{jk} + \boxed{\vec{s}_1 \bullet \vec{r}_{jk}}$$

Projection of $\vec{r}_{jk}$ on $\vec{s}_1$

$$= (\vec{s}_1 - \vec{s}_0) \bullet \vec{r}_{jk} = \vec{s} \bullet \vec{r}_{jk}$$

Definition: momentum transfer

$$\vec{q} = (2\pi / \lambda)\vec{s}$$

$$q = |\vec{q}| = (4\pi / \lambda)\sin\theta$$

Phase change: (radian)

$$\Delta\phi = 2\pi * \frac{\Delta}{\lambda} = \vec{q} \bullet \vec{r}_{jk}$$

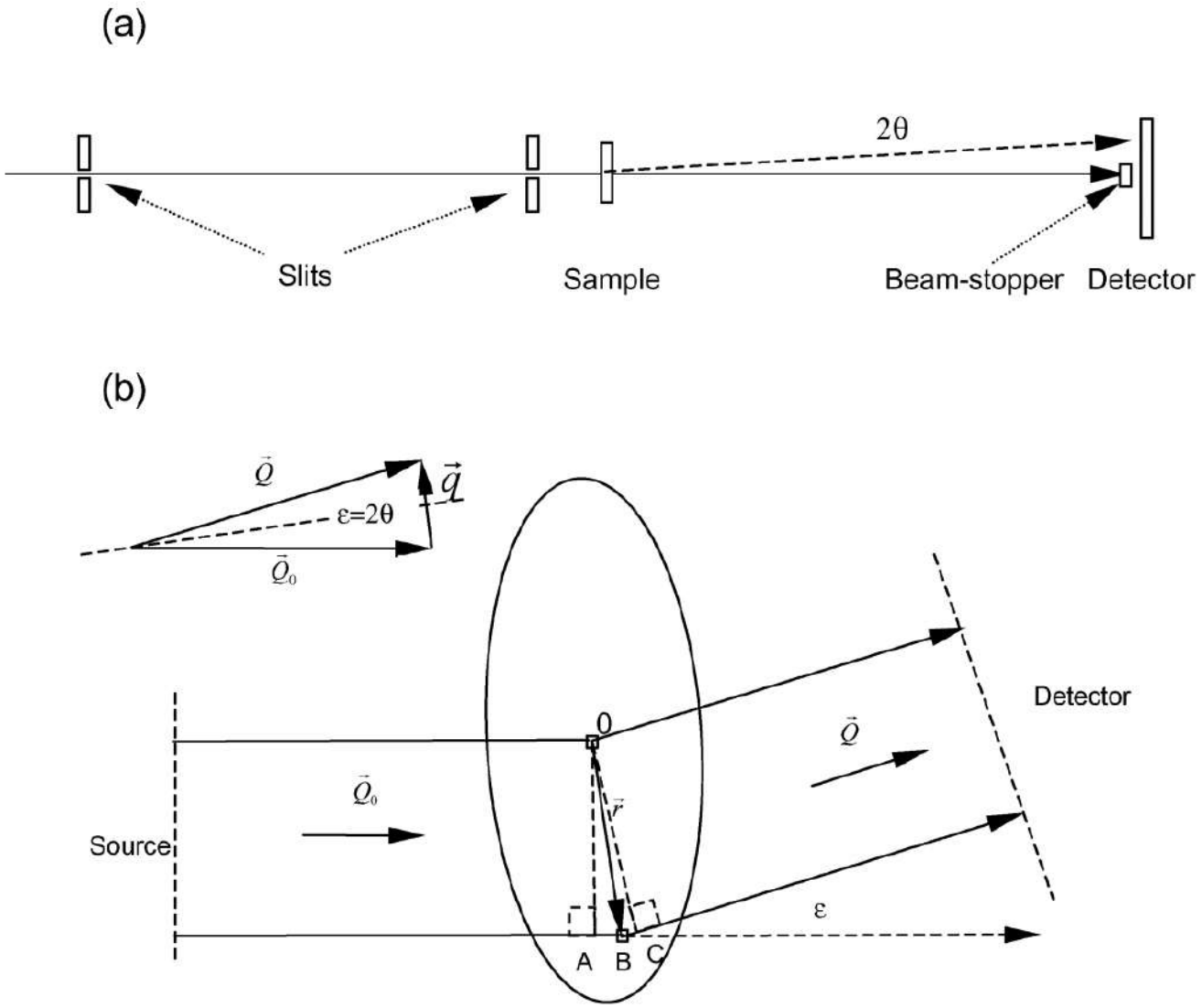

Figure 8-1. (a) Schematic SAXS setup. (b) X-ray beam paths from the source to the detector, both elements located far away from the sample. The segment $\overline{AB} + \overline{BC}$ is the optical path difference from which the phase shift is determined.

The total scattering amplitude is given by the integral, over the whole sample volume V, of the electron density function multiplied by a phase factor $e^{i\varphi}$, which depends on the position $\vec{r}$ of the volume element. The path difference between two generic wavelets propagating along the paths shown in *Figure 8-1(b)* is equal to $\overline{AB} + \overline{BC}$. It can easily be demonstrated that the corresponding phase shift $\varphi = (2\pi/\lambda) \cdot (\overline{AB} + \overline{BC})$ can also be written as $\varphi = -\vec{q} \cdot \vec{r}$. Thus the total scattering amplitude (setting $A_e = 1$) is given by (Glatter, 1982; Guinier, 1955):

$$A(\vec{q}) = \int_V \rho(\vec{r}) \mathrm{e}^{-i\vec{q}\cdot\vec{r}} \, \mathrm{d}v$$

Inversely, the electron density $\rho(\vec{r})$ can mathematically be obtained by the inverse Fourier transform of the amplitude function $A(\vec{q})$:

$$\rho(\vec{r}) = \frac{1}{(2\pi)^3} \int A(\vec{q}) \, \mathrm{e}^{i\vec{q}\cdot\vec{r}} \, \mathrm{d}v_q$$

The electron density $\rho(\vec{r})$ can be written as the integral of an average density ρ_a plus its local deviations defined by $\Delta\rho(\vec{r})$, so as $\rho(\vec{r}) = \rho_a + \Delta\rho(\vec{r})$. Substituting this form for $\rho(\vec{r})$ in equation (8-1), the scattering amplitude becomes

$$A(\vec{q}) = \int_V \rho_a \, \mathrm{e}^{-i\vec{q}\cdot\vec{r}} \, \mathrm{d}v + \int_V \Delta\rho(r) \, \mathrm{e}^{-i\vec{q}\cdot\vec{r}} \, \mathrm{d}v$$

For a macroscopic sample with a volume V and very large dimensions compared to the X-ray wavelength, the first integral yields non-zero values only over an extremely small q range, around $q = 0$, that is not reached in typical SAXS experiments. Thus, the scattering intensity, $I(\vec{q}) = A(q) \cdot A(q)^*$, over the accessible $\vec{q}$ range, is given by

$$I(\vec{q}) = \int_V \int_V \Delta\rho(\vec{r}_1) \cdot \Delta\rho(\vec{r}_2) \, \mathrm{e}^{-i\vec{q}\cdot(\vec{r}_1 - \vec{r}_2)} \, \mathrm{d}v_1 \, \mathrm{d}v_2$$

Making $\vec{r}_1 - \vec{r}_2 = \vec{r}$

$$I(\vec{q}) = V \int_V \gamma(\vec{r}) \, \mathrm{e}^{-i\vec{q}\cdot\vec{r}} \, \mathrm{d}v$$

$$\gamma(\vec{r}) = \frac{1}{V}\int_{V'} \Delta\rho(\vec{r}\,') \cdot \Delta\rho(\vec{r}\,' + \vec{r})\,\mathrm{d}v' = \overline{\Delta\rho(\vec{r}\,') \cdot \Delta\rho(\vec{r}\,' + \vec{r})}$$

The function $\gamma(\vec{r})$—named correlation function (Debye, 1949)—is the volume average of the product of $\Delta\rho(\vec{r})$ in two volume elements $\mathrm{d}v$, located at $\vec{r}_1$ and $\vec{r}_2$, connected by a vector $\vec{r}$. The function $\gamma(\vec{r})$ can directly be determined from an experimental scattering intensity function $I(\vec{q})$ by a Fourier transformation:

$$\gamma(\vec{r}) = \frac{1}{(2\pi)^3 V}\int I(\vec{q})\,\mathrm{e}^{i\vec{q}\cdot\vec{r}}\,\mathrm{d}v_q$$

In the particular case of isotropic systems, the correlation function is independent of the direction of the vector $\vec{r}$, i.e., $\gamma(\vec{r})$ can be written as $\gamma(r)$. Consequently, the scattering intensity is also isotropic. In this case, the function $e^{-i\vec{q}\cdot\vec{r}}$ is replaced in equation (8-5) by its spherical average $\langle e^{-i\vec{q}\cdot\vec{r}}\rangle = \sin qr/qr$ (Guinier, 1955). Thus, for isotropic systems, equation (8-5) becomes

$$I(q) = V\int_0^\infty 4\pi r^2\gamma(r)\frac{\sin q\cdot r}{q\cdot r}\,\mathrm{d}r \qquad \gamma(r) = \frac{1}{(2\pi)^3 V}\int_0^\infty 4\pi q^2 I(q)\frac{\sin q\cdot r}{q\cdot r}\,\mathrm{d}q$$